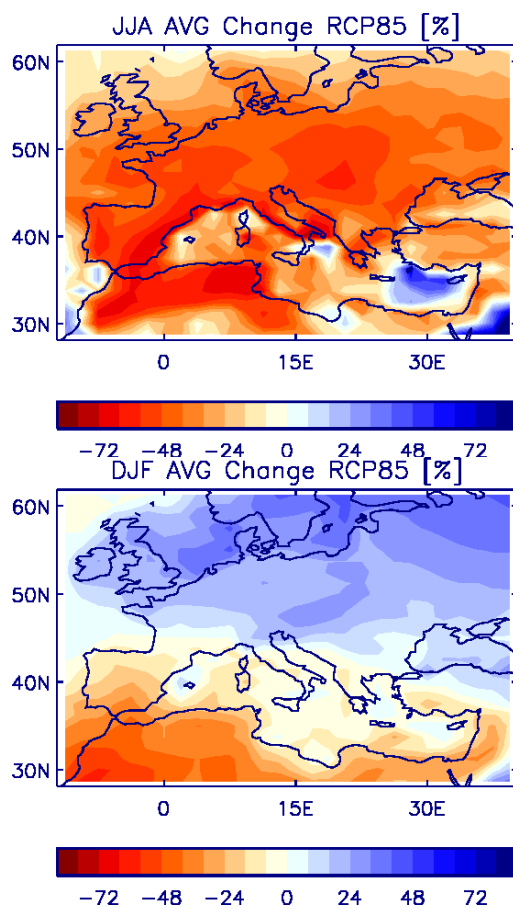# Changes in precipitation characteristics and extremes

Comparing Mediterranean to north-western European precipitation change

Master Thesis

April 2012

Author

David Vogel (04-919-502)

dvogel@student.ethz.ch

Supervisors

Dr Richard Allan (University of Reading)

Prof Dr Martin Wild (ETH Zurich)

Swiss Federal Institute of Technology Zurich
Institute of Atmospheric and Climate Science

University of Reading
Department of Meteorology

ETH

Eidgenössische Technische Hochschule Zürich
Swiss Federal Institute of Technology Zurich

University of Reading

Abstract

The global hydrological cycle is expected to alter with climate change, with potentially severe impacts on human society and ecosystems. This study analyses projected changes in precipitation characteristics (amount, frequency, intensity, duration), as well as heavy rainfall events and droughts, compared for the Mediterranean region and north-western Europe. The recent version 2 of the coupled Hadley Centre Global Environment Model (HadGEM2) is used to examine changes in two different climate scenarios.

In the Mediterranean region, precipitation amount, frequency and duration is projected to decrease 10-20 %, most pronounced during summer. In contrast, the precipitation intensity increases slightly. In north-western Europe, the precipitation amount remains constant on annual average, but increases during winter and decreasing in summer. The intensity of rainfalls rises 10-20 %, while precipitation frequency is reduced.

Heavy one- and five-day precipitation events are projected to increase 10-30 % in the Mediterranean region as well in north-western Europe, predominantly during winter. More consecutive dry days are simulated in both regions, 30-40 days in north-western Europe and 30-50 days in the Mediterranean area.

The model simulations of present climate are compared with monthly and daily precipitation data from the Global Precipitation Climatology Project. HadGEM2 underestimates the precipitation amount, especially in north-western Europe. While frequency is overestimated, the intensity is simulated too low. One-day precipitation extremes are over- or underestimated, depending on the considered region.

Keywords

Precipitation characteristics, extremes, HadGEM2, GPCP, precipitation intensity, precipitation frequency, Mediterranean, North-western Europe.

Cover: Percentage change of average precipitation during summer (top) and winter (down) simulated in HadGEM2-ES for emission scenario RCP85.

Table of contents

Table of tables

Table of figures

1 Introduction

πάντα ῥεῖ

(greek: panta rhei, "everything flows", attributed Heraclitus)

1.1 Motivation

Water continually moves between the oceans, the atmosphere and the land, forming the hydrological cycle. It is of outstanding importance for life on earth: ecosystems and the human society depend critically on the abundance of water. The hydrological cycle is fundamental for developed and developing countries likewise, for example for fresh water supply, agriculture, infrastructure or economical production (*IPCC*, 2007). Extreme events are thereby of especial significance, with potential loss of lives and severe destructions (*Seneviratne et al.*, 2012).

The global hydrological cycle is expected to alter with global climate change. In a human-induced climate change regime, changes of the energy budget at the Earth's surface and in the atmosphere influence the hydrological cycle (*Allen and Ingram*, 2002). Due to the major significance of the hydrological cycle, it is important to quantify its possible future change and to analyse the underlying mechanisms.

General circulation models are a powerful tool to explore potential changes in a future climate. A changing climate requires the society to start planning for adaption with potentially high cost in infrastructure measurements. Projections on regional scales enable informed decisions to be made regarding such investments.

1.2 Objective

In this study, results of the most recent version 2 of the Hadley Centre Global Environmental Model are used to examine the projected change for two regions: the Mediterranean area and north-western Europe. It aims to assess changes in amount, intensity, frequency, and duration of precipitation, as well as heavy precipitation events and droughts. The change is analysed for two different climate scenarios: a medium emission scenario and a high "business-as-usual" scenario.

2 Scientific Background

2.1 The global hydrological cycle

2.1.1 Water balance

The hydrological cycle is a major process in the earth's climate system. It describes the flow of water in between the atmosphere, land and oceans. Water evaporates from land or ocean surfaces, is transported within the atmosphere, condenses to clouds and eventually falls back to earth as rain or snow. The land fallen precipitation reevaporates or flows back to the oceans, closing the hydrological cycle (*Trenberth*, 2011).
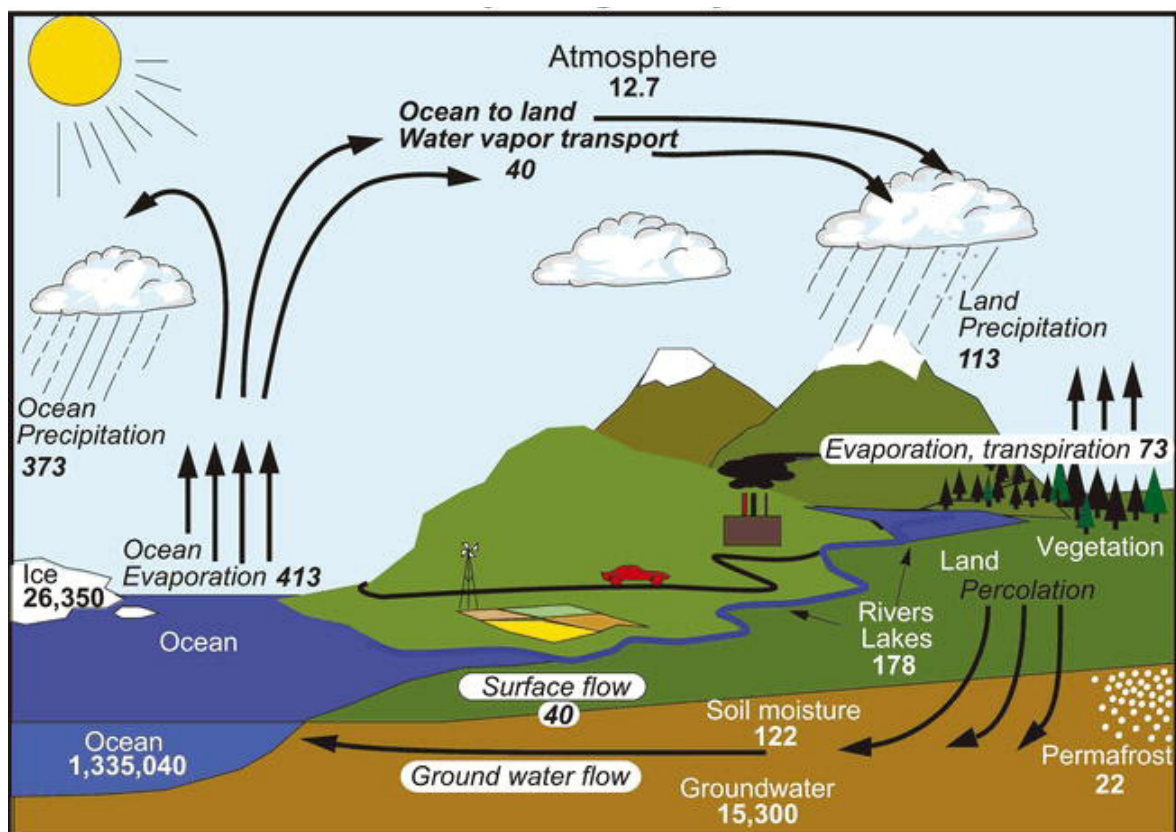
Figure 2-1 The hydrological cycle Estimates of main water storages (in 10^3 km^3) and flows (in 10^3 km^3/a) in the climate system, based on mean values form 1988-2004 (*Trenberth et al.*, 2007a).

Trenberth et al. (2007a) present an updated estimation of storages and flows in the hydrological cycle (Figure 2-1) based on mean values of the period 1988-2004, which was further analysed by *Trenberth et al.* (2011). The oceans are the most important storage by far, whereas the atmosphere has only minor storage. Evaporation fluxes are considerably larger than atmospheric storage, resulting in short residence time of water in the atmosphere (*Wild and Liepert*, 2010). Hence, global evaporation and precipitation must balance even on short time periods (*Wentz et al.*, 2007; *Wild and Liepert*, 2010). Estimates of annual daily precipitation and evaporation are given in Table 2-1. Both precipitation and evaporation data are affected by several sources of uncertainty, amongst them measurement inhomogenities, undercatch and shortcomings in remote sensing (*Trenberth et al.*, 2011).

Table 2-1 Annual global daily precipitation and evaporation values Values in mm/day. Ocean surfaces show an average surplus in evaporation, compared to a deficit of land surfaces. (*Trenberth*, 2011)

	Precipitation	Evaporation	Evaporation - Precipitation
Ocean	2.9	3.2	0.3
Land	2.1	1.4	-0.7
Total	2.7	2.7	

Evaporation exceeds precipitation over oceans, as moisture is advected from sea to land. Therefore the difference precipitation minus evaporation is positive on land and negative over the ocean. The surplus of 0.7 mm/day on land corresponds to the total runoff in surface flow. The proportion of advection to land precipitation is under debate (*van der Ent et al.*, 2010). According to the estimates in *Trenberth et al.* (2011), it is at least 35 %. *Bichet et al.* (2011) find a similar value. However, *van der Ent et al.* (2010) calculated in a reanalysis a ratio of 60 % of land precipitation advected from oceans.

2.1.2   Relationship to earth's energy budget

The hydrological cycle is closely linked to the earth's global energy budget (*Allen and Ingram*, 2002; *Boer*, 1993; *Held and Soden*, 2006; *Mitchell et al.*, 1987; *Wild and Liepert*, 2010). Water vapour is a strong greenhouse gas (GHG) and contributes to about 50 % of the total greenhouse effect (*Schmidt et al.*, 2010). Figure 2-2 depicts the global annual energy fluxes (*Trenberth et al.*, 2009). The net surface radiation balance, that is the net

radiation, is the key driver for evaporation. It is quantified by incoming minus outgoing solar (shortwave) and thermal (longwave) radiation. This available energy of 97 W/m^2 on global average is balanced by latent and sensible heat flux to the atmosphere. Thereby the latent heat is the dominant flux and the energy equivalent to the evaporation. The net radiation is positive on global scale, as on average an energy surplus at the surfaces is equalised by a deficit in the atmosphere (*Wild and Liepert*, 2010).
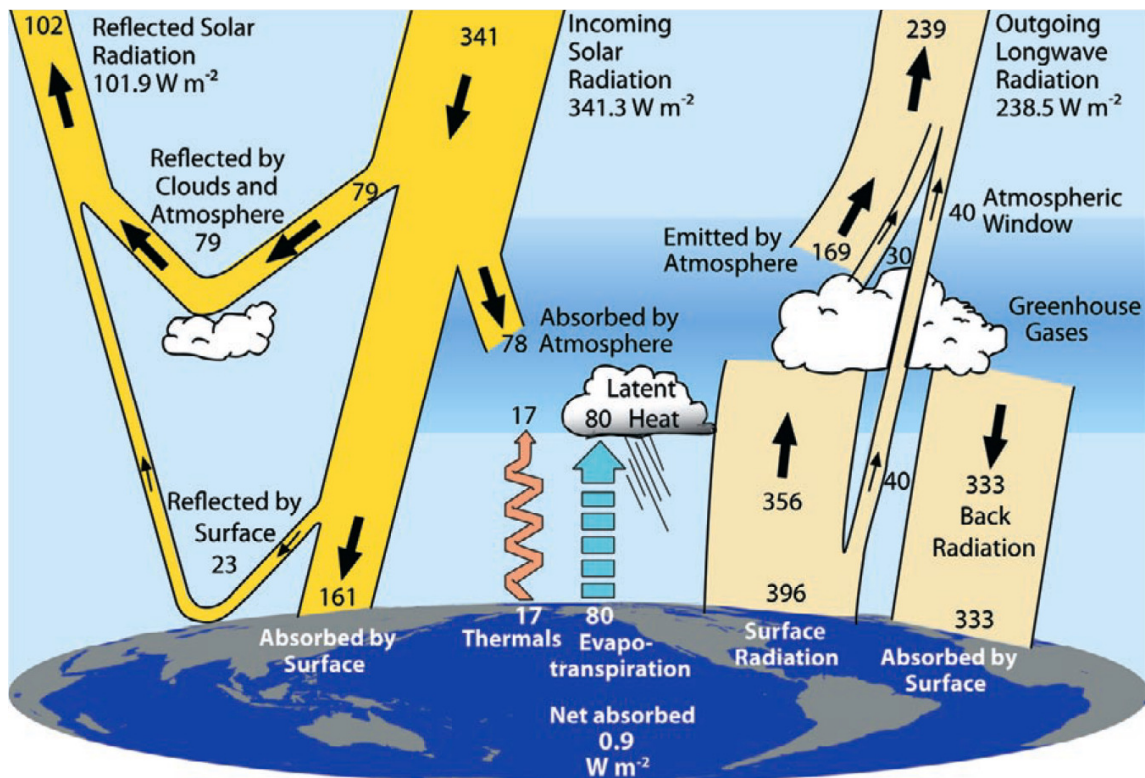
Figure 2-2 The global annual mean Earth's energy budget Energy fluxes of solar and thermal radiation as well as latent and sensible heat in W/m^2 (Trenberth et al., 2009)

The upward latent heat flow is an important contributor of the energy reallocation in the climate system, and as well a driver of the dynamical processes. The hydrological cycle affects the local energy balance in return. Clouds reflect incoming radiation, therefore cooling the climate, but heat it as well by absorbing outgoing longwave radiation. The net effect is complex and depends on the cloud structure and height (*Chahine*, 1992).

2.1.3   Influencing factors on evaporation

Evaporation shows two distinguished regimes: energy or moisture restriction. Energy restriction occurs if the surface could provide more moisture to evaporated, but the available energy is not sufficient. Moisture restriction describes the opposite case of sufficient energy supply but a lack of evaporatable moisture. This is often observed in hot and arid regions (*Hartmann*, 1994). Energy restriction applies always on sea surfaces, as moisture availability is infinite.

Locally, the strength of evaporation is influenced by additional factors: the relative humidity, wind speed, surface temperature and vegetation (*Richter and Xie*, 2008; *Zhang et al.*, 2004). Evaporation is found to be strongly dependent on sea surface temperature (SST) in a modelling experiment by *Bichet et al.* (2011). Vegetation absorbs water from the soil and transports it to the leaves, where it evaporates. This transpiration can have a substantial impact on the evaporation rate too (*Hartmann*, 1994).

2.1.4   Precipitation characteristics and extremes

Precipitation is complex and is be explored under different aspects. Not only how much precipitation is important, but also how often, how intense, how long and in which mode (rain, snow). These aspects are called precipitation characteristics and include amount, frequency, intensity, duration and type (*Trenberth et al.*, 2003). The knowledge of these characteristics is of general interest. For example, frequent precipitation with low intensities is more favourable regarding flood protection then the opposite. A change of type from snow to rain is of a major concern for the winter tourism industry (*Trenberth et al.*, 2003).

Extremes are generally associated as events with severe impacts to the environment, the society or both (*Trenberth et al.*, 2007b). In regard of precipitation they are often described as heavy precipitation, floods or droughts (*Easterling et al.*, 2000; *Trenberth*, 2008). Thereby it should be noted, that precipitation itself shows a considerable internal natural variability on various spatial and temporal scales. Long term variations are mostly coupled to atmospheric regimes like El Niño-Southern Oscillation (ENSO) or the North Atlantic Oscillation (NAO) (*Dai et al.*, 1997; *Trenberth et al.*, 2007b). This coupling influences the incidence of precipitation extremes (*Seneviratne et al.*, 2012).

Seneviratne et al. (2012) define extreme events in a general approach as the "occurrence of a value of a weather or climate variable above (or below) a threshold value near the upper (or lower) ends of the range of observed values of the variable". This implies that the local climate defines what an extreme event for that region is. They note as well that many extreme events occur as a result of the natural variability of the climate system. Extremes emerge as well as a combination of weather or climate phenomena which are not extreme themselves. In these so called compound or multiple events, the accumulation or combination itself is extreme. In contrast, although not being an extreme value in this statistical sense, events are anticipated as extreme based on their heavy impacts (*Seneviratne et al.*, 2012).

2.1.5   Significance to ecosystems and human society

The importance of the hydrological cycle is fundamental. It is the largest transport of any substance on earth, controlling earth's evolution in past, present and future (*Chahine*, 1992). The large scale redistribution of fresh water is crucial for human society and ecosystems. The availability of water impacts freshwater resources, agricultural production, ecosystems and most of industrial sectors (*Allan*, 2011; *Wild and Liepert*, 2010).

Extreme events in the hydrological cycle are often connected with severe impacts on human society and economy. The possibility of loss of human lives, destruction of properties, infrastructure and agricultural resources illustrate their significance (*IPCC*, 2007; *Trenberth*, 2008). Droughts caused wildfires as recently highlighted in California, associated with 2000 burned houses and 1 million displaced people in autumn 2007. Heavy precipitation and floods cause damage in comparable or even higher order (*Changnon et al.*, 2000; *Easterling et al.*, 2000; *Jonkman*, 2005). A highly developed infrastructure is becoming increasingly more sensible to climate extremes, as are less developed regions too due to lack of protective measures. Species, already endangered due to pressure on habitats, can be affected by extremes events, for example droughts, too (*Easterling et al.*, 2000).

2.2 The hydrological cycle in a changing climate

2.2.1 Atmospheric water vapour content

It is well understood that with an increasing concentration of anthropogenic greenhouse gases in the atmosphere, the downward thermal radiation will rise, consequently augmenting the net radiation (*Wild and Liepert*, 2010). A warmer climate is also capable of holding more moisture, a physical process governed by the Clausius-Clapeyron equation (1). Through the strong greenhouse effect of water vapour, an increase subsequently causes additional warming, the water vapour feedback (*Schmidt et al.*, 2010).

Clausius-Clapeyron describes an exponential increase in saturation water vapour pressure (e_s) with temperature (T) as:

$$\frac{d(ln e_s)}{dT} = \frac{L}{R_w T^2} \qquad\qquad (1)$$

which is approximately 7 % for a temperature rise of 1 Kelvin near the surface (L: latent heat of water vaporisation, R_w: specific gas constant for water) (*Held and Soden*, 2006; *Trenberth et al.*, 2003). The temperature dependence signifies a higher rise of saturation vapour pressure at colder temperatures, as much as 15 %/K at 200 K (*O'Gorman and Muller*, 2010). Models and observations show that the relative humidity of the atmosphere remains unchanged, consequentially resulting in an increase in specific humidity in a warming climate (*Held and Soden*, 2006; *Trenberth*, 2011). However, zonal differences exist (*O'Gorman and Muller*, 2010). In a detailed study by *O'Gorman and Muller* (2010), global mean moisture content is estimated to increase by 7.3 %/K, whereas surface specific humidity increases at a lower rate of 5.7 %/K. The total column of atmospheric water vapour was found to follow closely the SST in spatial pattern and time (*Trenberth*, 2011).

2.2.2 Energy constraints

The strength of the hydrological cycle, expressed as the amount of precipitation and evaporation, does not scale with Clausius-Clapeyron, in spite of the proportional increase in atmospheric mean moisture (*Allen and Ingram*, 2002; *Held and Soden*, 2006). Global mean precipitation sensitivity is modelled to increase on a lower rate of 2-3 %/K (1.4-

3.4 %/K, *Lambert and Webb* (2008); 2.3 %/K, *Stephens and Ellis* (2008); 1.7 %/K, *Held and Soden* (2006); 3.4 %/K, *Allen and Ingram* (2002)).

The reason for the difference between moisture and precipitation sensitivity is that the strength of the hydrological cycle is controlled more by energy than moisture availability. The constraining factor is the ability of the troposphere to radiate away the energy released during condensation of the latent heat transported from surface (*Allen and Ingram*, 2002; *Lambert and Webb*, 2008). The heat capacity of the atmosphere is negligible compared to the oceans. Therefore any change in released latent energy (LΔP) has to equal a change in radiative or sensible cooling (ΔR) of the troposphere. Conserving energy and following *Lambert and Allen* (2009), ΔR can be linearised as:

$$L\Delta P \approx k_T \Delta T + \Delta R_C + \Delta R_S \qquad (2)$$

with net change in cooling (a positive sign denotes an increase) due to: changes in tropospheric temperature ($k_T\Delta T$, inclusive change in sensible cooling), changes in longwave absorbing species concentration in the troposphere (ΔR_C) and changes in net solar shortwave radiation at the tropopause (ΔR_S). *Lambert and Allen* (2009) argue that ΔR_C and ΔR_S are expected to be negative in future, reducing LΔP. Model studies yield k_T values of 1.3-3.4 W/m^{2}K (*Lambert and Webb*, 2008) and 0.84-1.97 W/m^{2}K (*Lambert and Allen*, 2009). The temperature dependent change ($k_T\Delta T$) adjusts over a few years to achieve equilibrium, as the temperature depends on the heat uptake of the oceans, whereas the two other terms adjust instantaneously. *Andrews et al.* (2010) analyse the precipitation response for several radiative forcing mechanisms, differentiated into fast and slow responses. The fast precipitation response is sensitive to the applied forcing mechanism, whereas the slow response is independent. For future precipitation an increase in $k_T\Delta T$ is expected to be dominant (*Allen and Ingram*, 2002; *Held and Soden*, 2006; *Lambert and Allen*, 2009). Precipitation shows high sensitivity to changes in solar radiation, as further discussed in Chapter 2.2.3.

Allan (2006) calculated a longwave clear-sky radiative cooling (Q) of 3.6-4.6 W/m^{2}K, based on surface temperature (T_s). Thus we can write (2) as a differential precipitation change (dP) with T_s as:

$$\frac{dP}{dT_s} \approx \frac{1}{\rho_w L} \frac{dQ}{dT_s} \qquad (3)$$

which is 3-4 %/K (ρ_w is water density and L the latent heat of water vaporisation) (*Allan and Soden*, 2007).

As the precipitation does not scale with low-level moisture, the coupling atmospheric circulation is suggested to decrease (*Emori and Brown*, 2005; *Held and Soden*, 2006). Such a weakening is observed in a simulation of the Walker Circulation (*Vecchi and Soden*, 2007) as well in a smaller extent for the Hadley Circulation, which is additionally expected to expand polewards (*Lu et al.*, 2007).

Despite this proposed constraint, the response of the hydrological cycle is still under debate. A GCM surface evaporation analysis by *Richter and Xie* (2008) suggest that changes in other factors are also related to the muted increase: increases in surface relative humidity and surface stability, expressed as temperature gradient, and a decrease in wind speed damp the growth of evaporation. *Allan and Soden* (2007) detect considerable disagreement between models and observations in the tropics, underestimating trends in ascending and descending regions. In a global analysis, *Wentz et al.* (2007) found higher precipitation sensitivity in observations over two decades, questioning the damped increase of precipitation. However, the period of 20 years may be too short to assess trends, as observations can be affected by interdecadal variability (*Previdi and Liepert*, 2008). A sound understanding of the physical processes is still to be achieved (*Richter and Xie*, 2008; *Wild and Liepert*, 2010).

2.2.3   Atmospheric transmission

Not only greenhouse gases alter the available net energy for evaporation, but also fluctuations in solar radiation. Precipitation shows a higher sensitivity to forcing by solar radiation than by GHGs: solar radiation heats the surface efficiently by directly altering the surface energy balance, whereas GHGs enhance the downward thermal radiation of a warmer atmosphere as discussed in Chapter 2.2.2 (*Andrews et al.*, 2009; *Liepert et al.*, 2004). Studies attribute solar radiation a larger influence on precipitation for recent decades (*Bichet et al.*, 2011; *Feichter et al.*, 2004; *Liepert et al.*, 2004; *Wild et al.*, 2008). Beside natural variability of solar insolation, aerosols are an important determinant of the strength of solar radiation, displayed by "dimming" and "brightening" phases during the last century (*Wild et al.*, 2005). The atmospheric transmission of solar radiation is affected

by the presence of aerosols in several ways: directly by reflection of solar insolation, semi-directly by dissolving clouds due to heating of the aerosol layer. First and second indirectly through an increase of the cloud albedo due to more cloud condensation nuclei and through prolonging the lifetime of clouds (*Liepert et al.*, 2004). Except the semi-direct effect, all effects are thereby a reduction of the transmitted solar radiation (*Feichter et al.*, 2004; *Liepert et al.*, 2004; *Ramanathan et al.*, 2001).

Moreover it is assumed that aerosols, especially carbonaceous "black" aerosols, contribute to the slowdown of the hydrological cycle. Their strong absorption heat the aerosol layer which otherwise would have been heated by latent heat release (*Andrews et al.*, 2010; *Pendergrass and Hartmann*, 2012; *Trenberth et al.*, 2007b). In summary, increasing aerosol concentrations are expecting to dampen the hydrological cycle (*Bichet et al.*, 2011).

2.2.4   Moisture transport

More available moisture causes horizontal moisture transport to gain importance, with impact on precipitation characteristics, extremes and wet-dry regimes. In a constant circulation, convergent regions receive a higher moisture inflow and divergent regions are affected by a higher moisture outflow, making dry regions drier and wet regions wetter (*Allan and Soden*, 2007; *Allan et al.*, 2010; *Emori and Brown*, 2005).

In contrast to global mean precipitation, energy constraint is not necessarily applicable on smaller scales where moisture convergence and divergence is dominant (*Lambert and Allen*, 2009). Convective systems extend to about 3-5 times their radius to collect sufficient moisture, as the air remains typically still 70 % saturated after a precipitation event (*Trenberth et al.*, 2003).

The abundance of more moisture in the atmosphere and therefore moist energy will likely lead to more intense convective systems. The increase in precipitation intensity could even exceed the moisture increase. Intensity of precipitation is also expected to increase in areas where total precipitation decreases (*Allan and Soden*, 2008).

This gives rise to stronger precipitation extreme events (*Trenberth*, 2011; *Trenberth et al.*, 2003). *Pall et al.* (2007) found water vapour change a better predictor for extreme precipitation increase than mean precipitation change, although differences between

latitudes exist. However, contrary to a proportional increase with water vapour an analysis by *O'Gorman and Schneider* (2009) highlights the importance of changes in the moist-adiabatic lapse rate, vertical velocity and temperature for scaling of extreme precipitation in a future climate. Eventually, other phenomena are suggested to be important for extreme events. Moisture is spatially not uniformly distributed, but in so called Atmospheric rivers or moisture conveyor belts. Their influence and possible changes in future need further analysis as well (*Lavers et al.*, 2011).

The total amount of precipitation is coupled to the intensity and the frequency of precipitation events, given that the amount is a product of the frequency and the intensity of the precipitation. More frequent and intense events lead to higher precipitation amounts. As precipitation amount is expected to rise less than intensity, consequently frequency has to decrease. This makes precipitation more unpredictable and enhances the vulnerability for intense and prolonged droughts (*Trenberth*, 2008, 2011).

2.2.5   North Atlantic Oscillation (NAO)

The NAO is closely related to precipitation patterns in Europe through changes in the moist and warm westerlies. The NAO has its maximum signal in winter, and evidence suggest that it is connected to tropical and extratropical SST (*Hurrell et al.*, 2004; *Trenberth et al.*, 2007b). During a positive phase with a strong Iceland Low and Azores High, enhanced northward shifted westerlies bring increased precipitation in northern Europe winter, and reduced precipitation in southern Europe (*Hurrell and Van Loon*, 1997; *Trenberth et al.*, 2007b). *Meehl et al.* (2007) report an increasing trend in the NAO index in climate model projections. This is consistent with a projected poleward shift of storm tracks (*Yin*, 2005).

2.2.6   Seasonal patterns

Warmer temperatures as expected with climate change lead to opposite effects on precipitation in summer and winter in higher latitudes. In winter, precipitation increases in general. Cold surface temperatures in winter constrain the precipitable water vapour amount in the air. This is accompanied by a reduction in snow amounts (*Trenberth*, 2011). A warmer climate allows the atmosphere to hold more water vapour and hence permit

more precipitation. Whereas in summer, limited soil-moisture over land constrain latent heat release. Sensible heat release is increased instead of latent heat, resulting in warm, dry periods (*Schär et al.*, 1999; *Trenberth and Shea*, 2005). In this context, the discrepancy in the amount of advected moisture (cf. Chapter 2.1.1) should be further studied.

2.3 Observed and projected change in precipitation

2.3.1 Observations

An overall increase in global land precipitation in observations is not significant for the period 1907-2005 (*Trenberth et al.*, 2007b). However, regional trends show an increase in northern Europe and a decrease in the subtropics (*Trenberth*, 2011; *Trenberth et al.*, 2007b). Trends in extreme precipitation and droughts are insignificant for Europe and the Mediterranean area. Extreme precipitation shows a more pronounced increase in central Europe in winter, as well as drier conditions in the Mediterranean during summer (*Seneviratne et al.*, 2012).

2.3.2 Projections

Climate models respond to global warming in general with a rise in precipitation, but with large discrepancies between regions (*Christensen and Christensen*, 2007; *Christensen et al.*, 2007). Figure 2-3 shows the projected precipitation change in a 21 climate model average for a medium emission scenario (A1B). The annual, winter and summer change patterns are depicted.
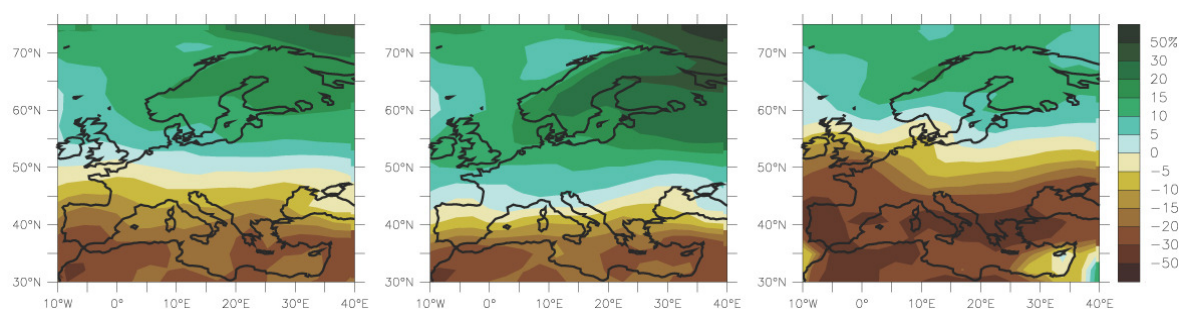
Figure 2-3 Projected precipitation changes Percentage precipitation change simulated in A1B scenario, averaged over 21 models. Annual (left), winter (middle) and summer (right) change (*Christensen et al.*, 2007).

Christensen et al. (2007) report median values for projected precipitation change. For northern and central Europe, an increase of 10-15 % is expected throughout all season except summer, where the signal is weak (2 %). For the Mediterranean Basin, average precipitation is expected to decrease for all seasons. The decrease ranges from 10 % in autumn to 29 % in summer.

The number of extreme precipitation events is projected to grow in northern and central Europe during winter. Less pronounced is an increase in summer dryness for this region. Southern and Mediterranean Europe show a consistent growth of areas affected by drought, but an inconsistent increase in the strength of heavy precipitation events (*Frei et al.*, 2006; *Seneviratne et al.*, 2012).

3 Data & Method

3.1 Global Precipitation Climatology Project (GPCP)

Monthly and daily values from the GPCP are used in this study as observational reference. The GPCP dataset combines microwave and infrared remote sensing with surface rain gauge measurements (*Adler et al.*, 2003; *Huffman et al.*, 2009). It provides monthly precipitation data from 1979 to 2010 on a 2.5° grid. The current version number 2.2 of the dataset is used for the analysis. Daily values are available from 1997 to 2009. The most recent version 1.1 is available on a one-degree grid and form the basis for daily precipitation analysis (*Huffman et al.*, 2001).

3.2 Hadley Centre Global Environment Model version 2 (HadGEM2)

General circulation models (GCMs) are of outstanding importance for analysing future climate change (*Meehl et al.*, 2007). The complexity of the climate system requires the integration of an atmosphere, ocean and earth-system component into a GCM to resolve the variety of coupled feedbacks (*Collins et al.*, 2011).

For the analysis of the future hydrological cycle, this study uses precipitation data from HadGEM2. HadGEM2 is a fully coupled GCM operated by the Met Office Hadley Centre, the climate research centre of the United Kingdom's Weather Service (*Martin et al.*, 2011).

3.2.1 Configurations

Two different configurations of HadGEM2 are used for this study: HadGEM2-ES (Earth System) and HadGEM2-A (Atmosphere-only). HadGEM2-ES is the complete model with all components of the climate system coupled and interacting: Troposphere, Land Surface & Hydrology, Aerosols, Ocean & Sea-ice, Terrestrial Carbon Cycle, Ocean Biogeochemistry and Tropospheric Chemistry. In the second configuration HadGEM2-A only the first three components are coupled (*Martin et al.*, 2011). Observational datasets

are used to pre-describe parts of the remaining components, as for example SSTs and sea ice concentration records (*Hurrell et al.*, 2008).

3.2.2   Temporal and spatial resolution

Simulations in HadGEM2 have a temporal resolution of 30 minutes, denoting the difference between two time steps. For this study monthly or daily output is used, depending on the analysis.

The spatial resolution of HadGEM2 is 1.25° latitude x 1.875° longitude, corresponding to a horizontal grid size of approximately 140 x 150 kilometres in Europe. Figure 3-2 illustrates the horizontal resolution in HadGEM2. Vertically, 38 levels are represented (*Martin et al.*, 2011).

3.2.3   Experiments

HadGEM2 contributes climate simulations for phase 5 of the international Coupled Model Intercomparison Project (CMIP5). The simulations from different GCMs in CMIP5 will be used in the fifth Assessment Report (AR5) of the Intergovernmental Panel on Climate Change (IPCC), to be released in 2013 (*Collins et al.*, 2011; *Jones et al.*, 2011). CMIP5 provides a set of standard experiment protocols to assess GCMs towards the AR5. They aim to provide improvements in climate projection, model evaluation and process understanding of the climate system. A variety of realistic and idealized simulations of the past and the future are covered. The experiment protocols include paths of natural and anthropogenic forcing factors, as for example emission and concentration paths of GHGs, solar insolation, land-use change or aerosol emissions (*Jones et al.*, 2011).

Simulations of the past are needed to evaluate the models ability to simulate processes and observations realistically (*Jones et al.*, 2011). Two experiments are used in this study: the "AMIP" and the "historical" experiment. The AMIP experiment, called after the Atmospheric Model Intercomparison Project, is an uncoupled simulation of the atmospheric system. The protocol for the AMIP experiment includes pre-described SST and sea ice concentration datasets. The oceans are thereby assumed to have an infinite heat uptake. This unidirectional forcing is physically incorrect, but allows to compare simulations with observations which are heavily depending on SSTs, such as annual or

decadal phenomena like ENSO (*Hurrell et al.*, 2008). In contrast, the experiment "historical" is simulated in the fully coupled HadGEM2-ES and driven by records of forcing factors from 1860 to 2005 (*Jones et al.*, 2011).

Future emissions depend heavily on development of key determinants in society, economy, and technology. Important indicators (also known as the Kaya factors) are thereby growth in population and economy, energy intensity of the economy and carbon intensity of the energy sources (*van Vuuren et al.*, 2011). Different plausible scenarios are built to explore the range of future states and to evaluate possible mitigation and adaption policies (*Moss et al.*, 2010).

For the upcoming AR5, four new Representative Concentration Pathways (RCPs) have been developed to be used in CMIP5 (*Meinshausen et al.*, 2011; *Moss et al.*, 2010; *van Vuuren et al.*, 2011). They represent a temporal and spatial discrete set of emissions and concentrations of GHG and air pollutants, as well as land-use projections. The RCPs lead to four clearly distinguished radiative forcing levels (2.6, 4.5, 6 and 8.5 W/m^2) at the end of the century, reflecting the range in literature (*van Vuuren et al.*, 2011). Different integrated assessment models were used to produce the pathways and further processed to ensure comparability (*Meinshausen et al.*, 2011). Parallel to the use in driving climate models, a variety of new socio-economic scenarios are assessed in respect to the RCPs (*Moss et al.*, 2010).
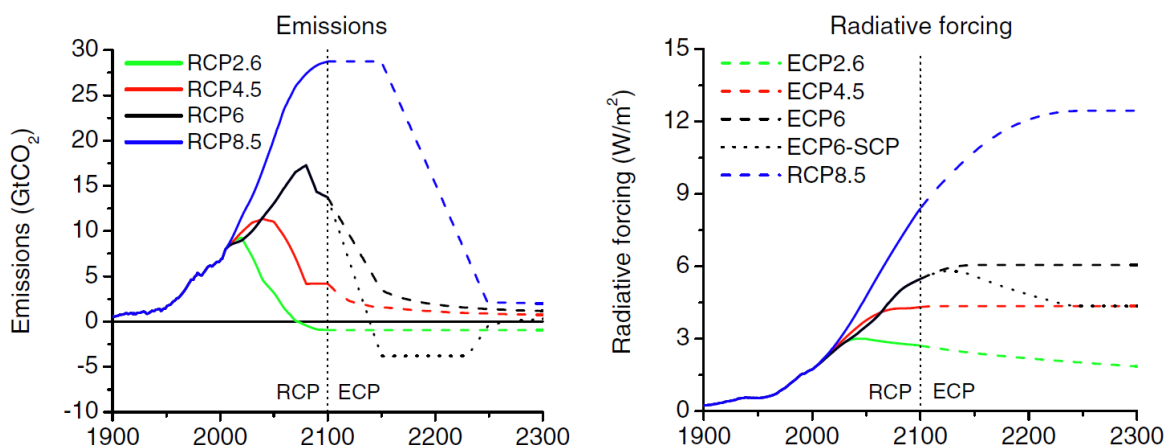
Figure 3-1 Emissions and radiative forcing in RCPs The different RCPs and their extension (ECPs) to 2300 are shown. CO$_2$ emissions (left) in GtCO$_2$ decrease for all RCPs but RCP85 to achieve stabilised radiative forcing (right) at the year 2100 (*van Vuuren et al.*, 2011).

Figure 3-1 shows CO_2 emissions and radiative forcing pathways of the RCPs. This study uses RCP45 and RCP85 to represent two different developments. The RCP45 experiment reflects a medium scenario with a stabilised radiative forcing level of 4.5 W/m^2 at the year 2100. This implies a reduction in global GHG emissions in the near future. The second used pathway RCP85 is a high level growth of GHG emissions in a "business-as-usual" manner, leading to an unstabilised radiative forcing level of 8.5 W/m^2 at the end of the century.

3.3 Study domains and reference periods

3.3.1 Study domains

This study assesses precipitation change in two study domains: north-western Europe (NWE) and the Mediterranean (MED). Hereafter, the acronyms denote specifically the study domains as defined in Table 3-1 and shown in Figure 3-3.

In Table 3-1, the regional definitions of this study are compared with regions used in the latest IPCC AR4 (*Christensen et al.*, 2007) and in Chapter 3 of the IPCC Special Report on Managing the Risks of Extreme Events and Disasters to Advance Climate Change Adaptation (SREX) by *Seneviratne et al.* (2012).

Table 3-1 Study domain borders The borders of this study are similar to SREX and IPCC AR4 regions. NWE reaches less north- and eastwards, to achieve a more homogenous domain in the Köppen-Geiger classification system. MED shares the same southern and northern border with IPCC and SREX, the eastern border lies in between.

	Region	North	West	South	East
This study	NWE	60°N	10°W	45°N	19°E
	MED	45°N	10°W	30°N	38°E
IPCC AR4	Northern Europe	75°N	10°W	48°N	40°E
	Mediterranean Basin	45°N	5°W	30°N	35°E
SREX	Central Europe	(*)	10°W	45°N	40°E
	Mediterranean Basin	45°N	10°W	30°N	40°E

(*) Note that SREX has two almost triangular shaped northern European areas. Their border divides Central Europe from the British Isles and Scandinavia.

The spatial setting is analysed in respect to the Köppen-Geiger system. The Köppen-Geiger system is a climate classification system, combining temperature and precipitation averages to distinguishable types of climate zones. Originally developed in 1900 by W. P. Köppen to classify areas with similar vegetation, it is still the most frequently used climate classification system (*Kottek et al.*, 2006; *Peel et al.*, 2007). The Köppen-Geiger system provides useful information for evaluations of GCMs. It has been successfully applied by *Lohmann et al.* (1993) as a diagnostic for the validation of GCM simulations.

The mid-latitudinal north-western European climate is represented by the Cfb climate (Temperate, dry winter & warm summers). Consequently, this is the dominant type in NWE, with exceptions of colder continental climate in the eastern area, the French Massif Central and the Alps. The characteristic class of the subtropical Mediterranean climate is the Csa climate (Temperate, dry & hot summer). MED is a more heterogeneous domain. Notable discrepancies are a considerable area of more arid regions of type B in the southern part: in northern Africa, Anatolia and central Spain. Colder climates are found on the Balkan Peninsula, and more humid areas in the Pyrenees (*Peel et al.*, 2007).
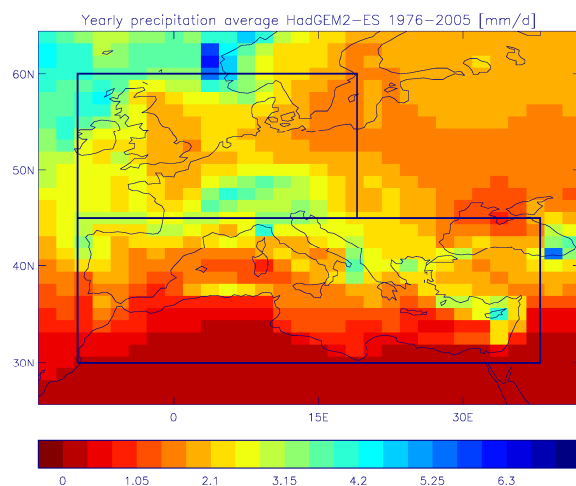
Figure 3-2 Study domains and resolution of HadGEM2 The two boxes indicate the study domains NWE (top) and MED (down). The model grid is shown, illustrating the horizontal resolution of 1.25° latitude x 1.875° longitude. The figure displays the annual precipitation average in HadGEM2-ES for the period 1976-2005 in mm/d.
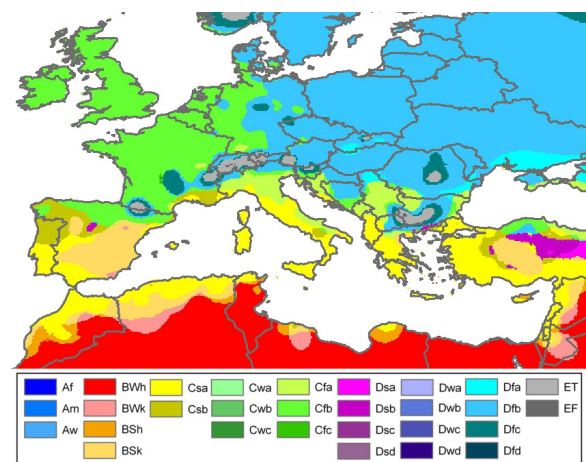
Figure 3-3 Köppen-Geiger map for Europe and Mediterranean Updated map of climate classification after W. P. Köppen. NWE is dominantly the Cfb class, with exceptions in the eastern part and the alpine ridge. MED is more heterogeneous, including areas of the characteristic Mediterranean Csa climate and more arid zones in the south (*Peel et al.*, 2007).

3.3.2   Reference periods

Climate refers to the average condition of the atmosphere over a long period, mostly 30 years (*CH2011*, 2011). Wherever possible, a 30 year was defined as reference period. The historical HadGEM2-ES simulations end in 2005. Therefore, the period 1976-2005 is chosen as reference period for the present climate (PRE) in this study. As future reference period (FUT), 2070-2099 is defined.

The available time periods of the datasets constrain the duration of the reference period for comparisons with observations. Monthly data reference period is 1979-2005, as model data of the historical experiment are available till 2005. The daily GPCP observations are even shorter, with an available period from 1997-2005. Table 3-2 gives an overview of the datasets and their characteristics used in this study.

Table 3-2 Overview of model and observational data used in this study The temporal and horizontal resolution (latitude x longitude), experiment for models or version for observations, reference periods and number of ensemble members is shown. For observational comparisons, high resolution data is interpolated to fit the coarser resolution.

Model, Observations	Temporal resolution	Horizontal resolution	Experiment, version	Reference period	Ensemble members
HadGEM2-ES	daily & monthly	1.25° x 1.875°	historical	1976-11/2005	4
			RCP45, RCP85	2070-2099	4
HadGEM2-A	monthly	1.25° x 1.875°	AMIP	1979-11/2005	6
	daily			1997-2008	1
GPCP	monthly	2.5° x 2.5°	V 2.2	1979-11/2005	-
	daily	1° x 1°	V 1.1	1997-2008	-

The meteorological seasons are abbreviated in the conventional manner: JJA (June-July-August) for summer, SON (September-October-November) for autumn, DJF (December-January-February) for winter and MAM (March-April-May) for spring.

3.4 Diagnostics

3.4.1   Precipitation diagnostics

This study analyses projected changes in a set precipitation characteristics and extremes: amount, frequency, intensity and duration, as well as heavy rain events and droughts. Changes in precipitation type (snow, rain) are not considered. Secondly, the model deviations to observational dataset GPCP are diagnosed. For the analysis of extremes, indices compliant to the recommendations by the Expert Team on Climate Change Detection and Indices (*Klein Tank et al.*, 2009) are used. The definition of the used indices is presented in Table 3-3.

Table 3-3 Precipitation diagnostics Definition of indices used in this analysis (*Frei et al.*, 2006; *Klein Tank et al.*, 2009).

	Index	Definition	Unit
Amount	AVG	Average precipitation	mm/d
Frequency	FRQ	Wet day frequency, days with precipitation ≥ 1 mm	fraction
Intensity	INT	Wet day intensity, mean precipitation on days with precipitation ≥ 1 mm	mm/d
Duration	CWD	Consecutive wet days, average of largest number of consecutive days with precipitation ≥ 1 mm	Number of days
Heavy rain events	RX1	Average maximum one-day precipitation in a year	mm/d
	RX1-30	Maximum one-day precipitation in a 30 years period (lowest ensemble member)	mm/d
	RX5	Average maximum precipitation during five consecutive days in a year	mm/d
	RX5-30	Maximum precipitation during five consecutive days in a 30 years period (lowest ensemble member)	mm/d
Droughts	CDD	Consecutive dry days, average of largest number of consecutive days with precipitation < 1 mm in a year	Number of days
	CDD-30	Consecutive dry days. Largest number of consecutive days with precipitation < 1 mm in a 30 years period (lowest ensemble member)	Number of days

The indices are calculated on an annual and seasonal basis, then averaged over the reference periods (cf. Chapter 3.3.2), and thirdly averaged over all ensemble members (where applicable). The indices CDD and CWD are not seasonally diagnosed.

For heavy rain events and droughts, maxima of a one year and 30 year period are analysed. For the first (RX1, RX5, CDD), the procedure is identical to the other indices. Hence, RX1 indicates the average of the annual heaviest daily rainfall in the reference period. The second approach enquires more extreme, thus rarer, events. The index maxima of the whole 30 year period are calculated for each ensemble member. The lowest of the four ensemble members is used for the analysis. This is a precaution to constrain outliers.

3.4.2 Change diagnostics

The change of the indices from present to future is evaluated. The signal is calculated between HadGEM2-ES (RCP45 & RCP85) FUT minus PRE (historical). The alteration is presented as percentage change of the present value:

$$\Delta\% = \frac{\mathrm{FUT}-\mathrm{PRE}}{\mathrm{PRE}} \times 100\,\% \qquad\qquad (4)$$

HadGEM2 simulations of the recent past are compared with GPCP observations, to identify deviance of the model from the records. Coupled simulations as HadGEM2-ES do not necessarily simulate interdecadal processes synchronously with observations. This causes additional bias for short time periods. To minimise this error source, AMIP simulations with pre-described SST are used. However, this procedure does not reflect possible bias due to the coupling of all model components. Therefore monthly observations are as well compared with HadGEM2-ES simulations, as there is a period of 27 years available for comparison. For daily values HadGEM2-ES is not compared to GPCP, due to the fact that only 9 years overlap.

3.4.3 Statistical analysis

To illustrate the spread of the signal in the domains, the changes are presented as boxplots. The underlying data used for the boxplot calculation is the entity of percentage change signals on all grid points in the ensemble members. The 25 %, median and 75 % quantiles form the box, and the whiskers depict the 2.5 % and 97.5 % quantiles of the data. It is important to note that the boxplot is a visualisation of the variation in the domain and not a statement about the probability of the diagnosed change signal.

The entity of the present and future average indices from ensemble members of a domain is used to perform a Wilcoxon-Mann-Whitney rank-sum test. The Wilcoxon-Mann-Whitney test is used to take into account that the data do not necessarily follow a standard normal distribution (*Wilks*, 1995). The rank-sum test indicates if the future climate average of index, the 30 year average, is statistically different from the present climate for the whole domain.

3.5 Discussion

3.5.1 GPCP

The approach of combined satellite and in-situ measurement aims to use the individual advantages of the data sources to reach a reliable set of precipitation values. Still, accurate precipitation measurements are difficult to achieve. Errors sources are for example wind-effects and land-ocean bias for in-situ measurements or coverage and calibration issues for remote sensing (*Allan et al.*, 2010; *Trenberth et al.*, 2007b).

A comparison of six different precipitation records (*Fekete et al.*, 2004), amongst them GPCP, shows that largest relative difference exists in mean values and seasonality in semi-arid and arid regions, whereas absolute difference is highest in tropic regions. The overall precipitation pattern is in good agreement (*Fekete et al.*, 2004). *Rubel et al.* (2002) analysed the daily GPCP precipitation data compared to a dataset of 3100 rain gauge measurements over the European Alps. Based on a two months period, a mean error of 0.18 mm/d, or approximately 5 % was reported. However, the mean absolute error is calculated to be 3.44 mm/d, or almost 100 % of the daily precipitation of this period. A detailed study over the Mississippi River Basin (*Gebremichael et al.*, 2005) reports a lower mean absolute deviation of 48 % for daily GPCP data. For monthly GPCP data, a mean absolute deviation of 22 % was calculated in an analysis of a 6 month period over 23 years in North Dakota (*Gebremichael et al.*, 2003).

For this study, the large horizontal resolution of monthly observations and the restricted available time period for daily values, imply some additional uncertainty for the results.

3.5.2   Uncertainties associated with climate projections

Projections on climate change are affected by three types of uncertainty sources: natural variability, scenario uncertainty and model uncertainty (*CH2011*, 2011; *Hawkins and Sutton*, 2009). Natural variability is of importance up to decadal predictions. For long term predictions, uncertainty is dominated by scenario uncertainty (*Hawkins and Sutton*, 2009). Scenario uncertainty refers to the difficulty to estimate future GHG and aerosol emissions, which depend strongly on the development in society and economy.

Model uncertainty is caused either by a lack of understanding of processes, the limited ability to describe processes accurately or the too low resolution in climate models, which therefore have to parameterise relevant processes. Uncertainty in initial and boundary conditions of climate models is of minor importance on long-term projections (*Knutti et al.*, 2010). To account for model uncertainty, different models are used in projections, which use independently developed parameters. Their results are combined as multi-model ensembles (*Knutti et al.*, 2010). Additionally, Regional Climate Models (RCMs) are nested into GCMs, and driven by boundary conditions derived from GCMs. They are able to resolve processes on higher resolutions (*Hawkins and Sutton*, 2009). A third approach is to obtain several ensemble of the same climate model, through perturbation of atmosphere-ocean initial conditions (*van der Linden and Mitchell*, 2009). Multi-model ensembles are reported to be superior to single-model ensembles (*Palmer et al.*, 2005).

To cope with the scenario uncertainty, this study analyses two different emission scenarios: RCP45 and RCP85. They represent a medium and a high "business-as-usual" emission development. The model uncertainty is considered with the use four ensembles of HadGEM2-ES. Further GCMs or RCMs are not used. Hence, the projection uncertainty is not fully represented by the results, and therefore no confidence intervals are presented.

3.5.3   Reliability of GCMs for precipitation and extremes

Despite of increased complexity and continuous improvements in GCM, projections of the hydrological cycle are still ambiguous (*Bony et al.*, 2006; *Schaller et al.*, 2011). They are more heterogeneous for precipitation than for other parameters, as for example for temperature. Clear statements are not possible in particular on regional scale, as models

show little consistency (*Anderson et al.*, 2009; *Pendergrass and Hartmann*, 2012). This is also the case for precipitation extremes (*Orlowsky and Seneviratne*, 2012; *Seneviratne et al.*, 2012). These circumstances have to be considered in the interpretation of the results.

Alongside, studies show that GCMs fail to simulate the intensity and frequency of precipitation accurately (*Dai*, 2006; *Sun et al.*, 2006). On the one hand, they overestimate the frequency for light precipitation (<10 mm/d) while correctly reproducing the intensity. On the other hand, they underestimate the intensity of heavy precipitation (<10 mm/d) while correctly reproducing the frequency (*Sun et al.*, 2006). *Martin et al.* (2011) describe improvements in precipitation, specific and relative humidity simulation in HadGEM2 compared to the previous version HadGEM1. Compared to GCMs in the previous CMIP3, HadGEM2 is superior (*Martin et al.*, 2010). The analysis of model-observation differences may deliver some insights.

The coarse grid spacing in HadGEM2 implies that the topography and land-sea distribution is only limitedly resolved, mesoscale and smaller scale processes have to be parameterised (*Frei et al.*, 2006). This affects the ability to resolve the precipitation process. An improvement could be achieved by downscaling the GCM data to high resolution observations, such as a dense rain gauge dataset (*Schmidli et al.*, 2007). In a simple method by *Schmidli et al.* (2006) the downscaling is obtained by adjusting frequency and intensity values of the GCM predictions. Due to time constraints, this is not implemented.

3.5.4   Diagnostics

Overall, the diagnostics give a robust impression of the most important precipitation characteristics and extremes. A minimal error originates from missing December values for 2005 in the historical simulations.

The analysis of precipitation duration, the consecutive wet days, differs from the other characteristics diagnostics. They do not deliver a diagnostic per day, but only one annual value is calculated. This index could suggest a more extreme event for longer periods of wet days.

Impacts of extreme events, as flooding, landslides or a drought period do not necessarily have to be connected with single extreme events. An accumulation of high, although not

extreme events can have similar impacts. Furthermore, vulnerability and accompanying conditions of the affected region are of importance, as for example soil saturation. Conversely, a climatic extreme event does not have to indicate an event with high impact (*Seneviratne et al.*, 2012). Therefore no strong causality to changes in extreme impacts can be made from the extreme indices.

The RX1-30, RX5-30 and CDD-30 values are not tested if a second largest event in an ensemble member exceeds the largest in another ensemble. Therefore, these extremes cannot necessarily be interpreted as the fourth largest event in all years in the combined ensembles.

The diagnostics of extremes do not use a locally definition as suggested by *Seneviratne et al.* (2012). For this purpose a definition based for example on the 95 % quantiles would have had to be used. But the selected indices are in agreement with *Klein Tank et al.* (2009) and used in analysis of climate predictions such as *CH2011* (2011). Hence, no curtailing of the validity of the results is expected.

A more detailed analysis would require the use of extreme value technique (*Frei et al.*, 2006). In extreme value technique the entity of block maxima or peaks over a threshold is used to fit a generalised extreme value distribution. This distribution is then used to calculate a return value of a chosen return period T. The return value is expected to be exceeded by an event with the probability of 1/T, for example once every 100 years (*Frei et al.*, 2006). Due to time constraints, this is not realised.

Changes in extremes can not only be caused by changes in the climate mean, but also in its variance or shape of probability distributions. It may also be due to a combination of this factors (*Seneviratne et al.*, 2012). Hence, probability distributions of precipitation and extremes could also be analysed.

4 Results

4.1 Precipitation amount

4.1.1 Comparison with observations
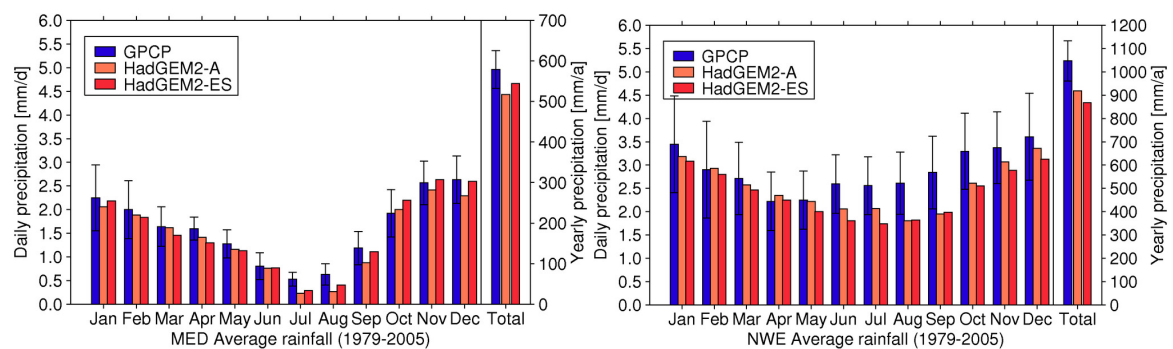
Figure 4-1 Deviation of precipitation amount between GPCP, HadGEM2-A & -ES Monthly average from
1979-2005 for precipitation in mm/d and yearly precipitation in mm/a, depicted for GPCP (with
standard deviation bars), HadGEM2-A & HadGEM2-ES. Left: MED, right: NWE. Note the different
scales.

Figure 4-1 shows the monthly and annual precipitation average in GPCP, HadGEM2-A
and HadGEM2-ES. The average precipitation for each month and the total annual
precipitation are displayed with standard deviations of the observation. In MED, a strong
seasonal cycle of precipitation is visible. Most rainfall occurs during winter. HadGEM2
simulates too little precipitation compared with GPCP in both configurations. The
difference is more pronounced in NWE, where the difference in total annual precipitation
is larger than the standard deviation of precipitation in GPCP. In particular in the months
June to October, the precipitation amount is distinctively underestimated. In MED, total
annual precipitation of HadGEM2-ES lies within the range of the standard deviation of
GPCP, while HadGEM2-A lies outside. HadGEM2-ES matches monthly averages of daily
precipitation often accurately, while differences remain during summer however.
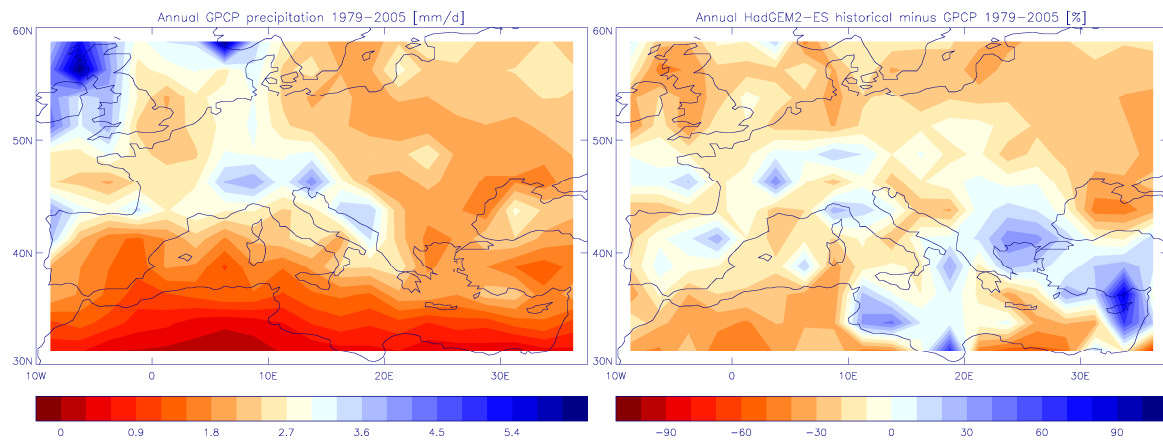
Figure 4-2 Average annual precipitation & deviation in HadGEM2-ES Left: annual average precipitation amount in GPCP in mm/d. Right: percentage deviation of HadGEM2-ES minus GPCP.

The spatial pattern of the difference between the model projections from GPCP observations is given in Figure 4-2. The spatial pattern of the deviation is similar for both model configurations. Over the British Isles, Scandinavia and the Black Sea, HadGEM2 underestimates the precipitation. On the other side, the areas of Turkey, Cypress and the Alps are modelled to be too wet. The deviation of average daily precipitation reaches thereby 80 % in Cypress. Absolute seasonal deviations for both model configurations are shown in Figure A-1 in the Appendix.

4.1.2   Mediterranean region
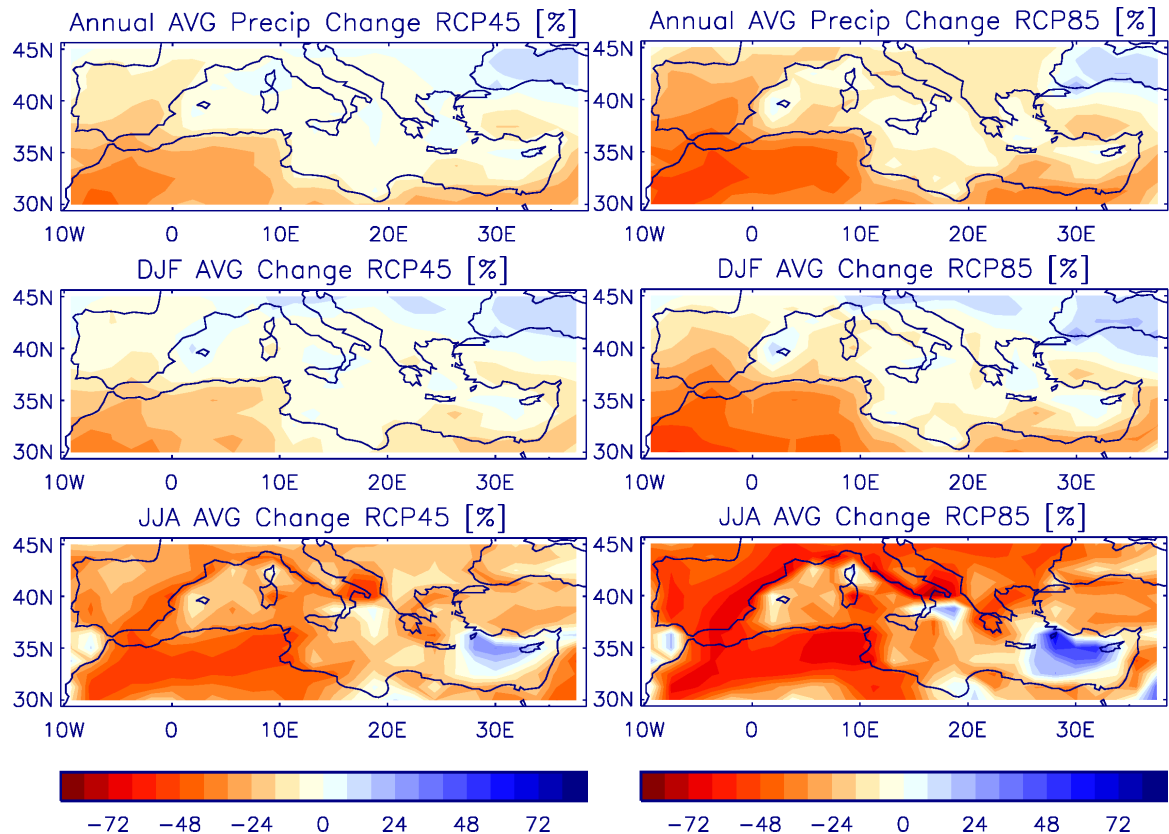
Figure 4-3 Average precipitation changes in MED Percentage change for period 2070-2099 of average precipitation in HadGEM2-ES are depcited for RCP45 (left column) and RCP85 (right column). The annual (top), DJF (middle) and JJA (bottom) changes are shown. Changes are significant on 5 % level, except DJF RCP45.

HadGEM2-ES simulates a decrease in average precipitation in the MED domain (Figure 4-3). Summer precipitation decreases up to 70 %, but contributing only a minor share of the annual precipitation amount. But the annual average declines in the medium RCP45 scenario too, by 10 %. For the RCP85 scenario the decrease is 20 %, distinctively higher. The highest percentage decreases are located in areas with low precipitation. HadGEM2-ES simulates an increase in north-eastern area during winter for RCP45. But the change of the domain is not significant for this season. RCP85 shows an overall decrease of average precipitation during winter.

A difference between land and sea surfaces is appearing, with higher reductions over land. The annual average rises over the Black Sea. Over Cypress, an anomalous strong precipitation increase is simulated. This could be related to modelling problems, as

precipitation deviates considerably from observations in this area. Further seasons and modelled present precipitation are shown in Figure A-2 in the Appendix.

4.1.3   North-western Europe

Comparing summer and winter in NWE, strong seasonal differences appear (Figure 4-4). Precipitation is increasing in winter season, whereas strongly decreasing during summer. The winter increase is larger in the north of the domain, summer decrease in the south. This is consistent with different change sign in annual precipitation (Figure 4-5). It may imply that the dominant change mechanism alters between 50°N and 55°N. Additional seasons and average precipitation amount is shown in Figure A-3 in the Appendix.
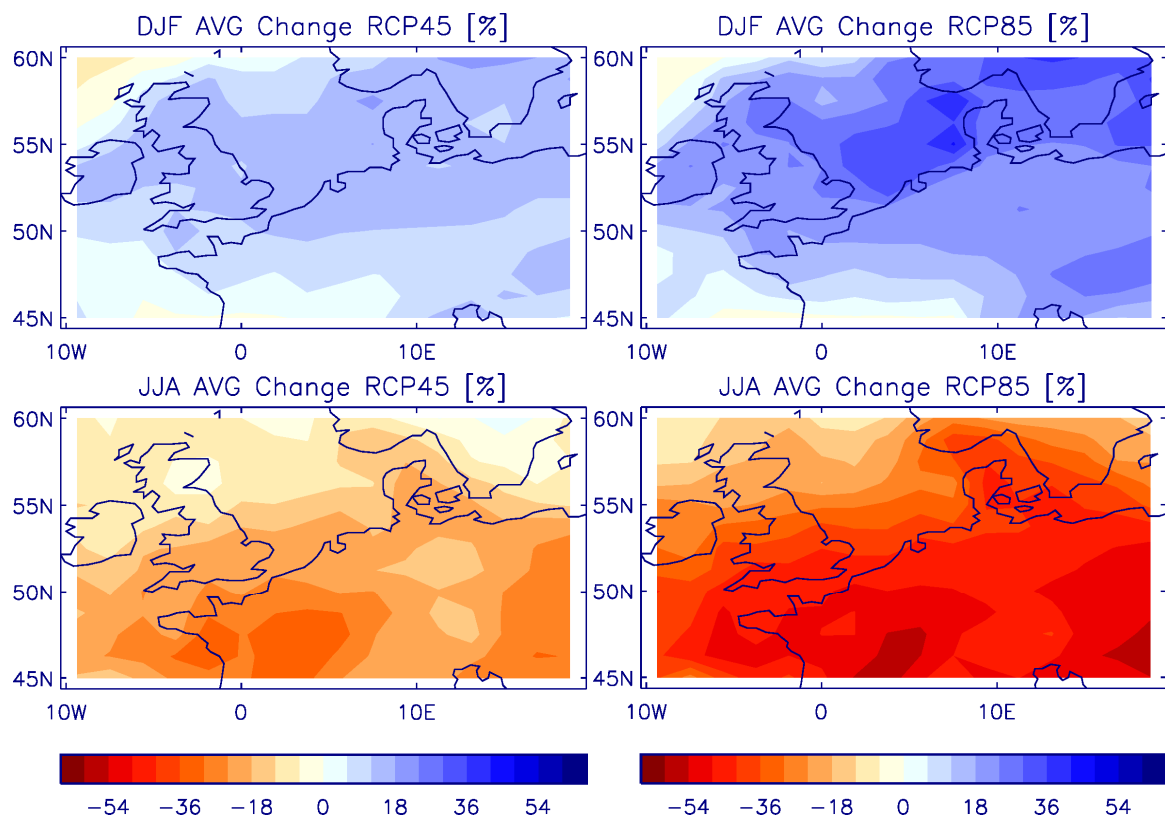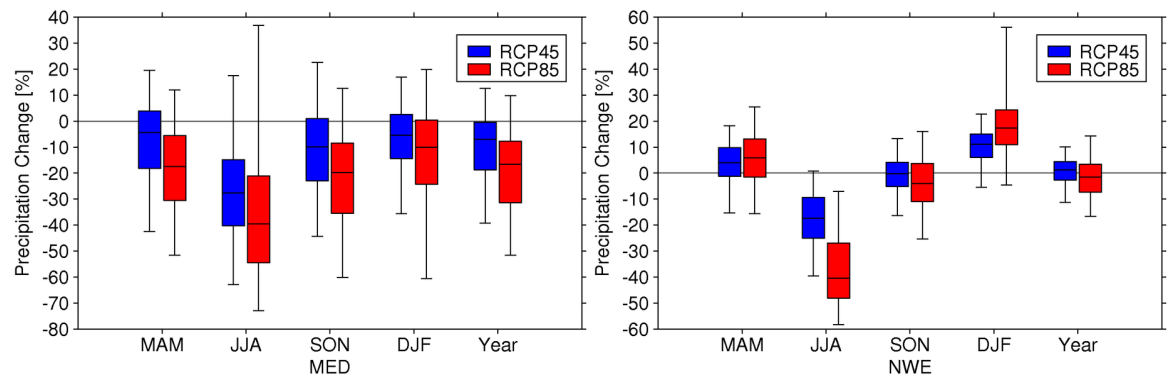

Figure 4-4 Seasonal average precipitation changes in NWE Percentage change for period 2070-2099 of average seasonal precipitation in HadGEM2-ES depicted for RCP45 (left column) and RCP85 (right column). The DJF (top) and JJA (bottom) changes are shown. Changes are significant on 5 % level.

The annual average is split into a weak increase in the northern part and a weak decrease in the southern part for RCP85. A change in annual average precipitation is thereby not significant on the 5 % level for RCP45.
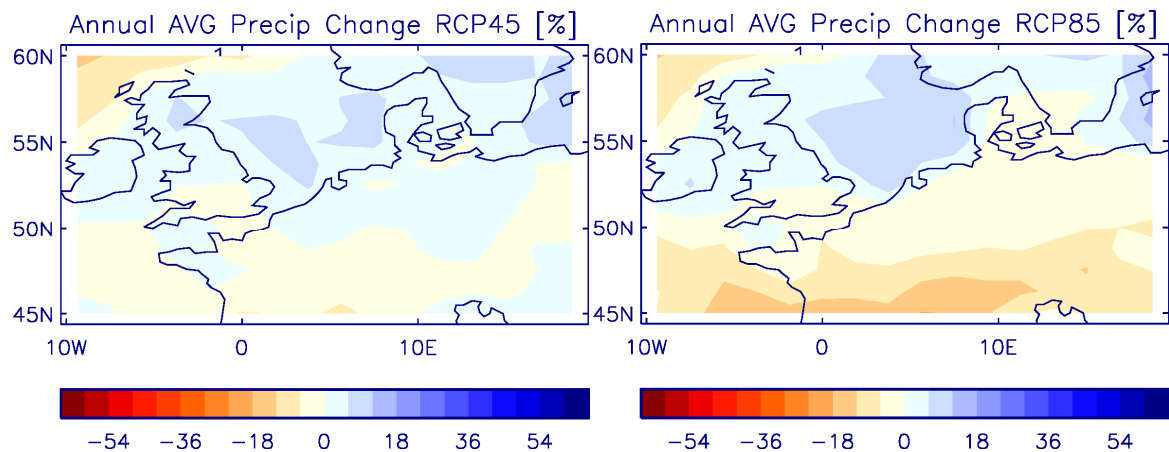
Figure 4-5 Annual average precipitation changes in NWE Percentage change for period 2070-2099 of annual average precipitation in HadGEM2-ES are depicted for RCP45 (left column) and RCP85 (right column). Changes are significant on 5 % level, except annual RCP45.

4.1.4   Regional differences

Figure 4-6 Boxplots of average precipitation changes Percentage change signals of average precipitation amount in MED (left) and NWE (right). RCP45 in blue, RCP85 in red, values for seasonal and annual changes. Boxes are 25 %, median and 75 % quantiles of change signal in the domain, whiskers are the 2.5 % and 97.5 % quantiles.

The Boxplots in Figure 4-6 outline the percentage changes within the domains. The two domains show a different pattern in change signals. The subtropical MED domain decreases consistently during all seasons, while NWE shows low changes in annual, spring (MAM) and autumn (SON) precipitation. Furthermore, precipitation in NWE

increases during winter, in contrast to MED. The signals in MED are more heterogeneous, with inter-quartile range exceeding 20 %. This coincides with the larger area of MED and more variety in the climate classifications. In general, the signal spread rises for the higher emission scenario RCP85.

The results agree with previous studies as described in Chapter 2.3.2: a general precipitation reduction in subtropical MED domain, and summer decrease and winter increase in NWE. The reduction of the subtropical divergent region is consistent with theoretical considerations described in Chapter 2.2.4. As well is the seasonal pattern of wetter winter and drier summer seasons (cf. 2.2.6).

4.1.5   Comparison with IPCC AR4 projections

In Figure 4-7, average precipitation amount from HadGEM2-ES is compared with an average of 21 models from IPCC AR4. The emission scenarios and reference periods are slightly different, although this should not affect the comparison. The spatial pattern in IPCC AR4 is more homogeneous. HadGEM2 depicts a more pronounced land-sea difference over the Mediterranean Sea. This may be due to the averaging of several model results in IPCC AR4. HadGEM2-ES shows a stronger signal in summer precipitation decrease, as well in northern winter increase.
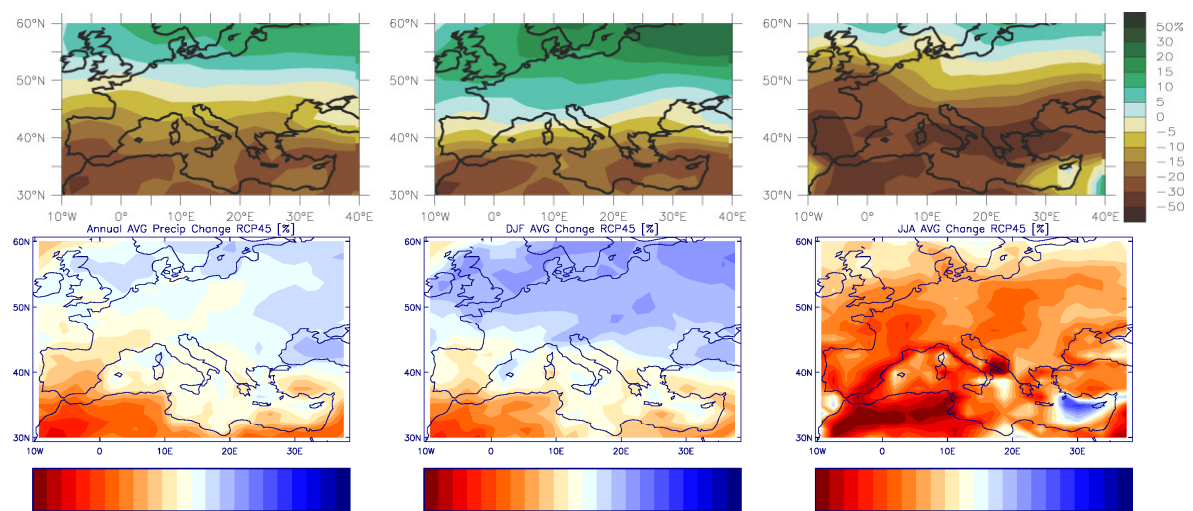

Figure 4-7 Comparison HadGEM2-ES with projections from IPCC AR4 Percentage precipitation change compared from IPCC AR4 (top) and HadGEM2-ES RCP45 (bottom). AR4 figure is edited from *Christensen et al.* (2007) and based on a 21 model average of the emission scenario A1B for the reference periods 1980-1999 and 2080-2099. Annual (left), DJF (middle) and JJA (right) precipitation change.

The balance line between areas with projected increase and areas of projected decrease for the annual average is approximately on 50°N in both projections. In contrast to the IPCC AR4 projections, the balance line describes an edge in HadGEM2-ES on 20°E, heading south to 40°N. In DJF, the balance line is at 45°N for both models. In JJA, the balance line at 60°N is moved 5° polewards in HadGEM2-ES compared to the model average in IPCC AR4.

4.2 Precipitation frequency and intensity

### 4.2.1 Comparison with observations
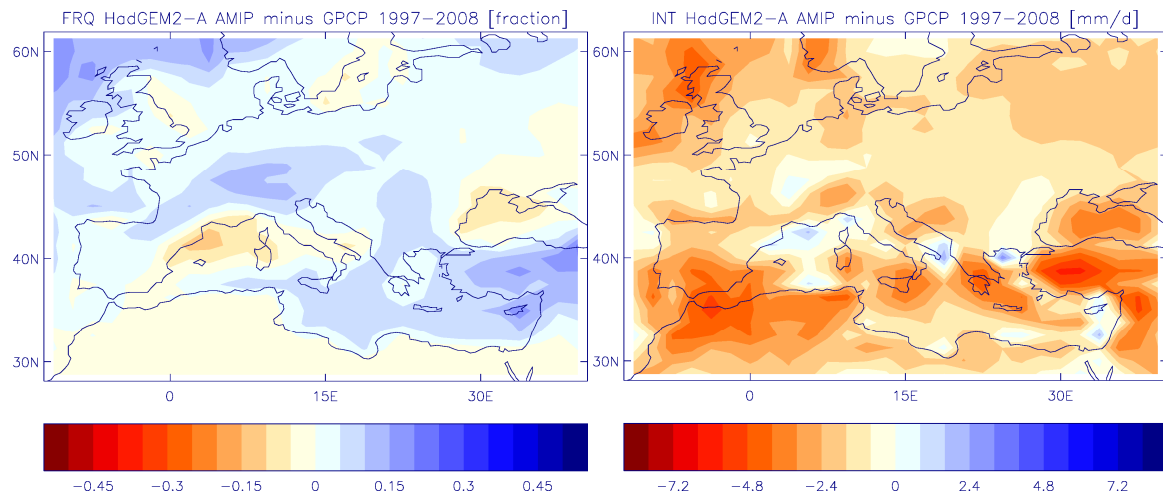
Figure 4-8 Deviation of average FRQ and INT between GPCP and HadGEM2-A Differences of annual averages. Absolute deviations calculated as HadGEM2-A AMIP experiment minus GPCP daily observation values for the period 1997-2008. Frequency deviation is shown in fraction (left), intensity in mm/d (right).

The observed and modelled frequencies and intensities deviate. HadGEM2-A overestimates precipitation frequency, but underestimates the intensity. The deviation signal is homogeneously positive (FRQ) or negative (INT) for large areas in both domains, but with differing amplitudes. The frequency overestimation is consistent with previous studies for light precipitation, the intensity underestimation is in agreement with studies for heavy precipitation (*Dai*, 2006; *Sun et al.*, 2006). However, this study does not analyse frequency and intensity separated by the strength of the precipitation amount. Seasonal deviation is shown in Figure A-4 in the Appendix.

4.2.2   Mediterranean region

Figure 4-9 shows the projected change in FRQ and INT for the JJA period. Precipitation frequency is projected to decrease in MED during summer. Thereby, the amplitude exceeds the reduction of average precipitation amount as shown in Figure 4-3. Individual grid points, notably in the Gulf of Genoa and over Cypress, show a strong relative increase in frequency and intensity, consistent in all four ensemble members. Although, absolute frequency of precipitation is low in MED during summer (cf. Figure A-5 in the Appendix). The change in intensity is varying over the domain. The median of the domain is thereby decreasing, as later shown in Figure 4-13. Present intensities of precipitation and changes in other seasons are presented Figure A-6 in the Appendix.
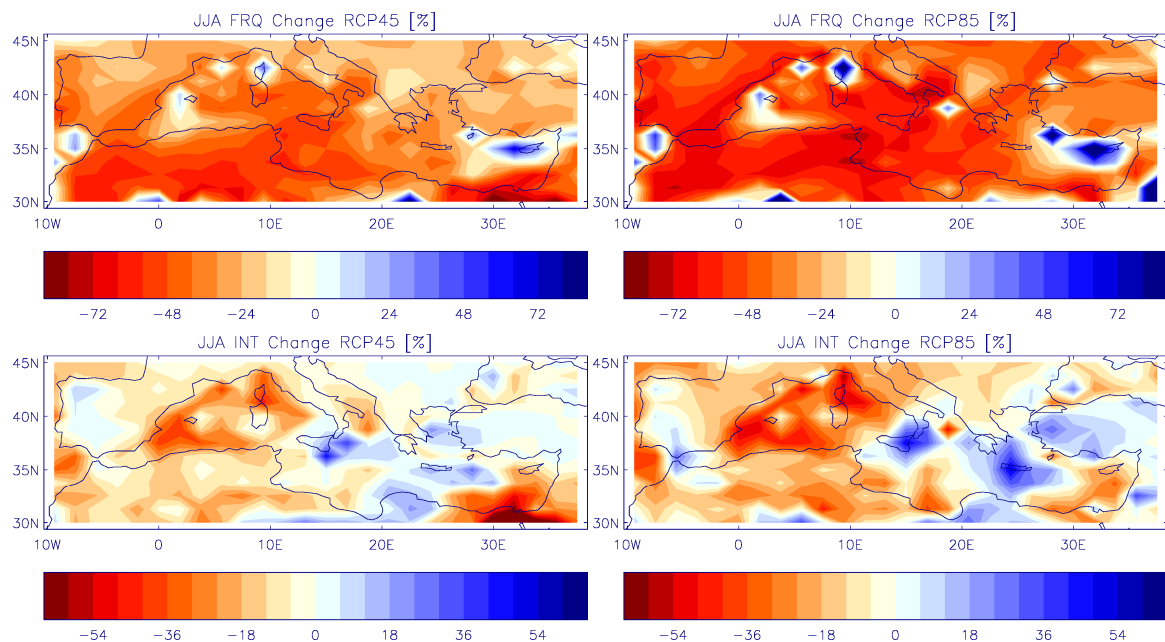
Figure 4-9 Average FRQ & INT changes in MED during summer Percentage change of precipitation frequency and intensity during summer simulated in HadGEM2-ES for RCP45 (left column) and RCP85 (right column) for period 2070-2099. Changes of FRQ (top) and INT (bottom) are shown. Changes are significant on 5 % level for all analysis.
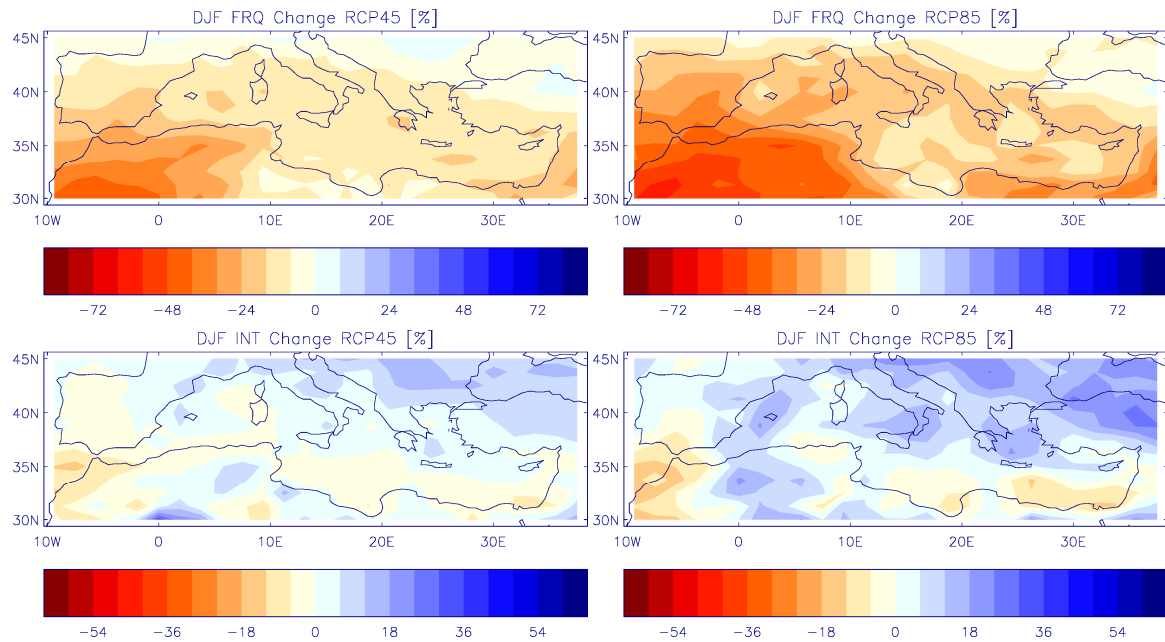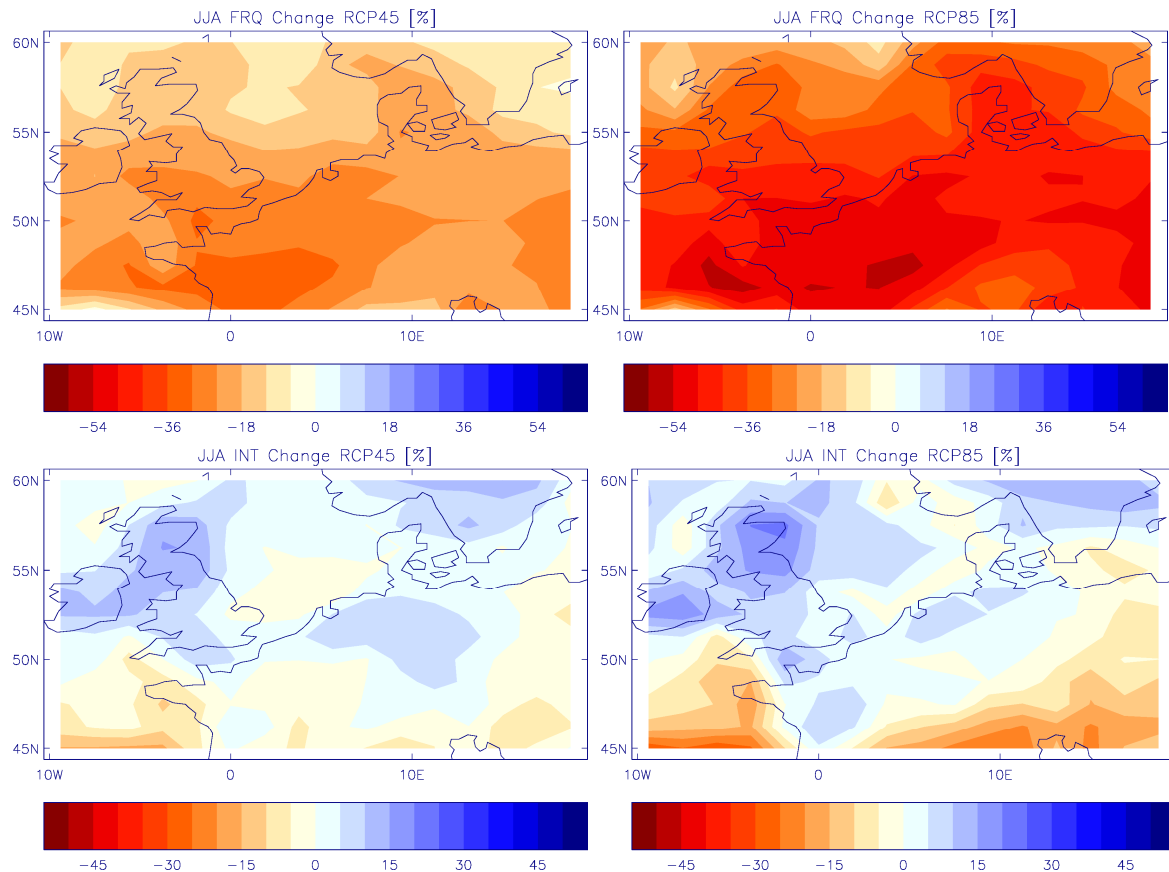
Figure 4-10 Average FRQ & INT changes in MED during winter Percentage change of precipitation frequency and intensity during winter simulated in HadGEM2-ES for RCP45 (left column) and RCP85 (right column) for period 2070-2099. Changes of FRQ (top) and INT (bottom) are shown. Changes are significant on 5 % level, except INT in RCP45 DJF.

Figure 4-10 shows the projected change for winter. Precipitation frequency decreases for both emission scenarios. Hence, both summer and winter precipitation frequency are diminished, but on a lower scale during winter. On the other hand, the intensity of precipitation events is projected to rise. The signal of intensity change is not significant for the RCP45 scenario.

In summary, the MED region is expecting a decrease in total amount for the whole year. This is accompanied by a decrease in frequency, whereas the intensity increases. The frequency decrease is more pronounced in summer in terms of relative change. In absolute numbers, the decrease of annual average FRQ and INT is similar to the decrease during winter (cf. Figure A-5 & Figure A-6).
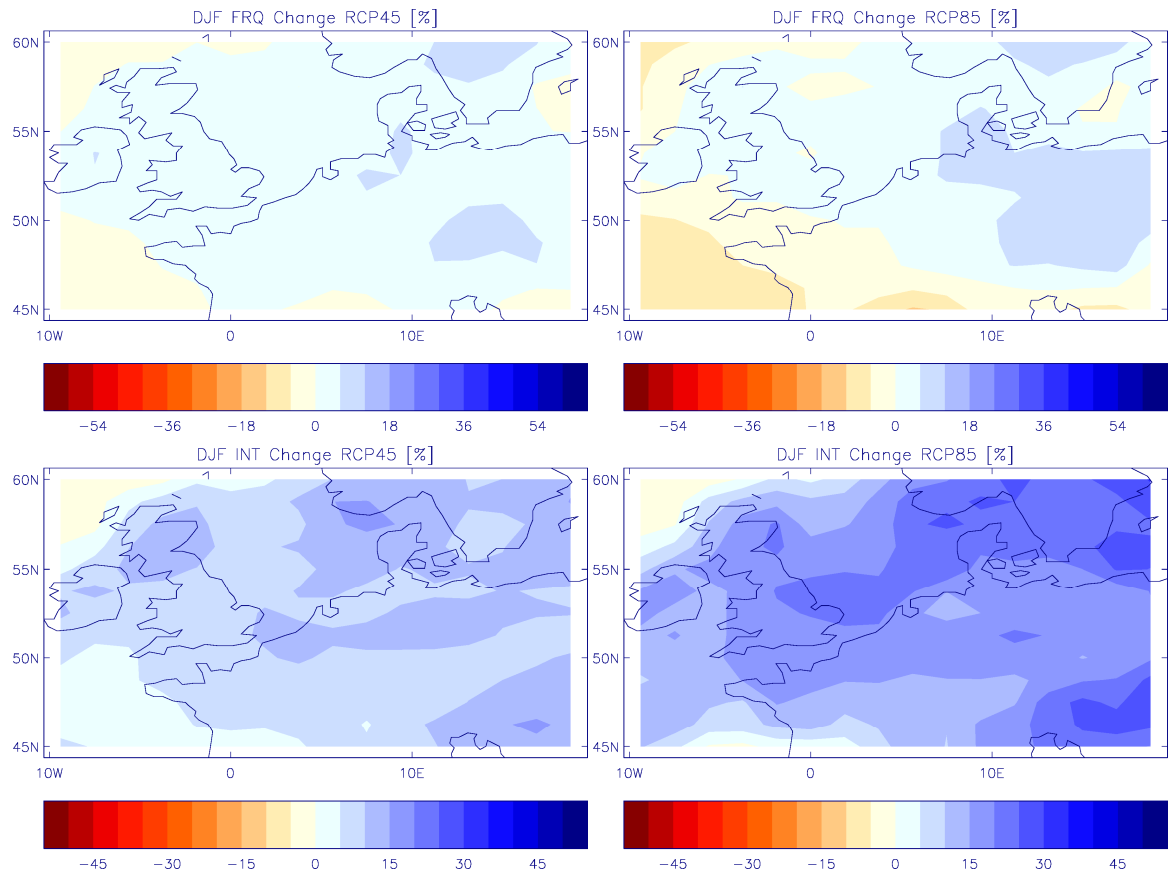
4.2.3   North-western Europe

Figure 4-11 Average FRQ & INT changes in NWE during summer Percentage change of precipitation frequency and intensity in summer simulated in HadGEM2-ES for RCP45 (left column) and RCP85 (right column) for period 2070-2099. Changes of FRQ (top) and INT (bottom) are shown. Changes are significant on 5 % level.

During summer, the precipitation frequency decreases strongly in NWE (Figure 4-11). The median is simulated to drop about 40 % for the higher RCP85 scenario. For RCP45 the decrease is half as large, distinctively lower.

In contrast, the intensity is simulated to increase. The amplitude of the intensity increase is smaller than the decrease in frequency, which is consistent with the overall decrease of the precipitation amount for this season.

Figure 4-12 Average FRQ & INT changes in NWE during winter Percentage change in winter simulated in HadGEM2-ES for RCP45 (left column) and RCP85 (right column) for period 2070-2099. Changes of FRQ (top) and INT (bottom) are shown. Changes are significant on 5 % level except DJF FRQ RCP85.

In projections of the winter season (Figure 4-12), precipitation frequency shows a weak and ambiguous change signal. The frequency increases slightly in the medium scenario RCP45. In RCP85 scenario, partial increase and partial decrease is simulated, and no statistical significance was achieved.

Precipitation intensity rises considerably during winter period, approximately 10 % for RCP45 and 20 % for the RCP85 scenario. Further seasonal analysis and present simulation are shown in Figure A-7 & Figure A-8 in the Appendix.

4.2.4   Regional differences
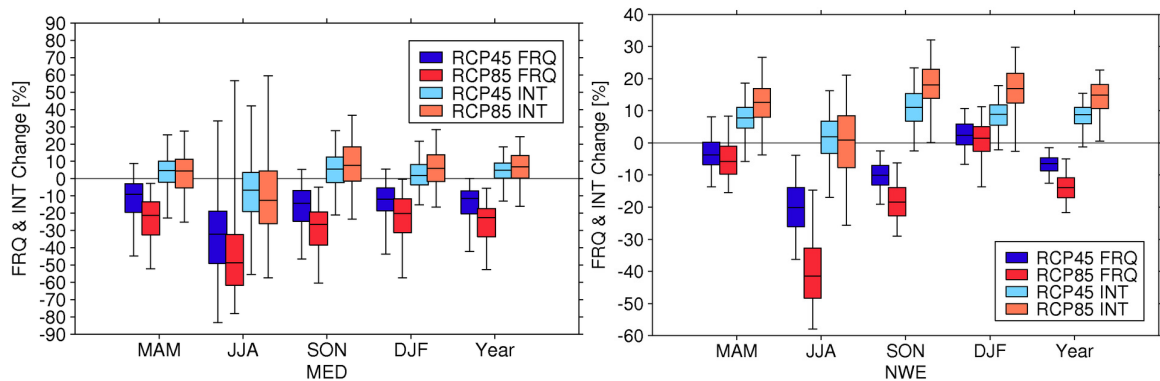
Figure 4-13 Boxplots of frequency and intensity changes Percentage change signals of precipitation intensity and frequency in MED (left) and NWE (right). RCP45 in blue, RCP85 in red, values for all seasonal and for the annual changes. Boxes are 25 %, median and 75 % quantiles of change signal in the domain, whiskers are the 2.5 % and 97.5 % quantiles. Note the different scales.

Frequency and intensity changes of the two domains are compared in Figure 4-13. Both regions simulate in general an increase in intensity and decrease in frequency. This agrees with theoretical concepts discussed in Chapter 2.2.4. Change signals are broader spread for MED than for NWE, equal to the pattern of average precipitation changes. Frequency is decreasing consistently and strongly for all seasons in MED, whereas the winter season in NWE shows a small increase (RCP45) or no change (RCP85). In contrast, intensity increase is slightly higher and more homogeneous in NWE compared to MED.
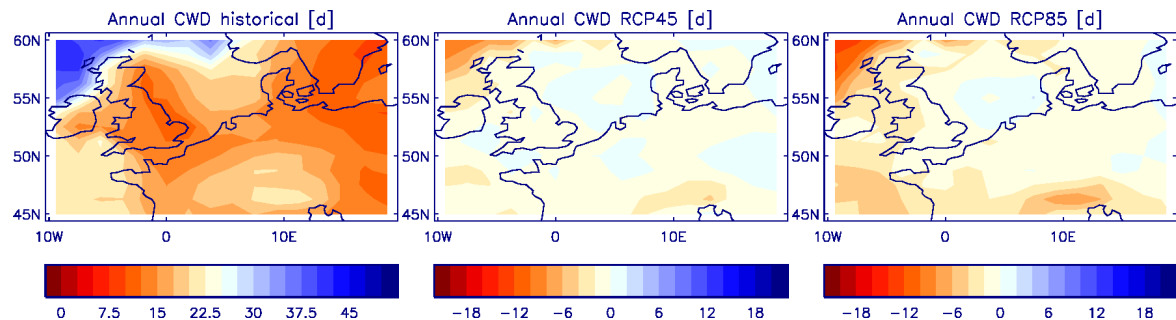
4.3   Precipitation duration

4.3.1   Mediterranean region
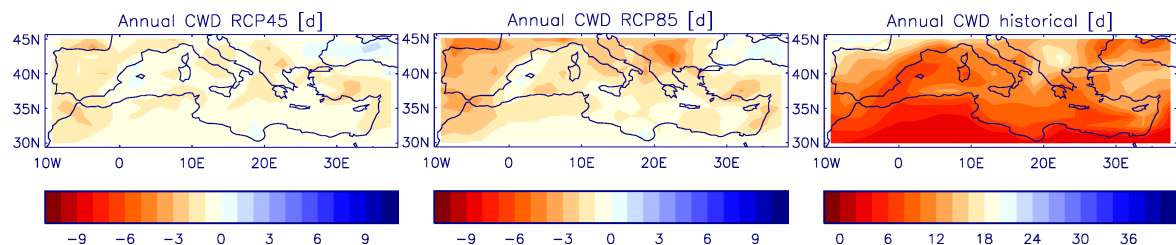
Figure 4-14 Present value and change in consecutive wet days for MED The left column shows HadGEM2-ES present climate (1976-2005) of annual average consecutive wet days CWD. On middle and right column, changes (in days) of RCP45 (middle) and RCP85 (right) for period 2070-2099 are shown.

Values of average consecutive wet days (Figure 4-14) in MED range from approximately 5 to 20 days. The longest durations are situated at the Pyrenees and Macedonia. In the two considered scenarios, a decrease of the CWD is projected. Already dry areas with short maximal precipitation duration remain less affected. The reduction is approximately a third in consecutive wet days for areas with longer precipitation duration in present climate. Notable is an increase of the indices over the Black Sea. The reduction is consistent with an overall drier precipitation regime as previously discussed.

4.3.2 North-western Europe

Figure 4-15 Present value and change in consecutive wet days for NWE The left column shows HadGEM2-ES present climate (1976-2005) of annual average consecutive wet days CWD. On middle and right column, changes (in days) for period 2070-2099 for RCP45 (middle) and RCP85 (right) scenarios are shown.

Consecutive wet days for NEW are highest in north-west of the British Isles (Figure 4-15). Values reach 45 days of consecutive rain. Other areas with higher values are over the sea and the Alps. For future projections, a reduction or increase of CWD is not consistent in the domain and the spatial pattern of change is varying.

4.4   Heavy precipitation extremes

For heavy precipitation extremes, results are presented for the higher RCP85 scenario. The signal pattern for the lower RCP45 scenario is similar, and the complete set of figures for RX1 and RX5 is presented in the Appendix.

4.4.1   Comparison with observations

The discrepancy between observed and modelled precipitation extremes is shown in Figure 4-16. The bias exceeds 100 % of the modelled extremes values in some areas (cf. Figure A-10 & Figure A-14). HadGEM2-A overestimates the one-day precipitation maximum in Central Europe and in the northern Mediterranean basin. An underestimation is diagnosed in Northern Africa, Turkey and the British Isles, most pronounced during winter. The remaining seasons are provided in Figure A-9 in the Appendix.
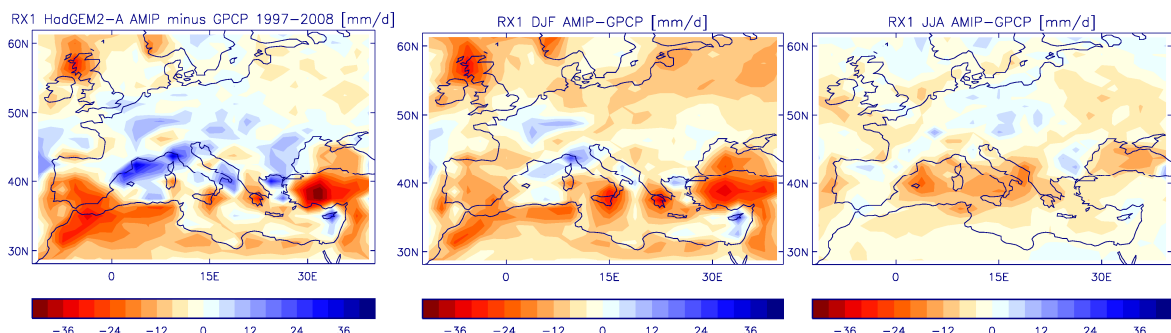

Figure 4-16 Deviation of RX1 between GPCP and HadGEM2-A Differences of averages are depicted for annual (left), winter (middle) and summer (right) one-day precipitation extremes in mm/d. Absolute deviations calculated as HadGEM2-A AMIP experiment minus GPCP daily observation values for the period 1997-2008. In GPCP, only the first 360 days are used to ensure comparability with model data.

4.4.2   Mediterranean region

In Figure 4-17, the average one-day (RX1) and five-day (RX5) precipitation change for the scenario RCP85 is presented. The spatial pattern is similar for both indices. The intense precipitation events increase during winter, but decrease in summer. However, northern Africa and southern Spain do not show a rise in winter heavy precipitation. During summer, heavy precipitation decreases around 50 %. In Turkey and Cypress, an opposite

signal of an increase in precipitation is visible. Further seasons are shown in Figure A-10 & Figure A-11 in the Appendix.
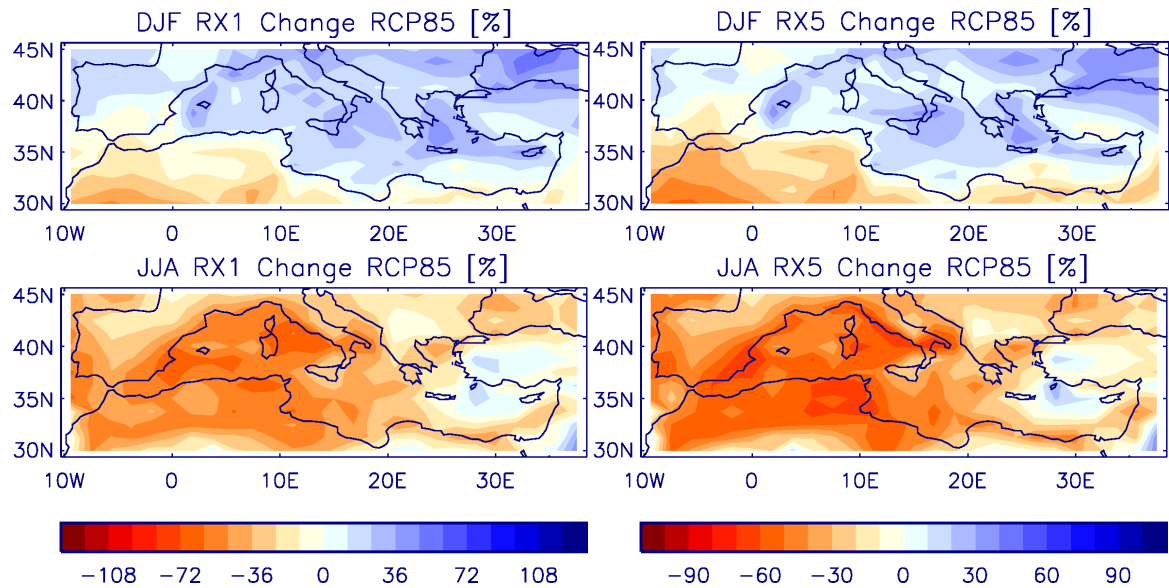
Figure 4-17 Average heavy precipitation change in MED Percentage changes for average heavy precipitation during one day (RX1, left) and five days (RX5, right) during winter (top) and summer (bottom) in RCP85 for period 2070-2099. Note the different scale. Changes are significant on 5 % level.
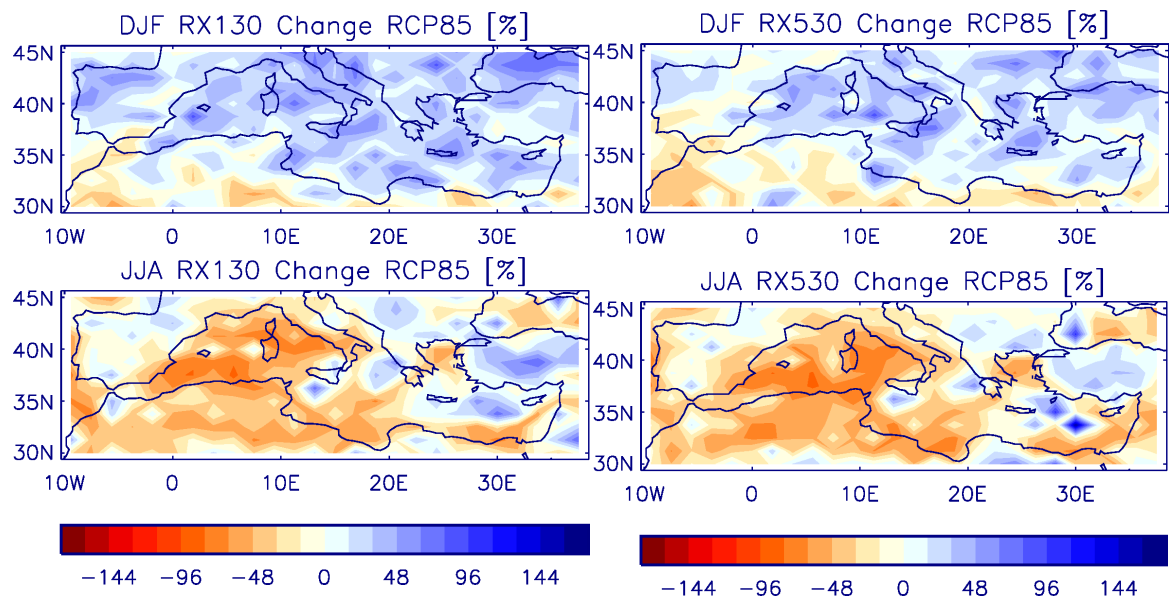
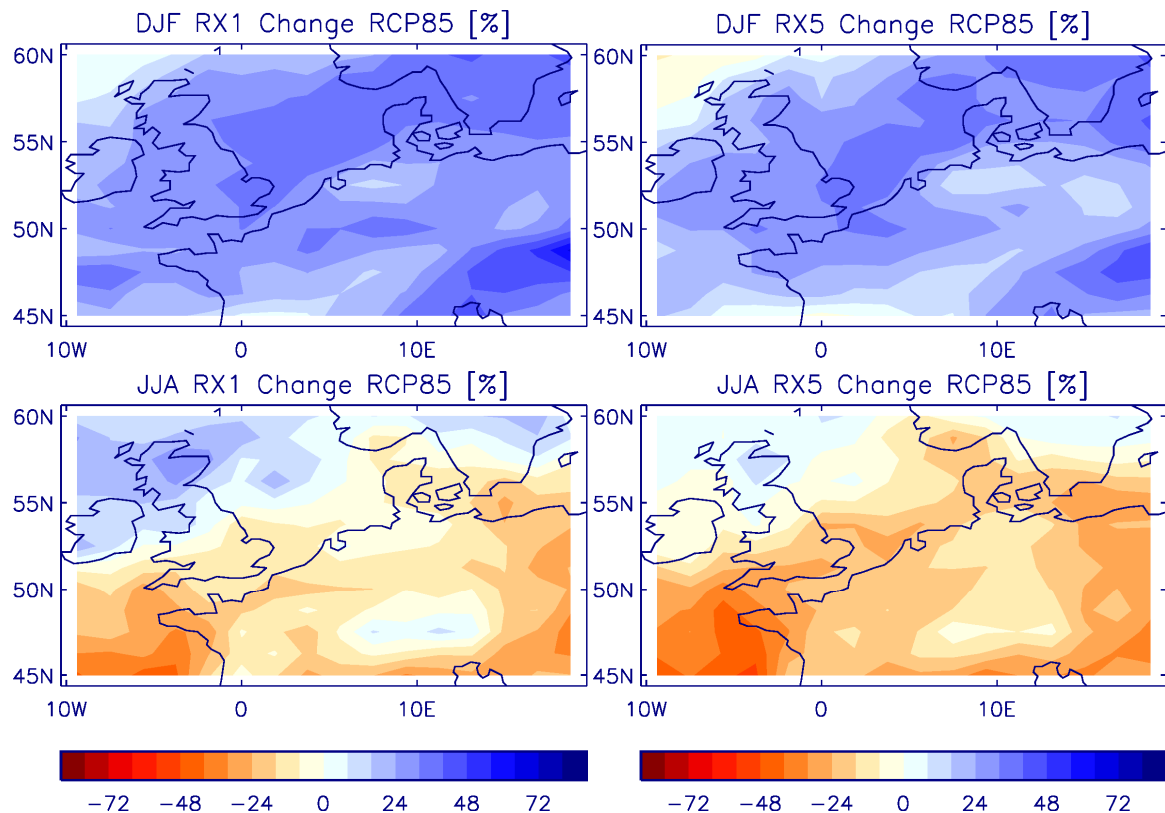**Figure 4-18 Maximum heavy precipitation change in MED** Percentage changes for 30 years maximum of heavy precipitation during one day (RX1-30, left) and five days (RX5-30, right) during winter (top) and summer (bottom) in RCP85 for period 2070-2099.

The changes for the 30 years extremes in one- and five-day precipitation (RX 1-30) are presented in Figure 4-18. The positive signal during winter is comparable for the average extremes in Figure 4-17. For summer extremes, the decrease is more heterogeneous compared to the average maximum precipitation. Considerable parts show an increase for those extreme precipitation events. Further seasons are shown in Figure A-12 & Figure A-13 in the Appendix.

4.4.3 North-western Europe

Figure 4-19 Average heavy precipitation change in NWE Percentage changes for average heavy precipitation during one day (RX1, left) and five days (RX5, right) during winter (top) and summer (bottom) in RCP85 for period 2070-2099.

Figure 4-19 shows the changes for heavy one- and five-day precipitation (RX1 & RX5) in NWE. A consistent increase between 20 and 30 % is simulated during winter. The pattern of change in RX1 and RX5 are in close agreement for both seasons. The summer heavy precipitation is simulated to increase over the British Isles, whereas the major part of

continental Europe shows a decrease. The reduction over the Alps (minus 10 %) is less pronounced than in the south western area (up to minus 50 %).

Further seasonal changes, as well as the RCP45 scenario are given in Figure A-14 & Figure A-15 in the Appendix.
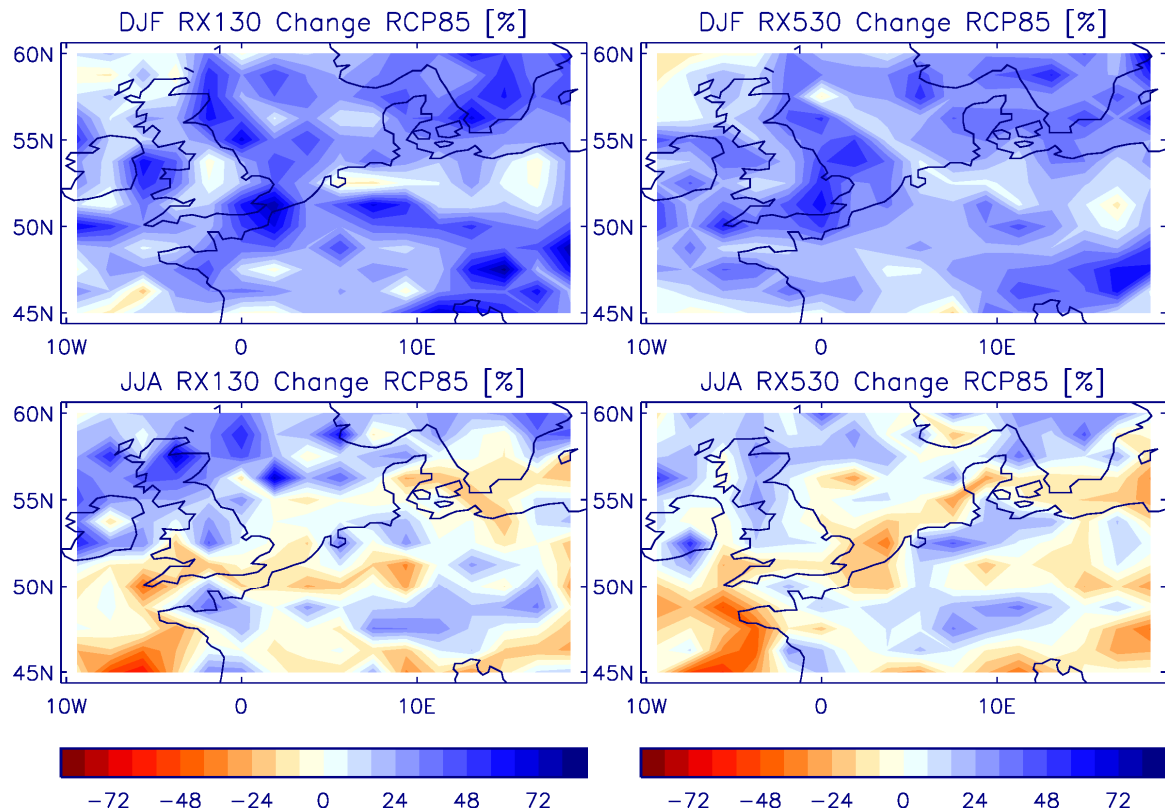

Figure 4-20 Maximum heavy precipitation change in NWE Percentage changes for 30 years maximum of heavy precipitation during one day (RX1-30, left) and five days (RX5-30, right) during winter (top) and summer (bottom) in RCP85 for period 2070-2099.

The change in the more extreme precipitation is more heterogeneous, as it is calculated from one ensemble each. Change signals for the summer season agree reasonably in spatial distribution with change in average maximum precipitation. As well do the changes in winter heavy precipitation. The percentage change is 20-40 %, also comparable to changes in RX1 and RX5. Further seasons are shown in Figure A-16 & Figure A-17 in the Appendix.

4.4.4   Regional differences
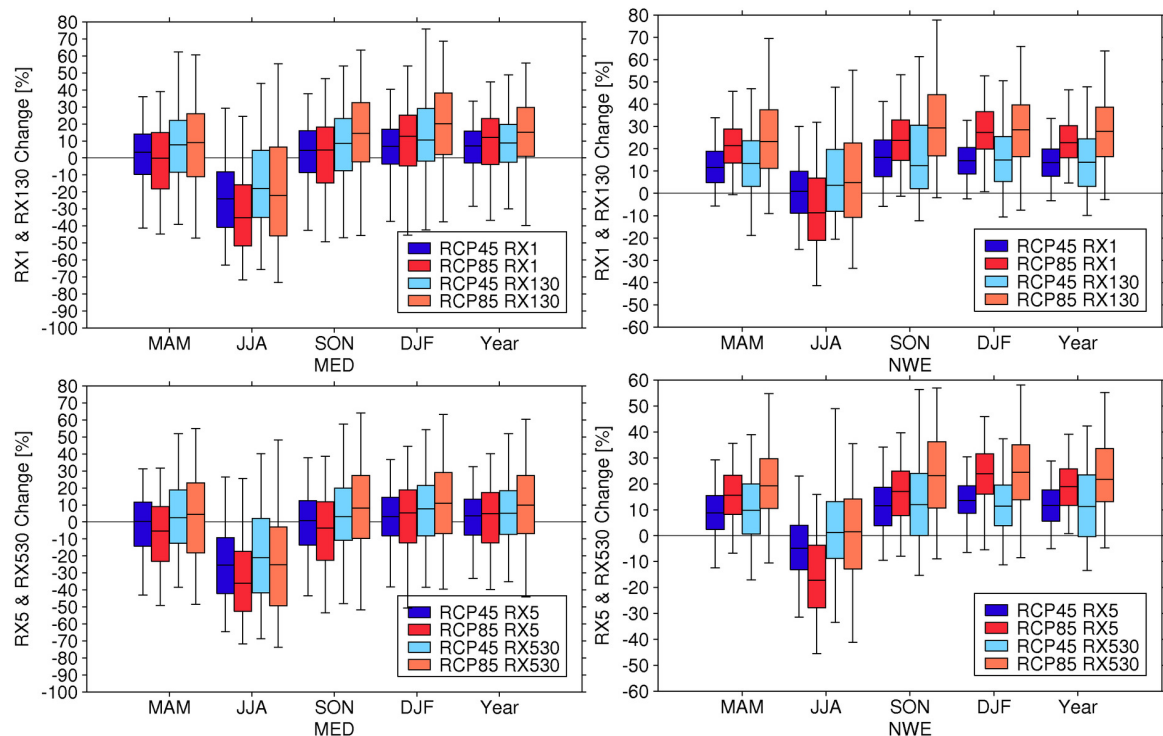
Figure 4-21 Boxplot of heavy precipitation changes Percentage precipitation changes of maximum one day (top) and 5 days (bottom) precipitation events for MED (left) and NWE (right). The average maximum and the 30 years maximum change is shown in each plot. Boxes are 25 %, median and 75 % quantiles of change signal in the domain, whiskers are the 2.5 % and 97.5 % quantiles. Note the different scales.

A comparison of the annual and seasonal change signals can be seen in Figure 4-21. The spread of the signal is larger for the MED than the NWE domain, as well for 30 years than for average maximum precipitation. RX1 and RX5 change in the same strength within each domain. The seasonal pattern of the projected changes agrees in both study domains, with JJA differing from the other season and the annual signals. In MED this signifies a strong decrease during summer and a weak increase during the remaining seasons. In NWE, RX1 & RX5 show a weak decrease during summer and a strong increase during the rest of the year. In contrast to RX1 & RX5, summer RX1-30 and RX5-30 do not show a decrease in NWE. This is consistent in MED, where 30 years extreme do not decrease as strongly either. In the other seasons, the 30 years extreme increase even stronger than the annual averages. Hence, heavy precipitation events do not increase in all seasons in HadGEM2-ES simulations, as it may be suggested in theory by

the higher moisture content (cf. Chapter 2.2.4). Other projections agree on a stronger increase in winter (cf. Chapter 2.3.2). However, more extreme events (RX1-30 & RX5-30) could develop differently.
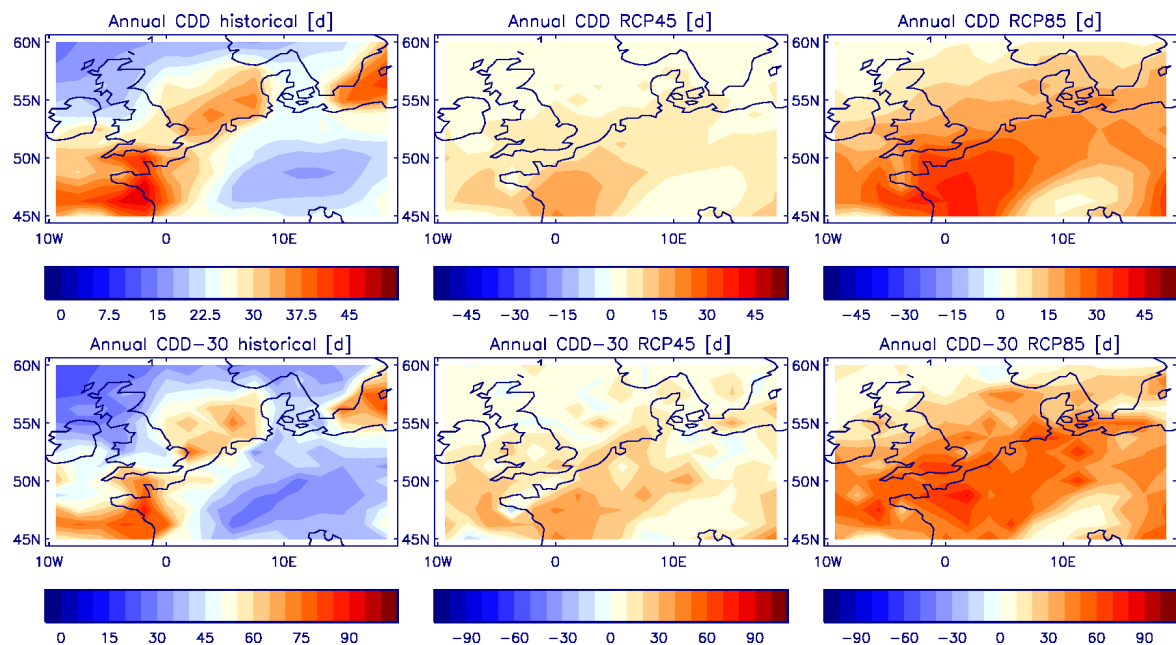
4.5 Droughts

4.5.1 Mediterranean region
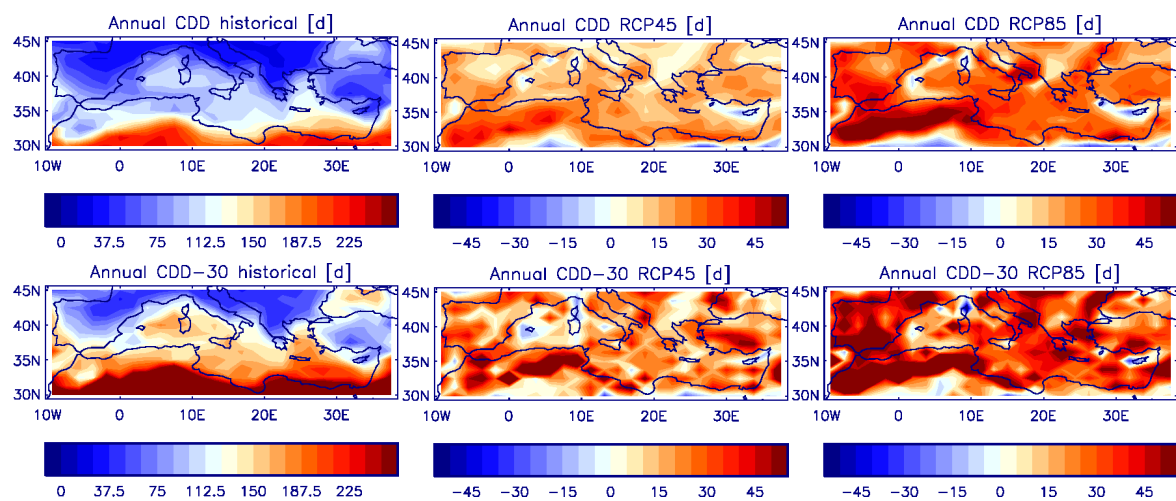
Figure 4-22 Present value and change in consecutive dry days for MED The left column shows HadGEM2-ES present climate (1976-2005) of annual average consecutive dry days CDD (top) and 30 years maximum CDD-30 (bottom). On middle and right column, changes (in days) for CDD and CDD-30 for RCP45 (middle) and RCP85 (right) for period 2070-2099 are shown.

Figure 4-22 presents the consecutive dry days, simulated for the present climate and the projected changes for the RCP45 and RCP85 scenario. In the present climate, three areas can be separated: in the north over land surfaces, an average of 30-40 consecutive dry days is simulated. Over the Mediterranean Sea and the Atlas ridge, the average is approximately 120 consecutive dry days. Thirdly in the arid regions in the south, values higher than 240 dry days are achieved. The first and the second region are thereby projected to have a pronounced increase in consecutive dry days. The Atlas Mountains and the south of Spain show a rise of over 50 days compared to present dry days. In the northern area, the number of consecutive dry days is almost doubled. The already dry south does not show a strong sign of increase. Isolated signs of decrease are simulated for Cypress and the Gulf of Genoa.

4.5.2   North-western Europe

The simulated present consecutive dry days show an inhomogeneous spatial distribution. Patches of longer periods are located over the oceanic areas, whereas over northern British Isles and the Alps short periods of 15-20 dry days simulated. These areas remain unchanged in future projections. Hence, a rise in droughts cannot be diagnosed for them. Whereas the already dry areas have an increase of up to 40 days in average maximum consecutive dry days. This pattern of different change is also visible in CDD-30 projections.

Figure 4-23 Present value and change in consecutive dry days for NWE The left column shows HadGEM2-ES present climate (1976-2005) of annual average consecutive dry days CDD (top) and 30 years maximum CDD-30 (bottom). On middle and right column, changes (in days) for CDD and CDD-30 for RCP45 (middle) and RCP85 (right) for period 2070-2099 are shown. Note the different scale.

5 Discussion & Conclusions

5.1 Precipitation characteristics

Amount, frequency, intensity and duration of precipitation have been analysed for the Mediterranean area (MED) and north-western Europe (NWE) in HadGEM2-ES.

The subtropical MED domain shows a distinct decrease in rain amount, frequency and duration over all seasons. The highest reduction is projected for the summer season. However, the indices of the remaining seasons decrease less, and so does the annual average. Nevertheless their reduction of 10 to 20 % is still considerable. In contrast, the intensity does not decline. The precipitation intensity on wet days increases approximately about 10 % on average, with the exception of a reduction in summer. Precipitation duration is simulated to decrease in this region.

In NWE, the precipitation amount increases during winter, decreases in summer and remain constant on annual average. The intensity increase ranges from 10-20 % on average, while the frequency declines in the same order of magnitude. This is accompanied with a more pronounced increase in precipitation intensity during winter and frequency decrease during summer. The signal of changes in consecutive precipitation duration is ambiguous.

The projections for the domains are similar in their seasonal pattern, as well are the differing developments of the precipitation characteristics: declining or steady frequency, steady or rising intensity. However, the Mediterranean will be more affected by an overall reduction in rainfall.

HadGEM2-ES underestimates the precipitation amount, especially in NWE. Although the frequency is overestimated, the precipitation intensity is diagnosed to be too low.

5.2 Extreme events

Heavy precipitation extremes, more precisely maximum one- and five-day precipitation amounts have been studied. Furthermore, changes in consecutive dry days have been analysed. The extremes have been evaluated subdivided into average annual extremes and 30 years maxima, besides the one- and five-day maxima. RX1 and RX5 do not show distinguished differences in spatial patterns and seasonal cycle. The seasons show the highest influence on the change signal.

Heavy precipitation is projected to increase predominantly during winter, for both MED and NWE. Summer heavy precipitation events are simulated to decrease in the domains. The consecutive dry days are not seasonally analysed. On annual average, both regions show rise in the numbers of dry days, except of northern NWE and arid southern MED.

5.3 Discussion

5.3.1 Analysis

The analysis of a single global model for a regional analysis is to be evaluated cautiously. The validity is constrained. Four ensembles are used to reduce uncertainty. Confidence can be gained by the circumstance that the results are consistent with previous models. Further discussion of methods and data can be found in Chapter 3.

The MED domain is more heterogeneous, with higher spreads in signals. The strength of the statistical analysis may be diminished when sub areas of a domain show an increase while other decrease, as the significance is calculated for the whole region. Therefore sub-domains are possible to have a significant change while no significance is shown for the whole domain. As changes are almost always significant, this is only a minor issue.

5.3.2 Results

The results are in good agreement with theoretical understanding and previous analysis of climate model projections. The subtropical MED region is projected to become drier. Precipitation intensity is increasing while frequency decreases. Extreme events are increasing generally. However, heavy rainfalls are diagnosed not to increase in summer season. Furthermore, droughts increase in MED, but not consistently in NWE.

The area near Cypress shows often a strongly opposite sign compared to the other area changes in MED. This is maybe unrealistic, as large differences of the model with observations have been found. However the IPCC AR4 projections show as well differing signs compared to the neighbouring areas. A detailed analysis of evaporation, radiation budget and flow pattern could deliver some insights. Other regions which behave differently in MED are the Black Sea and the Gulf of Genoa, what could be further analysed. In NWE, a discrepancy between northern and southern parts is appearing. Southern parts of NWE show differing changes compared to the northern parts. This may be associated a poleward shift of the storm tracks. Further analysis is suggested.

5.4 Outlook

To improve our knowledge in future climate change, this analysis should be extended to other ensembles of GCMs and RCMs. This allows analysing model agreement, to assess the projection uncertainty. High resolving RCMs are thereby especially valuable for such studies on regional scale. Applying an extreme value technique analysis at HadGEM2 data can improve the understanding of occurrences of future extremes.

Further observational dataset can be applied to account for uncertainty within observational data, in order to evaluate the model performance. A use of high resolution dataset would allow the implementation of a downscaling method, so that projections can be interpreted on local levels.

The analysis of model bias will help to improve model performance and hence confidence in their results. Last but not least, to reduce uncertainty in projections, we need further research in the physical principles how the hydrological cycle is altering.

6 References

Adler, R. F., G. J. Huffman, A. Chang, R. Ferraro, P. P. Xie, J. Janowiak, B. Rudolf, U. Schneider, S. Curtis, D. Bolvin, A. Gruber, J. Susskind, P. Arkin, and E. Nelkin, 2003: The version-2 global precipitation climatology project (GPCP) monthly precipitation analysis (1979-present). *Journal of Hydrometeorology*, **4,** 1147-1167, doi: 10.1175/1525-7541(2003)004<1147:tvgpcp>2.0.co;2.

Allan, R. P., 2006: Variability in clear-sky longwave radiative cooling of the atmosphere. *Journal of Geophysical Research-Atmospheres*, **111**, doi: 10.1029/2006jd007304.

Allan, R. P., 2011: Climate change: Human influence on rainfall. *Nature*, **470,** 344-345, doi: 10.1038/470344a.

Allan, R. P., and B. J. Soden, 2007: Large discrepancy between observed and simulated precipitation trends in the ascending and descending branches of the tropical circulation. *Geophysical Research Letters*, **34**, doi: 10.1029/2007gl031460.

Allan, R. P., and B. J. Soden, 2008: Atmospheric warming and the amplification of precipitation extremes. *Science*, **321,** 1481-1484, doi: 10.1126/science.1160787.

Allan, R. P., B. J. Soden, V. O. John, W. Ingram, and P. Good, 2010: Current changes in tropical precipitation. *Environ. Res. Lett.*, **5**, doi: 10.1088/1748-9326/5/2/025205.

Allen, M. R., and W. J. Ingram, 2002: Constraints on future changes in climate and the hydrologic cycle. *Nature*, **419,** 224-232, doi: 10.1038/nature01092.

Anderson, B. T., C. Reifen, and R. Toumi, 2009: Consistency in Global Climate Change Model Predictions of Regional Precipitation Trends. *Earth Interactions*, **13**, doi: 10.1175/2009ei273.1.

Andrews, T., P. M. Forster, and J. M. Gregory, 2009: A Surface Energy Perspective on Climate Change. *Journal of Climate*, **22,** 2557-2570, doi: 10.1175/2008jcli2759.1.

Andrews, T., P. M. Forster, O. Boucher, N. Bellouin, and A. Jones, 2010: Precipitation, radiative forcing and global temperature change. *Geophysical Research Letters*, **37**, doi: 10.1029/2010gl043991.

Bichet, A., M. Wild, D. Folini, and C. Schär, 2011: Global precipitation response to changing forcings since 1870. *Atmospheric Chemistry and Physics*, **11,** 9961-9970, doi: 10.5194/acp-11-9961-2011.

Boer, G. J., 1993: Climate change and the regulation of the surface moisture and energy budgets. *Climate Dynamics*, **8,** 225-239.

Bony, S., R. Colman, V. M. Kattsov, R. P. Allan, C. S. Bretherton, J.-L. Dufresne, A. Hall, S. Hallegatte, M. M. Holland, W. Ingram, D. A. Randall, B. J. Soden, G. Tselioudis, and M. J. Webb, 2006: How Well Do We Understand and Evaluate Climate

Change Feedback Processes? *Journal of Climate*, **19,** 3445-3482, doi: 10.1175/jcli3819.1.

CH2011, 2011: *Swiss Climate Change Scenarios CH2011.* C2SM, MeteoSwiss, ETH, NCCR Climate, OoCC, Zurich, Switzerland, 88 pp, ISBN: 978-3-033-03065-7.

Chahine, M. T., 1992: The hydrological cycle and its influence on climate. *Nature*, **359,** 373-380, doi: 10.1038/359373a0.

Changnon, S. A., R. A. Pielke, D. Changnon, R. T. Sylves, and R. Pulwarty, 2000: Human Factors Explain the Increased Losses from Weather and Climate Extremes. *Bulletin of the American Meteorological Society*, **81,** 437-442, doi: 10.1175/1520-0477(2000)081<0437:hfetil>2.3.co;2.

Christensen, J. H., and O. B. Christensen, 2007: A summary of the PRUDENCE model projections of changes in European climate by the end of this century. *Clim. Change*, **81,** 7-30, doi: 10.1007/s10584-006-9210-7.

Christensen, J. H., B. Hewitson, A. Busuioc, A. Chen, X. Gao, I. Held, R. Jones, R. K. Kolli, W.-T. Kwon, R. Laprise, V. Magaña Rueda, L. Mearns, C. G. Menéndez, J. Räisänen, A. Rinke, A. Sarr, and P. Whetton, 2007: Regional Climate Projections. In: *Climate Change 2007: The Physical Science Basis. Contribution of Working Group I to the Fourth Assessment Report of the Intergovernmental Panel on Climate Change*, [S. Solomon, D. Qin, M. Manning, M. Marquis, K. Averyt, M. M. B. Tignor, H. L. Miller, and Z. L. Chen (Eds.)], Cambridge University Press, Cambridge, United Kingdom and New York, NY, USA, 847-940, ISBN: 978-0-521-70596-7.

Collins, W. J., N. Bellouin, M. Doutriaux-Boucher, N. Gedney, P. Halloran, T. Hinton, J. Hughes, C. D. Jones, M. Joshi, S. Liddicoat, G. Martin, F. O'Connor, J. Rae, C. Senior, S. Sitch, I. Totterdell, A. Wiltshire, and S. Woodward, 2011: Development and evaluation of an Earth-System model-HadGEM2. *Geosci. Model Dev.*, **4,** 1051-1075, doi: 10.5194/gmd-4-1051-2011.

Dai, A., 2006: Precipitation characteristics in eighteen coupled climate models. *Journal of Climate*, **19,** 4605-4630, doi: 10.1175/jcli3884.1.

Dai, A., I. Y. Fung, and A. D. DelGenio, 1997: Surface observed global land precipitation variations during 1900-88. *Journal of Climate*, **10,** 2943-2962, doi: 10.1175/1520-0442(1997)010<2943:soglpv>2.0.co;2.

Easterling, D. R., G. A. Meehl, C. Parmesan, S. A. Changnon, T. R. Karl, and L. O. Mearns, 2000: Climate extremes: Observations, modeling, and impacts. *Science*, **289,** 2068-2074, doi: 10.1126/science.289.5487.2068.

Emori, S., and S. J. Brown, 2005: Dynamic and thermodynamic changes in mean and extreme precipitation under changed climate. *Geophysical Research Letters*, **32**, doi: 10.1029/2005gl023272.

Feichter, J., E. Roeckner, U. Lohmann, and B. Liepert, 2004: Nonlinear aspects of the climate response to greenhouse gas and aerosol forcing. *Journal of Climate*, **17,** 2384-2398, doi: 10.1175/1520-0442(2004)017<2384:naotcr>2.0.co;2.

Fekete, B. M., C. J. Vorosmarty, J. O. Roads, and C. J. Willmott, 2004: Uncertainties in precipitation and their impacts on runoff estimates. *Journal of Climate*, **17,** 294-304, doi: 10.1175/1520-0442(2004)017<0294:uipati>2.0.co;2.

Frei, C., R. Scholl, S. Fukutome, J. Schmidli, and P. L. Vidale, 2006: Future change of precipitation extremes in Europe: Intercomparison of scenarios from regional climate models. *Journal of Geophysical Research-Atmospheres*, **111**, doi: 10.1029/2005jd005965.

Gebremichael, M., W. F. Krajewski, M. L. Morrissey, G. J. Huffman, and R. F. Adler, 2005: A Detailed Evaluation of GPCP 1° Daily Rainfall Estimates over the Mississippi River Basin. *Journal of Applied Meteorology*, **44,** 665-681, doi: 10.1175/jam2233.1.

Gebremichael, M., W. F. Krajewski, M. Morrissey, D. Langerud, G. J. Huffman, and R. Adler, 2003: Error Uncertainty Analysis of GPCP Monthly Rainfall Products: A Data-Based Simulation Study. *Journal of Applied Meteorology*, **42,** 1837-1848, doi: 10.1175/1520-0450(2003)042<1837:euaogm>2.0.co;2.

Hartmann, D. L., 1994: *Global Physical Climatology.* Academic Press Limited, London, 411 pp, ISBN: 0-12-328530-5.

Hawkins, E., and R. Sutton, 2009: The potential to narrow uncertainty in regional climate predictions. *Bulletin of the American Meteorological Society*, **90,** 1095-+, doi: 10.1175/2009bams2607.1.

Held, I. M., and B. J. Soden, 2006: Robust responses of the hydrological cycle to global warming. *Journal of Climate*, **19,** 5686-5699, doi: 10.1175/jcli3990.1.

Huffman, G. J., R. F. Adler, D. T. Bolvin, and G. J. Gu, 2009: Improving the global precipitation record: GPCP Version 2.1. *Geophysical Research Letters*, **36**, doi: 10.1029/2009gl040000.

Huffman, G. J., R. F. Adler, M. M. Morrissey, D. T. Bolvin, S. Curtis, R. Joyce, B. McGavock, and J. Susskind, 2001: Global Precipitation at One-Degree Daily Resolution from Multisatellite Observations. *Journal of Hydrometeorology*, **2,** 36-50, doi: 10.1175/1525-7541(2001)002<0036:gpaodd>2.0.co;2.

Hurrell, J. W., and H. Van Loon, 1997: Decadal variations in climate associated with the north Atlantic oscillation. *Clim. Change*, **36,** 301-326, doi: 10.1023/a:1005314315270.

Hurrell, J. W., M. P. Hoerling, A. S. Phillips, and T. Xu, 2004: Twentieth century North Atlantic climate change. Part 1: assessing determinism. *Climate Dynamics*, **23,** 371-389, doi: 10.1007/s00382-004-0432-y.

Hurrell, J. W., J. J. Hack, D. Shea, J. M. Caron, and J. Rosinski, 2008: A new sea surface temperature and sea ice boundary dataset for the Community Atmosphere Model. *Journal of Climate*, **21,** 5145-5153, doi: 10.1175/2008jcli2292.1.

IPCC, 2007: *Climate Change 2007: Impacts, Adaptation and Vulnerability. Contribution of Working Group II to the Fourth Assessment. Report of the Intergovernmental Panel on Climate Change.* [M. L. Parry, O. F. Canziani, J. P. Palutikof, P. J. van der Linden, and C. E. Hanson (Eds.)], Cambridge University Press, Cambridge, UK, 976 pp, ISBN: 978-0521-70597-4.

Jones, C. D., J. K. Hughes, N. Bellouin, S. C. Hardiman, G. S. Jones, J. Knight, S. Liddicoat, F. M. O'Connor, R. J. Andres, C. Bell, K. O. Boo, A. Bozzo, N. Butchart, P. Cadule, K. D. Corbin, M. Doutriaux-Boucher, P. Friedlingstein, J. Gornall, L. Gray, P. R. Halloran, G. Hurtt, W. J. Ingram, J. F. Lamarque, R. M. Law, M. Meinshausen, S. Osprey, E. J. Palin, L. P. Chini, T. Raddatz, M. G. Sanderson, A. A. Sellar, A. Schurer, P. Valdes, N. Wood, S. Woodward, M. Yoshioka, and M. Zerroukat, 2011: The HadGEM2-ES implementation of CMIP5 centennial simulations. *Geosci. Model Dev.*, **4,** 543-570, doi: 10.5194/gmd-4-543-2011.

Jonkman, S. N., 2005: Global perspectives on loss of human life caused by floods. *Nat. Hazards*, **34,** 151-175, doi: 10.1007/s11069-004-8891-3.

Klein Tank, A. M. G., F. W. Zwiers, and X. Zhang, 2009: Guidelines on Analysis of extremes in a changing climate in support of informed decisions for adaptation. *WCDMP No. 72*, World Meteorological Organisation, Geneva, Switzerland, 56 pp.

Knutti, R., R. Furrer, C. Tebaldi, J. Cermak, and G. A. Meehl, 2010: Challenges in Combining Projections from Multiple Climate Models. *Journal of Climate*, **23,** 2739-2758, doi: 10.1175/2009jcli3361.1.

Kottek, M., J. Grieser, C. Beck, B. Rudolf, and F. Rubel, 2006: World map of the Koppen-Geiger climate classification updated. *Meteorologische Zeitschrift*, **15,** 259-263, doi: 10.1127/0941-2948/2006/0130.

Lambert, F. H., and M. J. Webb, 2008: Dependency of global mean precipitation on surface temperature. *Geophysical Research Letters*, **35**, doi: 10.1029/2008gl034838.

Lambert, F. H., and M. R. Allen, 2009: Are Changes in Global Precipitation Constrained by the Tropospheric Energy Budget? *Journal of Climate*, **22,** 499-517, doi: 10.1175/2008jcli2135.1.

Lavers, D. A., R. P. Allan, E. F. Wood, G. Villarini, D. J. Brayshaw, and A. J. Wade, 2011: Winter floods in Britain are connected to atmospheric rivers. *Geophysical Research Letters*, **38**, doi: 10.1029/2011gl049783.

Liepert, B. G., J. Feichter, U. Lohmann, and E. Roeckner, 2004: Can aerosols spin down the water cycle in a warmer and moister world? *Geophysical Research Letters*, **31**, doi: 10.1029/2003gl019060.

Lohmann, U., R. Sausen, L. Bengtsson, U. Cubasch, J. Perlwitz, and E. Roeckner, 1993: The Koppen climate classification as a diagnostic tool for general circulation models. *Climate Research*, **3,** 177-193, doi: 10.3354/cr003177.

Lu, J., G. A. Vecchi, and T. Reichler, 2007: Expansion of the Hadley cell under global warming. *Geophysical Research Letters*, **34**, doi: 10.1029/2006gl028443.

Martin, G. M., S. F. Milton, C. A. Senior, M. E. Brooks, S. Ineson, T. Reichler, and J. Kim, 2010: Analysis and Reduction of Systematic Errors through a Seamless Approach to Modeling Weather and Climate. *Journal of Climate*, **23,** 5933-5957, doi: 10.1175/2010jcli3541.1.

Martin, G. M., N. Bellouin, W. J. Collins, I. D. Culverwell, P. R. Halloran, S. C. Hardiman, T. J. Hinton, C. D. Jones, R. E. McDonald, A. J. McLaren, F. M. O'Connor, M. J.

Roberts, J. M. Rodriguez, S. Woodward, M. J. Best, M. E. Brooks, A. R. Brown, N. Butchart, C. Dearden, S. H. Derbyshire, I. Dharssi, M. Doutriaux-Boucher, J. M. Edwards, P. D. Falloon, N. Gedney, L. J. Gray, H. T. Hewitt, M. Hobson, M. R. Huddleston, J. Hughes, S. Ineson, W. J. Ingram, P. M. James, T. C. Johns, C. E. Johnson, A. Jones, C. P. Jones, M. M. Joshi, A. B. Keen, S. Liddicoat, A. P. Lock, A. V. Maidens, J. C. Manners, S. F. Milton, J. G. L. Rae, J. K. Ridley, A. Sellar, C. A. Senior, I. J. Totterdell, A. Verhoef, P. L. Vidale, A. Wiltshire, and G. E. M. D. T. Had, 2011: The HadGEM2 family of Met Office Unified Model climate configurations. *Geosci. Model Dev.*, **4,** 723-757.

Meehl, G. A., T. F. Stocker, W. D. Collins, P. Friedlingstein, A. T. Gaye, J. M. Gregory, A. Kitoh, R. Knutti, J. M. Murphy, A. Noda, S. C. B. Raper, I. G. Watterson, A. J. Weaver, and Z.-C. Zhao, 2007: Global Climate Projections. In: *Climate Change 2007: The Physical Science Basis. Contribution of Working Group I to the Fourth Assessment Report of the Intergovernmental Panel on Climate Change*, [S. Solomon, D. Qin, M. Manning, M. Marquis, K. Averyt, M. M. B. Tignor, H. L. Miller, and Z. L. Chen (Eds.)], Cambridge University Press, Cambridge, United Kingdom and New York, NY, USA, 747-846, ISBN: 978-0521-70596-7.

Meinshausen, M., S. J. Smith, K. Calvin, J. S. Daniel, M. L. T. Kainuma, J. F. Lamarque, K. Matsumoto, S. A. Montzka, S. C. B. Raper, K. Riahi, A. Thomson, G. J. M. Velders, and D. P. P. van Vuuren, 2011: The RCP greenhouse gas concentrations and their extensions from 1765 to 2300. *Clim. Change*, **109,** 213-241, doi: 10.1007/s10584-011-0156-z.

Mitchell, J. F. B., C. A. Wilson, and W. M. Cunnington, 1987: On CO2 climate sensitivity and model dependence of results. *Quarterly Journal of the Royal Meteorological Society*, **113,** 293-322, doi: 10.1256/smsqj.47516.

Moss, R. H., J. A. Edmonds, K. A. Hibbard, M. R. Manning, S. K. Rose, D. P. van Vuuren, T. R. Carter, S. Emori, M. Kainuma, T. Kram, G. A. Meehl, J. F. B. Mitchell, N. Nakicenovic, K. Riahi, S. J. Smith, R. J. Stouffer, A. M. Thomson, J. P. Weyant, and T. J. Wilbanks, 2010: The next generation of scenarios for climate change research and assessment. *Nature*, **463,** 747-756, doi: 10.1038/nature08823.

O'Gorman, P. A., and T. Schneider, 2009: The physical basis for increases in precipitation extremes in simulations of 21st-century climate change. *Proceedings of the National Academy of Sciences of the United States of America*, **106,** 14773-14777, doi: 10.1073/pnas.0907610106.

O'Gorman, P. A., and C. J. Muller, 2010: How closely do changes in surface and column water vapor follow Clausius-Clapeyron scaling in climate change simulations? *Environ. Res. Lett.*, **5**, doi: 10.1088/1748-9326/5/2/025207.

Orlowsky, B., and S. I. Seneviratne, 2012: Global changes in extreme events: regional and seasonal dimension. *Clim. Change*, **110,** 669-696, doi: 10.1007/s10584-011-0122-9.

Pall, P., M. R. Allen, and D. A. Stone, 2007: Testing the Clausius-Clapeyron constraint on changes in extreme precipitation under CO2 warming. *Climate Dynamics*, **28,** 351-363, doi: 10.1007/s00382-006-0180-2.

Palmer, T. N., G. J. Shutts, R. Hagedorn, E. Doblas-Reyes, T. Jung, and M. Leutbecher, 2005: Representing model uncertainty in weather and climate prediction. *Annual Review of Earth and Planetary Sciences*, **33,** 163-193, doi: 10.1146/annurev.earth.33.092203.122552.

Peel, M. C., B. L. Finlayson, and T. A. McMahon, 2007: Updated world map of the Köppen-Geiger climate classification. *Hydrol. Earth Syst. Sci. Discuss.*, **4,** 439-473, doi: 10.5194/hessd-4-439-2007.

Pendergrass, A. G., and D. L. Hartmann, 2012: Global-mean precipitation and black carbon in AR4 simulations. *Geophysical Research Letters*, **39**, doi: 10.1029/2011gl050067.

Previdi, M., and B. G. Liepert, 2008: Interdecadal Variability of Rainfall on a Warming Planet. *Eos Trans. AGU*, **89**, doi: 10.1029/2008eo210002.

Ramanathan, V., P. J. Crutzen, J. T. Kiehl, and D. Rosenfeld, 2001: Atmosphere - Aerosols, climate, and the hydrological cycle. *Science*, **294,** 2119-2124, doi: 10.1126/science.1064034.

Richter, I., and S.-P. Xie, 2008: Muted precipitation increase in global warming simulations: A surface evaporation perspective. *Journal of Geophysical Research-Atmospheres*, **113**, doi: 10.1029/2008jd010561.

Rubel, F., P. Skomorowski, and B. Rudolf, 2002: Verification scores for the operational GPCP-1DD product over the European Alps. *Meteorologische Zeitschrift*, **11,** 367-370, doi: 10.1127/0941-2948/2002/0011-0367.

Schaller, N., I. Mahlstein, J. Cermak, and R. Knutti, 2011: Analyzing precipitation projections: A comparison of different approaches to climate model evaluation. *Journal of Geophysical Research-Atmospheres*, **116**, doi: 10.1029/2010jd014963.

Schär, C., D. Lüthi, U. Beyerle, and E. Heise, 1999: The soil-precipitation feedback: A process study with a regional climate model. *Journal of Climate*, **12,** 722-741, doi: 10.1175/1520-0442(1999)012<0722:tspfap>2.0.co;2.

Schmidli, J., C. Frei, and P. L. Vidale, 2006: Downscaling from GC precipitation: A benchmark for dynamical and statistical downscaling methods. *International Journal of Climatology*, **26,** 679-689, doi: 10.1002/joc.1287.

Schmidli, J., C. M. Goodess, C. Frei, M. R. Haylock, Y. Hundecha, J. Ribalaygua, and T. Schmith, 2007: Statistical and dynamical downscaling of precipitation: An evaluation and comparison of scenarios for the European Alps. *Journal of Geophysical Research-Atmospheres*, **112**, doi: 10.1029/2005jd007026.

Schmidt, G. A., R. A. Ruedy, R. L. Miller, and A. A. Lacis, 2010: Attribution of the present-day total greenhouse effect. *Journal of Geophysical Research-Atmospheres*, **115**, doi: 10.1029/2010jd014287.

Seneviratne, S. I., N. Nicholls, D. Easterling, C. M. Goodess, S. Kanae, J. Kossin, Y. Luo, J. Marengo, K. McInnes, M. Rahimi, M. Reichstein, A. Sorteberg, C. Vera, and X. Zhang, 2012: Changes in climate extremes and their impacts on the natural physical environment. In: *Managing the Risks of Extreme Events and Disasters to Advance Climate Change Adaptation*, [C. B. Field, V. Barros, T. F. Stocker, D. Qin,

D. J. Dokken, K. L. Ebi, M. D. Mastrandrea, K. J. Mach, G.-K. Plattner, S. K. Allen, M. Tignor, and P. M. Midgley (Eds.)], Cambridge University Press, Cambridge, United Kingdom and New York, NY, USA, 109-230, ISBN: 978-1-107-60780-4.

Stephens, G. L., and T. D. Ellis, 2008: Controls of Global-Mean Precipitation Increases in Global Warming GCM Experiments. *Journal of Climate*, **21,** 6141-6155, doi: 10.1175/2008jcli2144.1.

Sun, Y., S. Solomon, A. Dai, and R. W. Portmann, 2006: How often does it rain? *Journal of Climate*, **19,** 916-934, doi: 10.1175/jcli3672.1.

Trenberth, K. E., 2008: The Impact of Climate Change and Variability on Heavy Precipitation, Floods, and Droughts. In: *Encyclopedia of Hydrological Sciences*, John Wiley & Sons, Ltd, ISBN: 978-0470848944.

Trenberth, K. E., 2011: Changes in precipitation with climate change. *Climate Research*, **47,** 123-138, doi: 10.3354/cr00953.

Trenberth, K. E., and D. J. Shea, 2005: Relationships between precipitation and surface temperature. *Geophysical Research Letters*, **32**, doi: 10.1029/2005gl022760.

Trenberth, K. E., J. T. Fasullo, and J. Kiehl, 2009: Earth's Global Energy Budget. *Bulletin of the American Meteorological Society*, **90,** 311-323, doi: 10.1175/2008bams2634.1.

Trenberth, K. E., J. T. Fasullo, and J. Mackaro, 2011: Atmospheric Moisture Transports from Ocean to Land and Global Energy Flows in Reanalyses. *Journal of Climate*, **24,** 4907-4924, doi: 10.1175/2011jcli4171.1.

Trenberth, K. E., A. Dai, R. M. Rasmussen, and D. B. Parsons, 2003: The changing character of precipitation. *Bulletin of the American Meteorological Society*, **84,** 1205-1217, doi: 10.1175/bams-84-9-1205.

Trenberth, K. E., L. Smith, T. Qian, A. Dai, and J. Fasullo, 2007a: Estimates of the global water budget and its annual cycle using observational and model data. *Journal of Hydrometeorology*, **8,** 758-769, doi: 10.1175/jhm600.1.

Trenberth, K. E., P. D. Jones, P. Ambenje, R. Bojariu, D. Easterling, A. Klein Tank, D. Parker, F. Rahimzadeh, J. A. Renwick, M. Rusticucci, B. Soden, and P. Zhai, 2007b: Observations: Surface and Atmospheric Climate Change. In: *Climate Change 2007: The Physical Science Basis. Contribution of Working Group I to the Fourth Assessment Report of the Intergovernmental Panel on Climate Change*, [S. Solomon, D. Qin, M. Manning, M. Marquis, K. Averyt, M. M. B. Tignor, H. L. Miller, and Z. L. Chen (Eds.)], Cambridge University Press, Cambridge, United Kingdom and New York, NY, USA, 235-336, ISBN: 978-0521-70596-7.

van der Ent, R. J., H. H. G. Savenije, B. Schaefli, and S. C. Steele-Dunne, 2010: Origin and fate of atmospheric moisture over continents. *Water Resources Research*, **46**, doi: 10.1029/2010wr009127.

van der Linden, P., and J. F. B. Mitchell (Eds.), 2009: *ENSEMBLES: Climate Change and its Impacts: Summary of research and results from the ENSEMBLES project*. Met Office Hadley Centre, Exeter, UK, 160 pp.

van Vuuren, D. P., J. Edmonds, M. Kainuma, K. Riahi, A. Thomson, K. Hibbard, G. C. Hurtt, T. Kram, V. Krey, J.-F. Lamarque, T. Masui, M. Meinshausen, N. Nakicenovic, S. J. Smith, and S. K. Rose, 2011: The representative concentration pathways: an overview. *Clim. Change*, **109,** 5-31, doi: 10.1007/s10584-011-0148-z.

Vecchi, G. A., and B. J. Soden, 2007: Global warming and the weakening of the tropical circulation. *Journal of Climate*, **20,** 4316-4340, doi: 10.1175/jcli4258.1.

Wentz, F. J., L. Ricciardulli, K. Hilburn, and C. Mears, 2007: How much more rain will global warming bring? *Science*, **317,** 233-235, doi: 10.1126/science.1140746.

Wild, M., and B. Liepert, 2010: The Earth radiation balance as driver of the global hydrological cycle. *Environ. Res. Lett.*, **5**, doi: 10.1088/1748-9326/5/2/025003.

Wild, M., J. Grieser, and C. Schär, 2008: Combined surface solar brightening and increasing greenhouse effect support recent intensification of the global land-based hydrological cycle. *Geophysical Research Letters*, **35**, doi: 10.1029/2008gl034842.

Wild, M., H. Gilgen, A. Roesch, A. Ohmura, C. N. Long, E. G. Dutton, B. Forgan, A. Kallis, V. Russak, and A. Tsvetkov, 2005: From dimming to brightening: Decadal changes in solar radiation at Earth's surface. *Science*, **308,** 847-850, doi: 10.1126/science.1103215.

Wilks, D. S., 1995: *Statistical Methods in the Atmospheric Sciences.* Academic Press, London, 467 pp, ISBN: 0-12-751965-3.

Yin, J. H., 2005: A consistent poleward shift of the storm tracks in simulations of 21st century climate. *Geophysical Research Letters*, **32**, doi: 10.1029/2005gl023684.

Zhang, L., K. Hickel, W. R. Dawes, F. H. S. Chiew, A. W. Western, and P. R. Briggs, 2004: A rational function approach for estimating mean annual evapotranspiration. *Water Resources Research*, **40**, doi: 10.1029/2003wr002710.

Appendix

Appendix A: Acknowledgements

The HadGEM2 data was acquired from the British Atmospheric Data Centre of the Natural Environment Research Council (http://badc.nerc.ac.uk). The primary web site for the GPCP dataset is the World Meteorological Organization's World Data Center at the National Climatic Data Center of the National Oceanic and Atmospheric Administration (http://lwf.ncdc.noaa.gov/oa/wmo/wdcamet-ncdc.html).

The author would like to thank Dr Richard Allan and Prof Dr Martin Wild for their supervision of this thesis. Richard Allan offered most gratefully guidance and support throughout the whole analysis and writing process. The University of Reading provided infrastructure and data access during my stay. I would like to thank Mrs Dawn Turner and Mr Andy Heaps for administrative and technical support and Dr George Dugdale for proof-reading of parts of Chapter 2 and 3.

Last but not least I would like to thank my parents for their continued generous support throughout my entire academic studies.

Appendix B: Declaration of originality

This signed "Declaration of originality" is a required component of any written work (including any electronic version) submitted by a student during the course of studies in Environmental Sciences. For Bachelor and Master thesis, a copy of this form is to be attached to the request for diploma.

I hereby declare that this written work is original work which I alone have authored and written in my own words, with the exclusion of proposed corrections.

Title of the work:	Changes in precipitation characteristics and extremes: Comparing Mediterranean to north-western European precipitation change

Author(s)

Last name:	Vogel
First Name:	David Alexander

With my signature, I hereby declare:

• I have adhered to all rules outlined in the form on „Citation etiquette", www.ethz.ch/students/exams/plagiarism_s_en.pdf.

• I have truthfully documented all methods, data and operational procedures.

• I have not manipulated any data.

• I have identified all persons who have substantially supported me in my work in the acknowledgements.

• I understand the rules specified above. I understand that the above written work may be tested electronically for plagiarism.

Reading, 24.04.2012

Place, Date   *Signature*

Appendix C: Abbreviations

AMIP	Atmospheric Model Intercomparison Project experiment
AR	Assessment Report of the IPCC
CMIP5	Coupled Model Intercomparison Project phase 5
DJF	Winter season December-January-February
ENSO	El Niño-Southern Oscillation
FUT	Future reference period 2070-2099
GCM	General Circulation Model
GHG	Greenhouse Gas
GPCP	Global Precipitation Climatology Project
HadGEM2	Hadley Centre Global Environment Model version 2
HadGEM2-A	HadGEM2 in Atmospheric-only configuration
HadGEM2-ES	HadGEM2 in complete Earth System configuration
IPCC	Intergovernmental Panel on Climate Change
JJA	Summer season June-July-August
MAM	Spring season March-April-May
MED	Study domain "Mediterranean"
NAO	North Atlantic Oscillation
NWE	Study domain "North-western Europe"
PRE	Present reference period 1976-2005
RCM	Regional Climate Model
RCP	Representative Concentration Pathway
SON	Autumn season September-October-November
SREX	Special Report on Managing the Risks of Extreme Events and Disasters to Advance Climate Change Adaptation
SST	Sea surface temperature

Appendix D: Additional figures
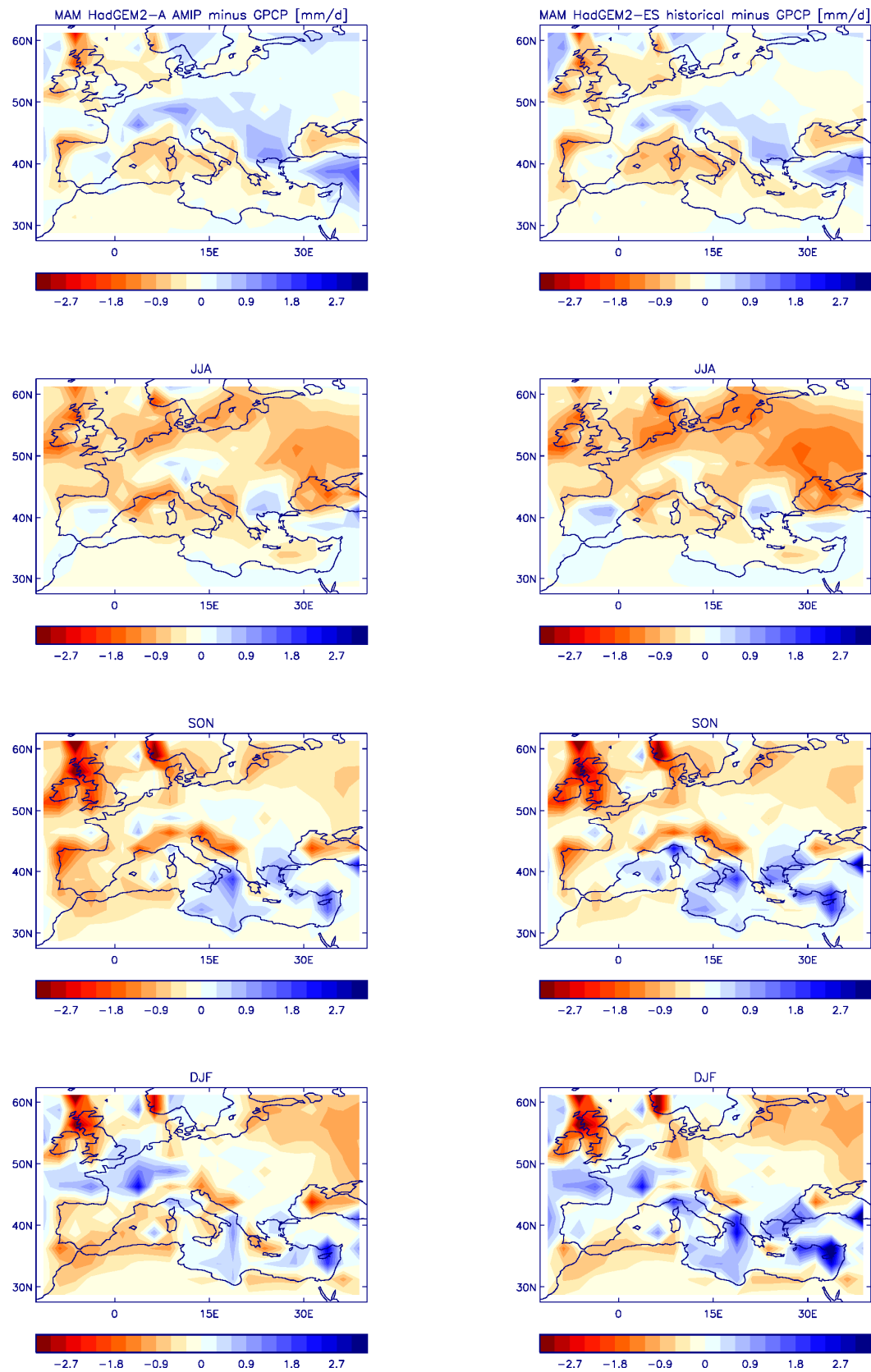
Figure A-1 Seasonal deviation of AVG between GPCP, HadGEM2-A & -ES Deviation of seasonal precipitation amount in mm/d. Left: HadGEM2-A minus GPCP, right: HadGEM2-ES minus GPCP.
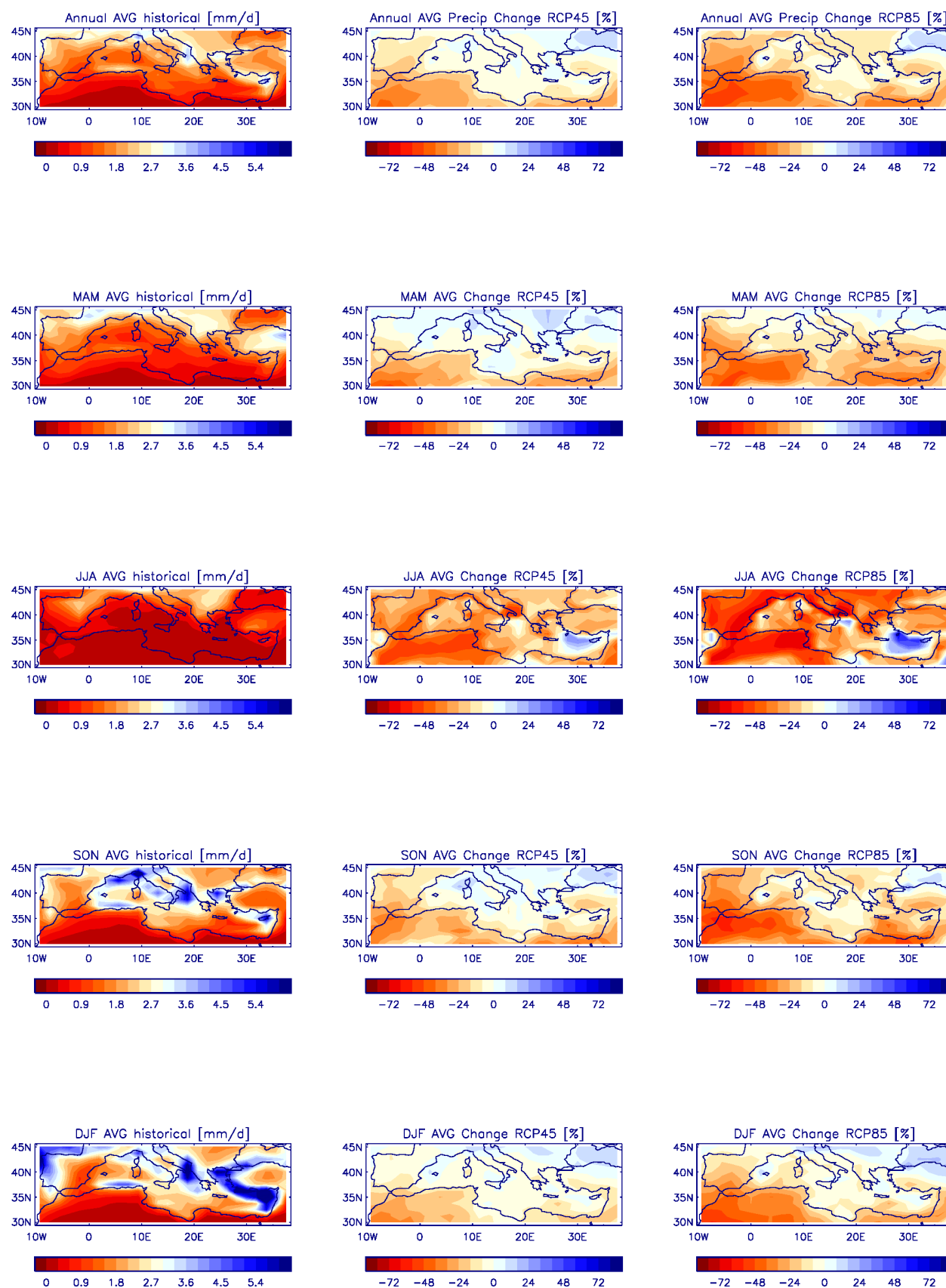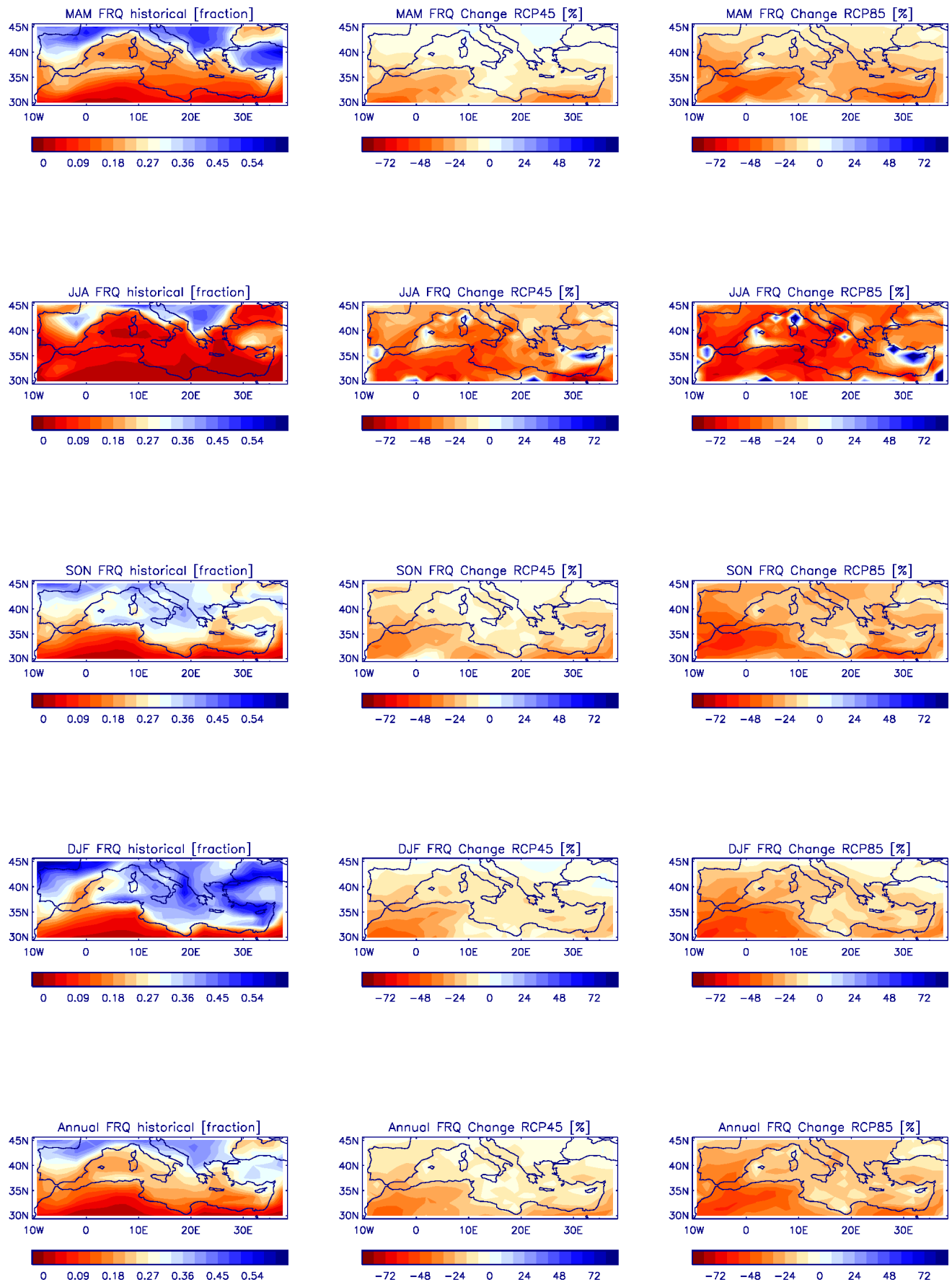
Figure A-2 Average precipitation change in MED Average annual and seasonal precipitation in mm/d for period 1976-2005 (left column). Percentage change simulated in HadGEM2-ES for RCP45 (middle column) and RCP85 (right column) for period 2070-2099. Changes are significant on 5 % level except for RCP45 DJF and MAM change.
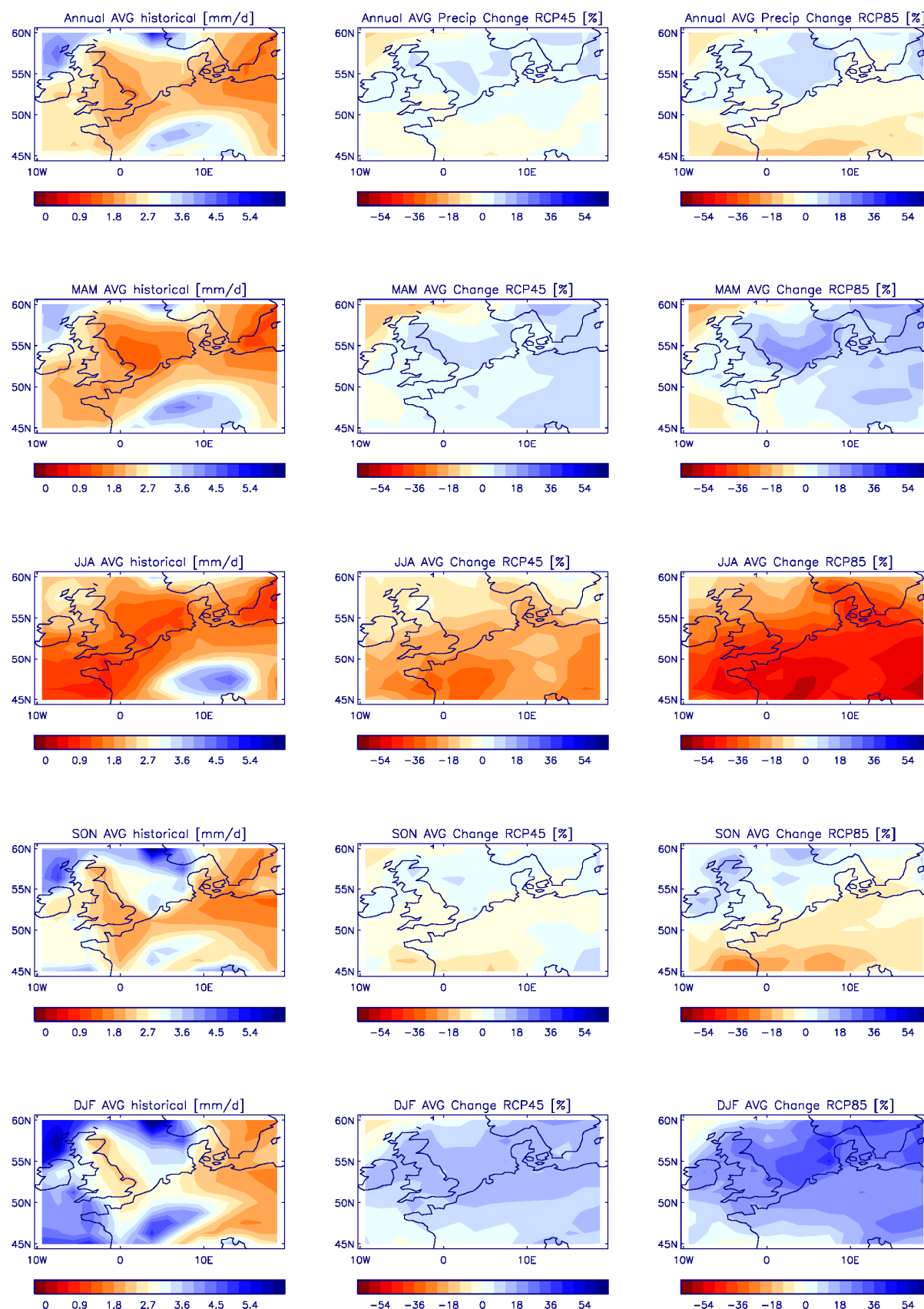
Figure A-3 Average precipitation change in NWE Average annual and seasonal precipitation in mm/d for period 1976-2005 (left column). Percentage change simulated in HadGEM2-ES for RCP45 (middle column) and RCP85 (right column) for period 2070-2099. Changes are significant on 5 % level except for RCP45 annual and SON change.
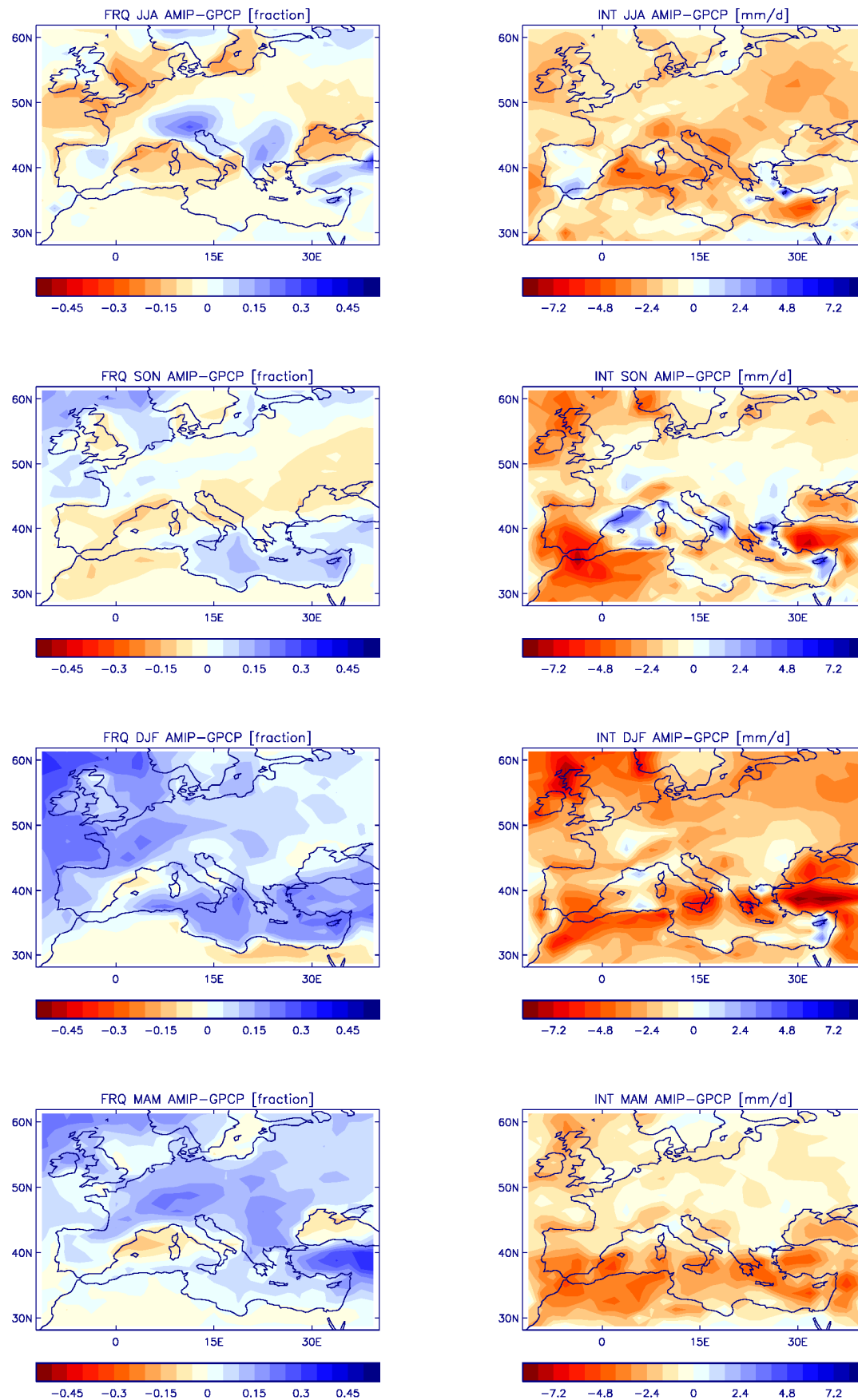
Figure A-4 Seasonal deviation of FRQ & INT between GPCP and HadGEM2-A Differences of annual averages calculated as HadGEM2-A AMIP experiment minus GPCP daily observation values for the period 1997-2008. Frequency deviation is shown in fraction (left), intensity in mm/d (right).

Figure A-5 Present precipitation frequency and projected change in MED Annual and seasonal simulation of present (1976-2005) precipitation FRQ (left), as well as percentage change in RCP45 (middle) and RCP85 (right) for period 2070-2099.
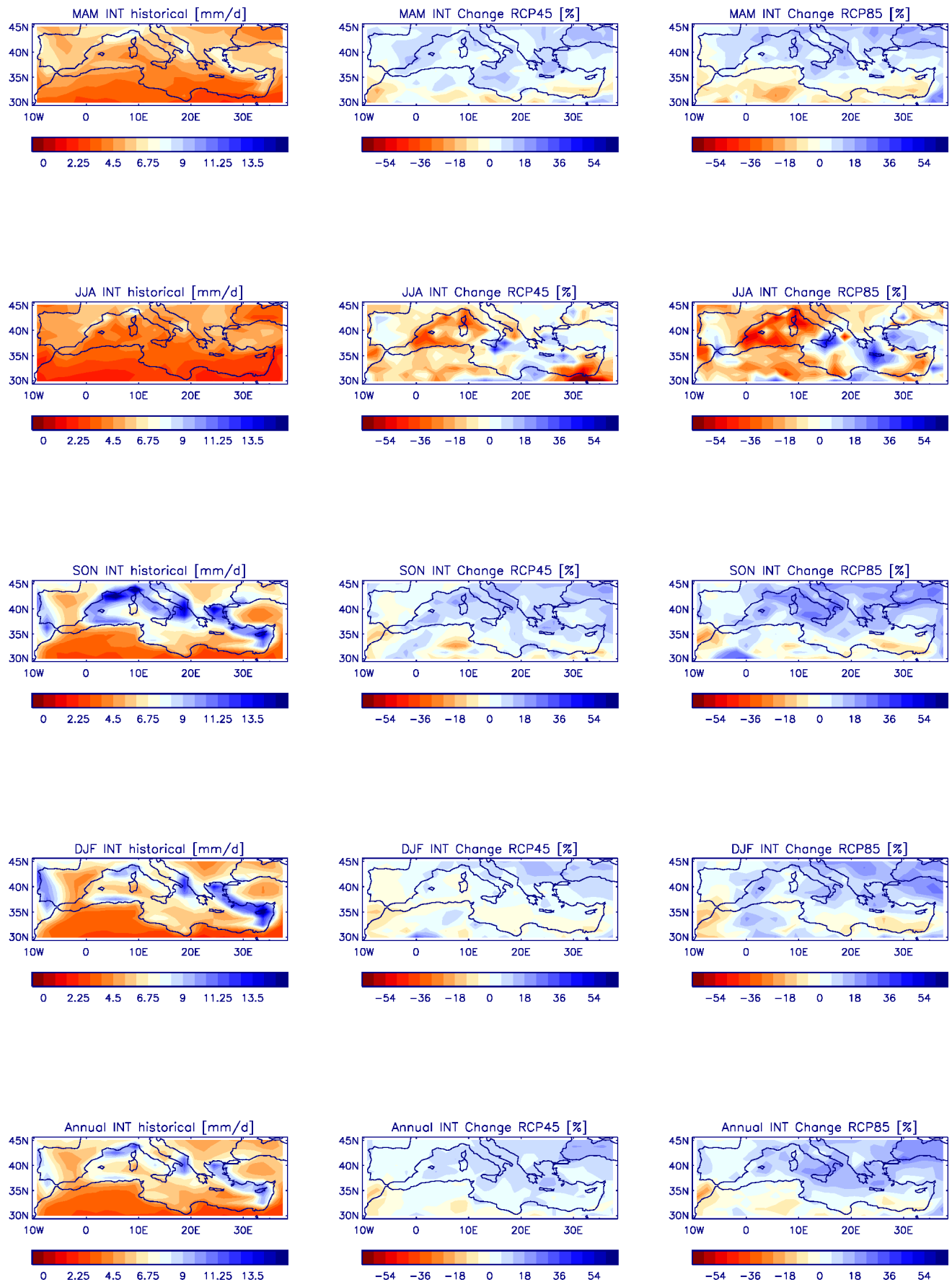
Figure A-6 Present precipitation intensity and projected change in MED Annual and seasonal simulation of present (1976-2005) precipitation INT (left), as well as percentage change in RCP45 (middle) and RCP85 (right) for period 2070-2099.
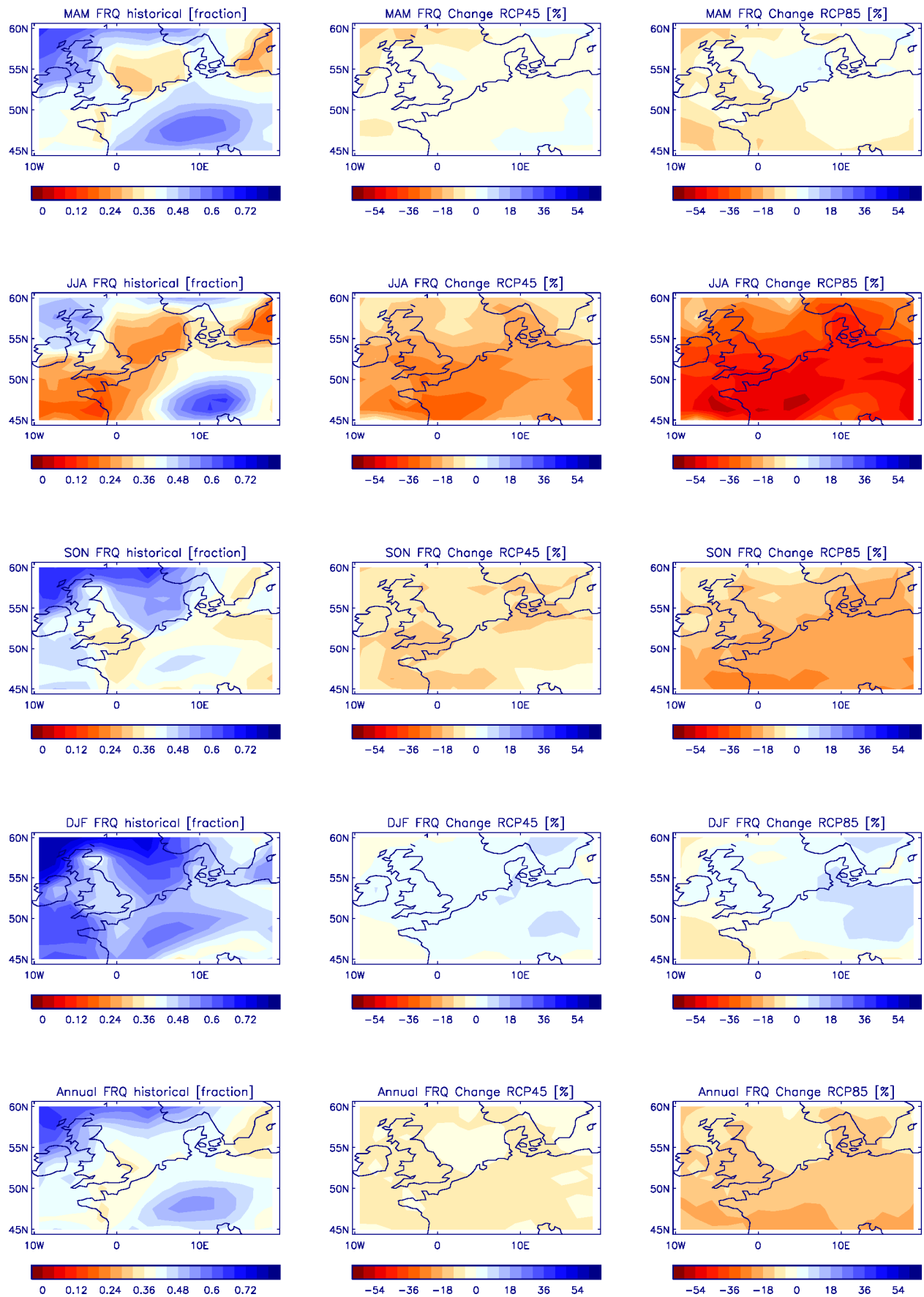
Figure A-7 Present precipitation frequency and projected change in NWE Annual and seasonal simulation of present (1976-2005) precipitation FRQ (left), as well as percentage change in RCP45 (middle) and RCP85 (right) for period 2070-2099.
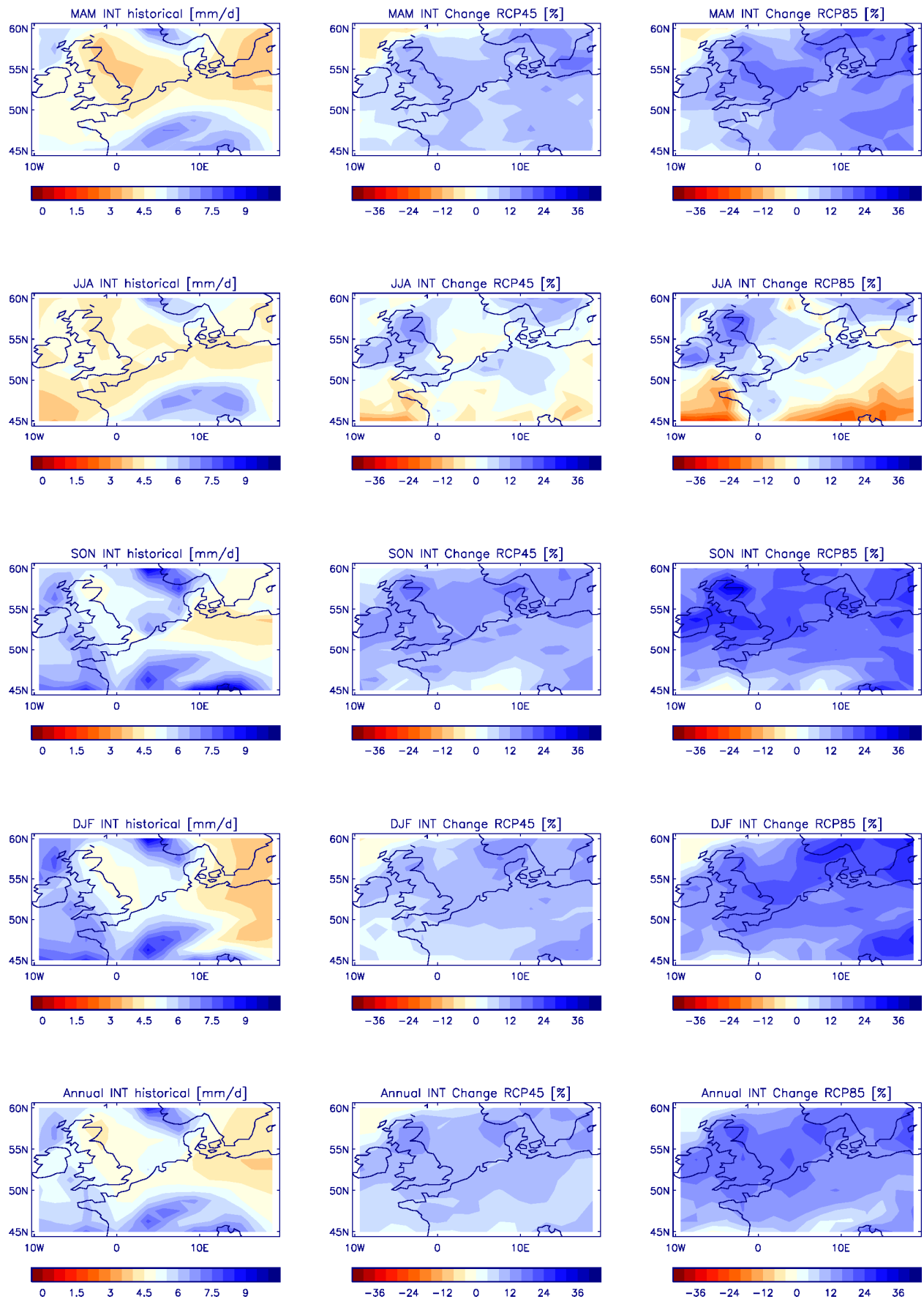
Figure A-8 Present precipitation intensity and projected change in NWE Annual and seasonal simulation of present (1976-2005) precipitation INT (left), as well as percentage change in RCP45 (middle) and RCP85 (right) for period 2070-2099.
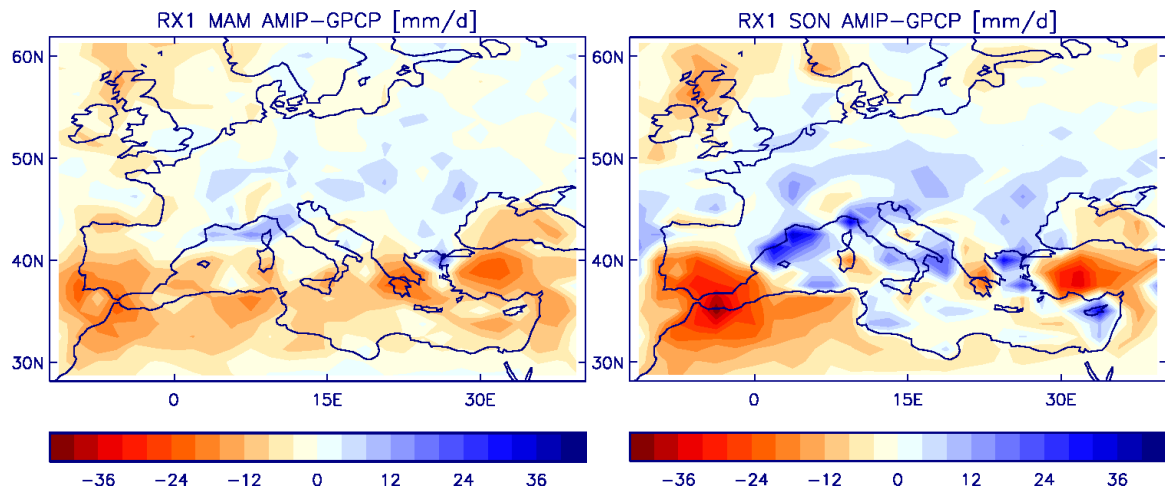
Figure A-9 Seasonal deviation of RX1 between GPCP and HadGEM2-A Differences of average spring (left) and autumn (right) one-day precipitation maxima in mm/d, calculated as HadGEM2-A AMIP experiment minus GPCP daily observation values for the period 1997-2008.
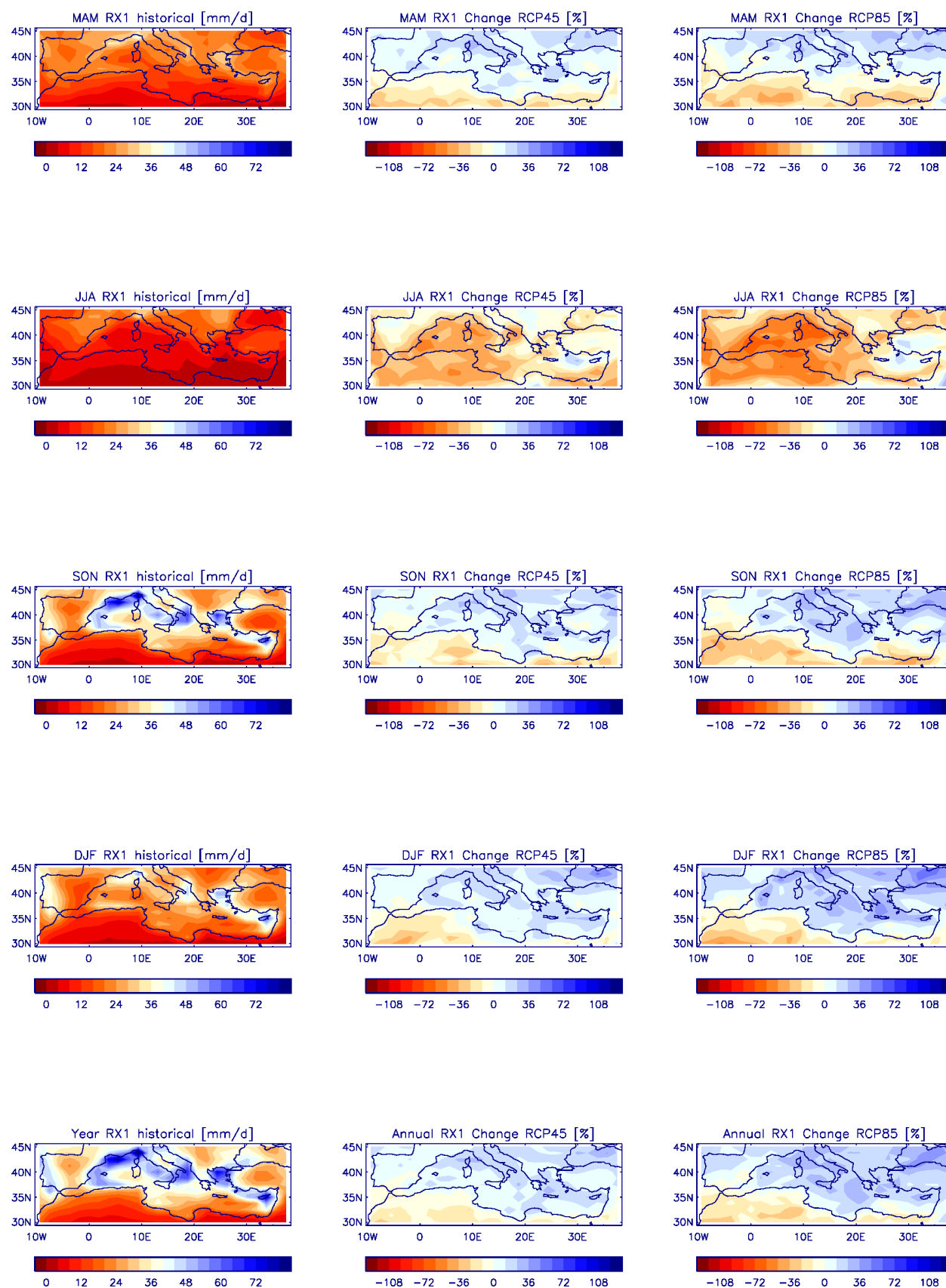
Figure A-10 Present value and change in RX1 for MED The left column shows HadGEM2-ES present climate (1976-2005) of average maximum one-day precipitation RX1. On middle and right column, percentage changes for RCP45 (middle) and RCP85 (right) for period 2070-2099 are shown. Changes are significant on 5 % level.
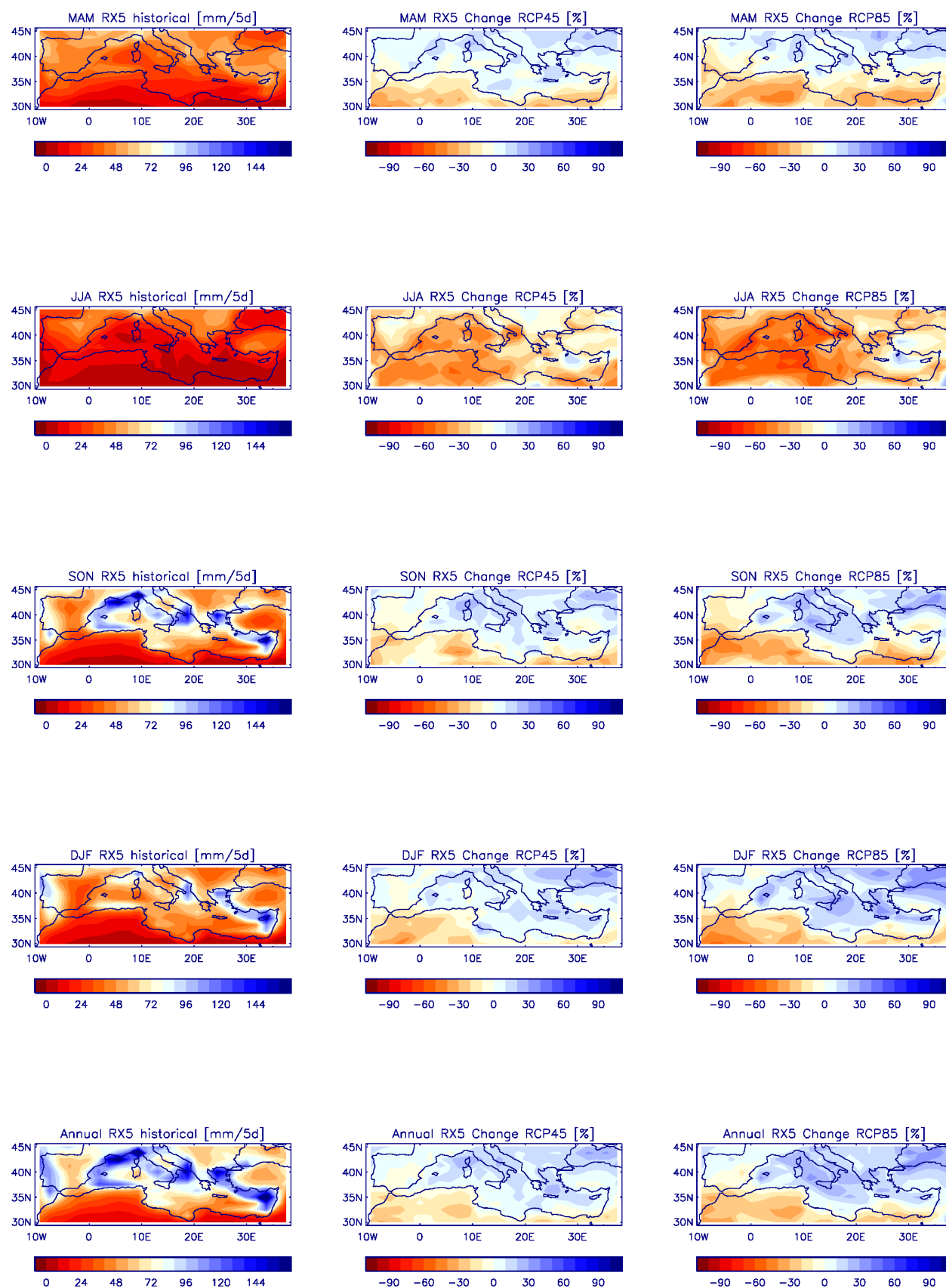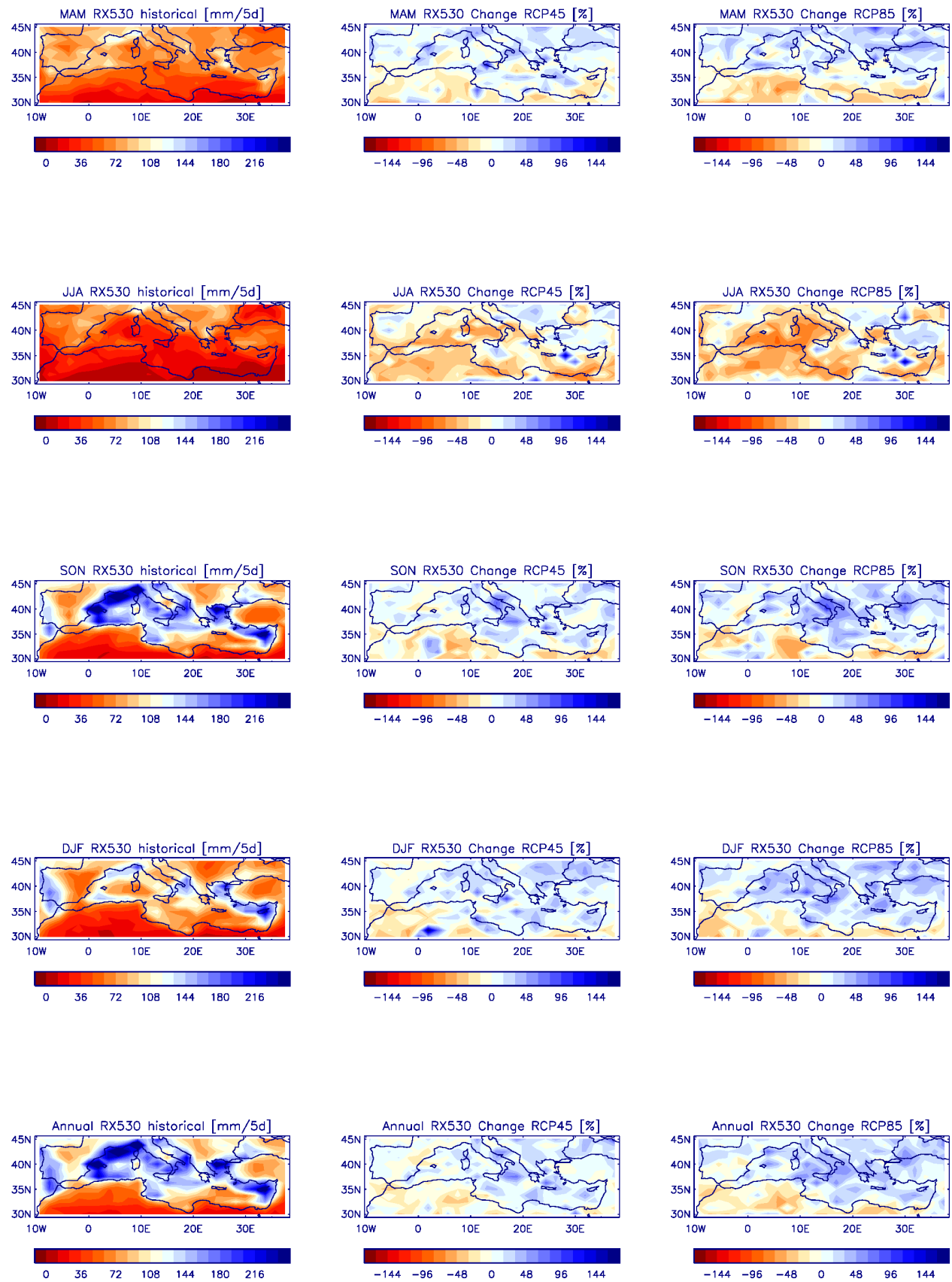
Figure A-11 Present value and change in RX5 for MED The left column shows HadGEM2-ES present climate (1976-2005) of average maximum five-day precipitation RX5. On middle and right column, percentage changes for RCP45 (middle) and RCP85 (right) for period 2070-2099 are shown. Changes are significant on 5 % level except for RX5 change in MAM & SON for both scenarios. Changes are significant on 5 % level.
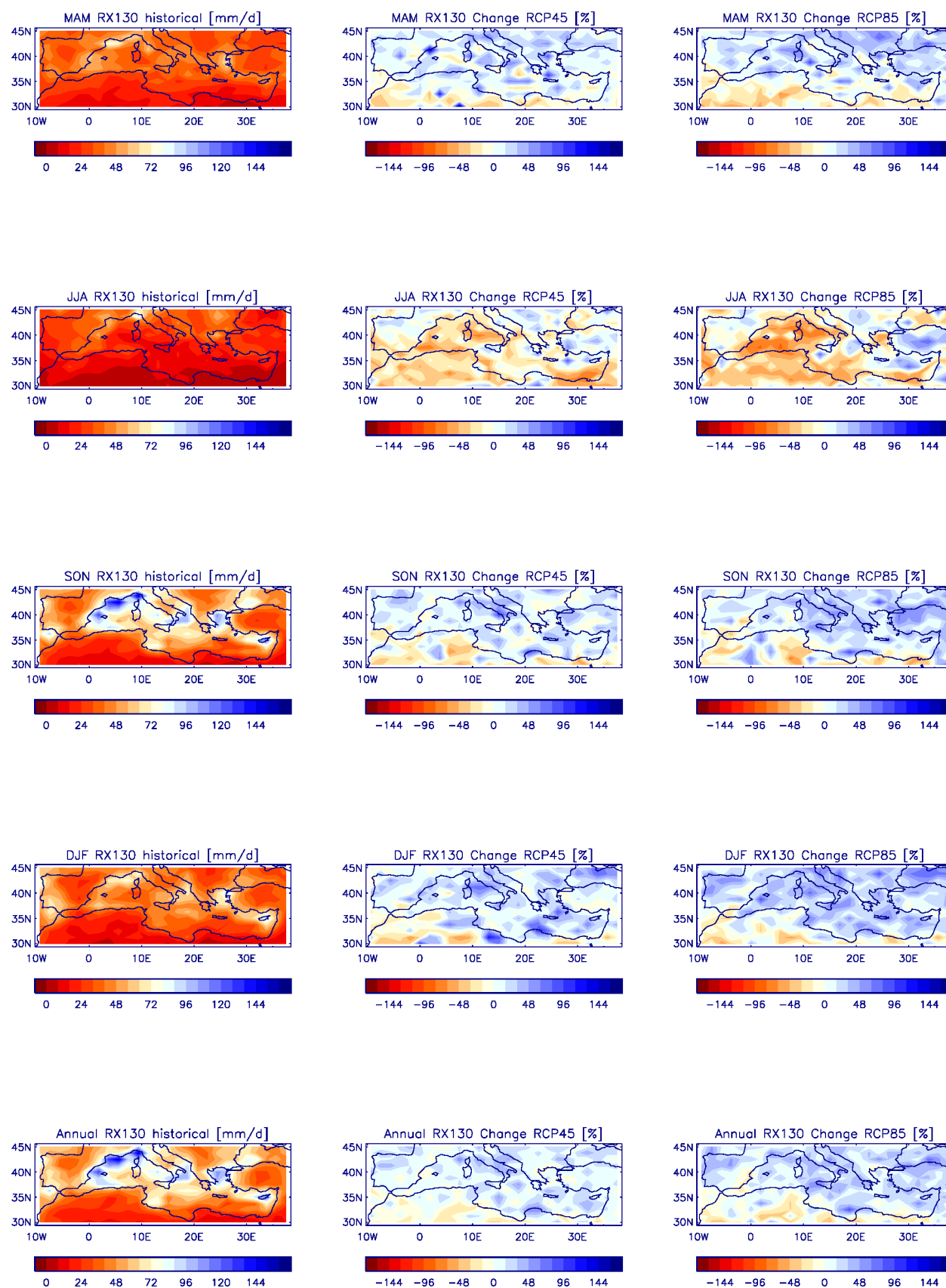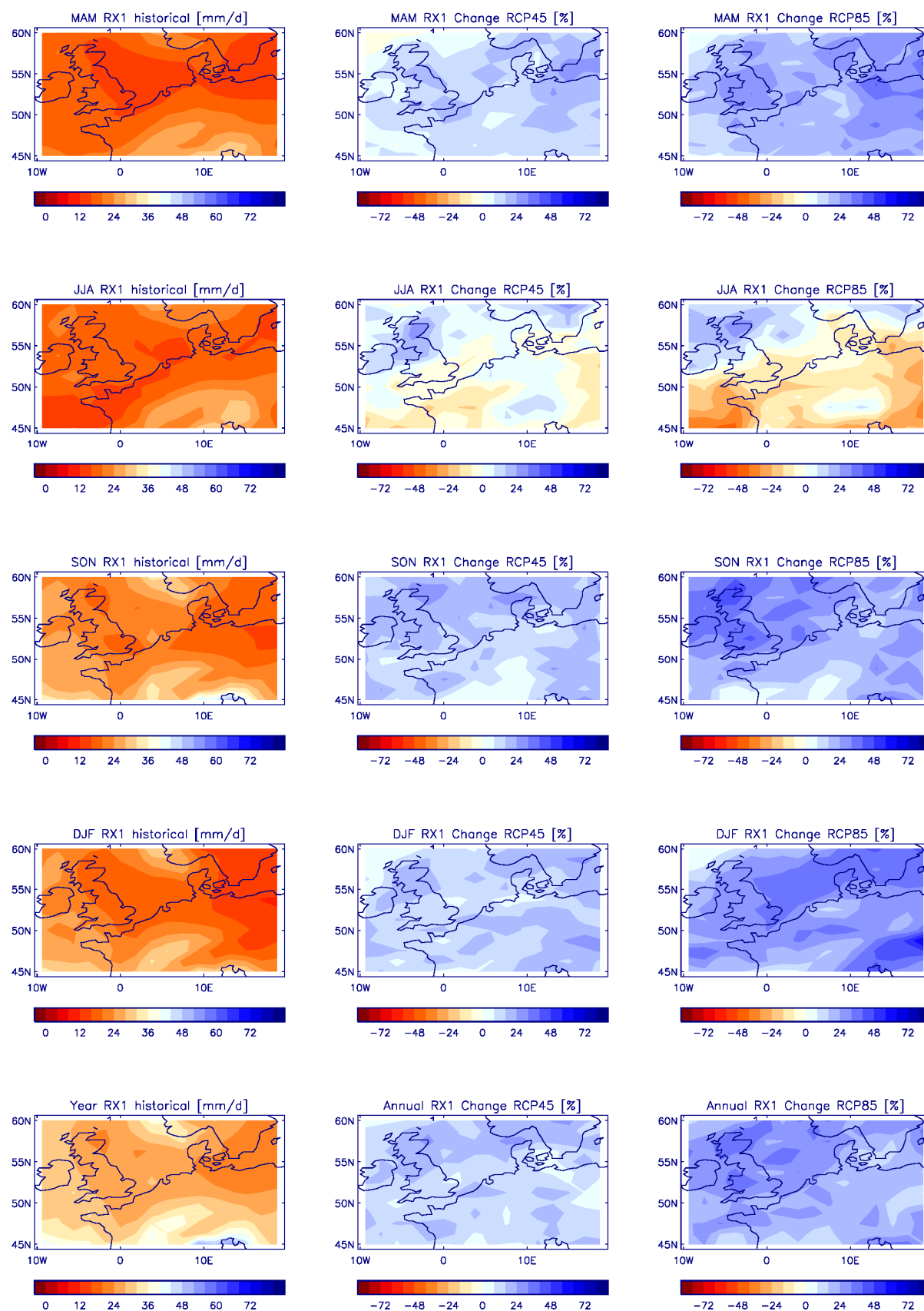
Figure A-12 Present value and change in RX1-30 for MED The left column shows HadGEM2-ES present climate (1976-2005) of maximum one-day precipitation in 30 years RX1-30. On middle and right column, percentage changes for RCP45 (middle) and RCP85 (right) for period 2070-2099 are shown. Changes are significant on 5 % level.
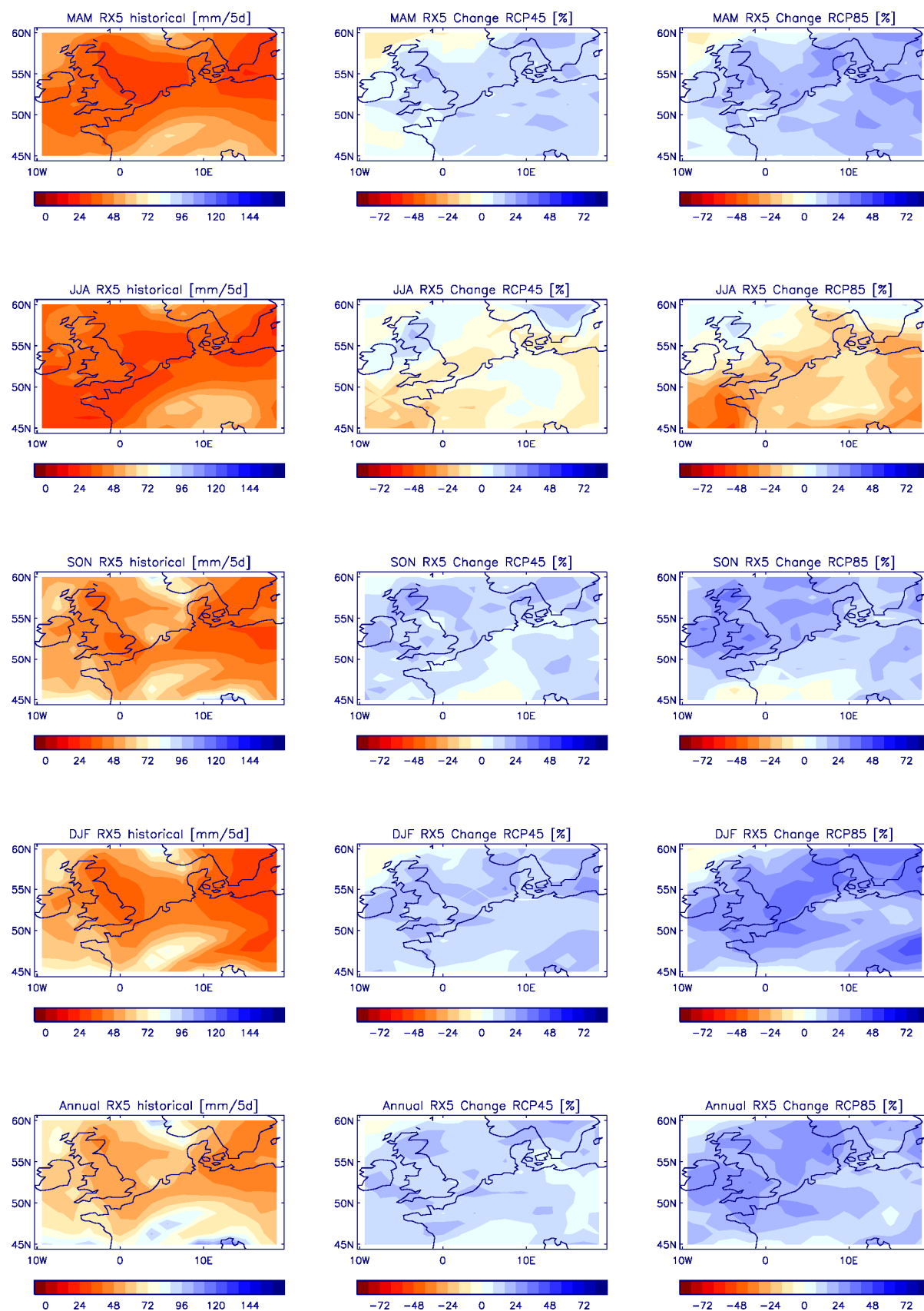
Figure A-13 Present value and change in RX5-30 for MED The left column shows HadGEM2-ES present climate (1976-2005) of maximum five-day precipitation in 30 years RX5-30. On middle and right column, percentage changes for RCP45 (middle) and RCP85 (right) for period 2070-2099 are shown. Changes are significant on 5 % level.
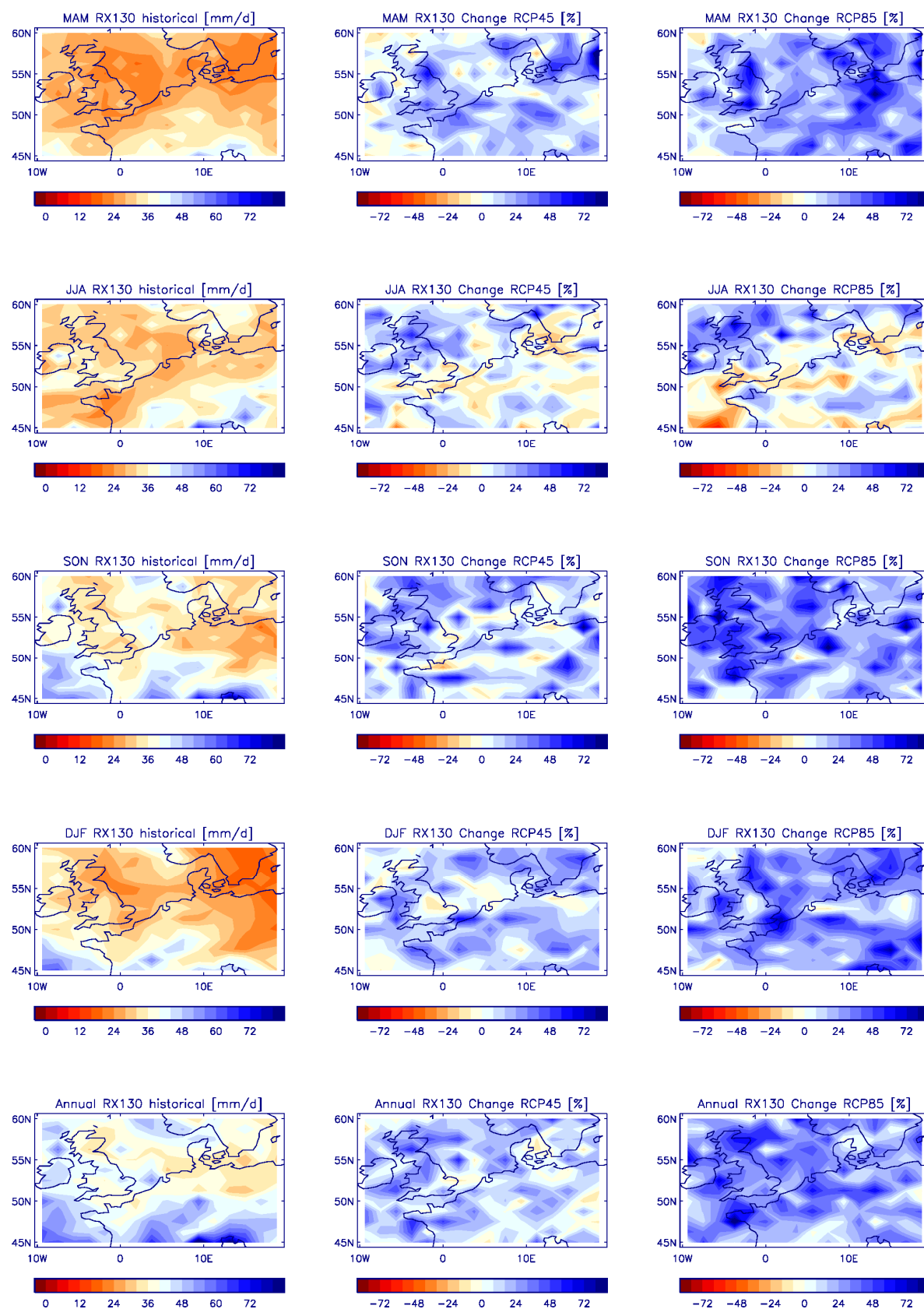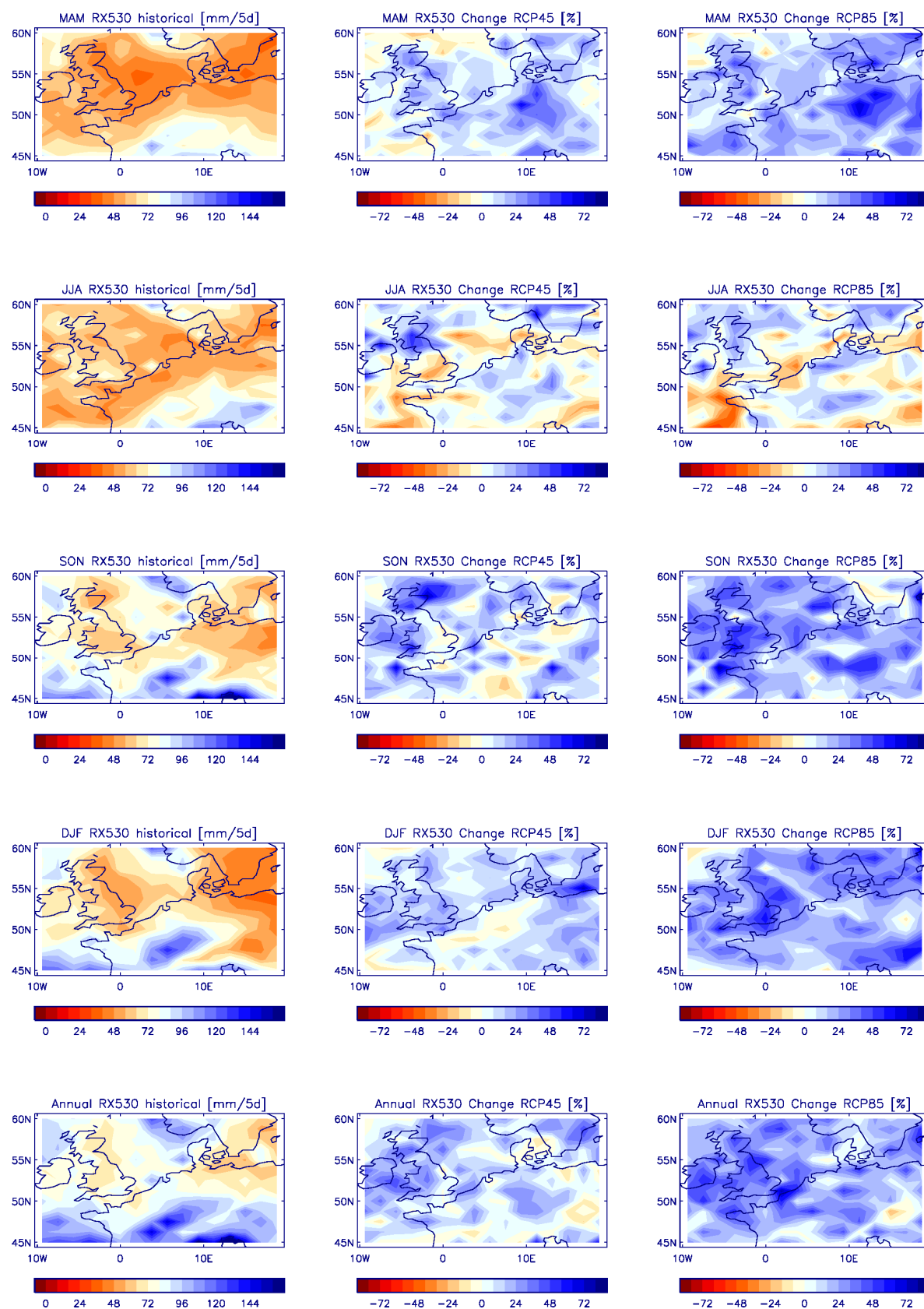
Figure A-14 Present value and change in RX1 for NWE The left column shows HadGEM2-ES present climate (1976-2005) of average maximum one-day precipitation RX1. On middle and right column, percentage changes for RCP45 (middle) and RCP85 (right) for period 2070-2099 are shown. Changes are significant on 5 % level except for JJA RCP45 scenario.

Figure A-15 Present value and change in RX5 for NWE The left column shows HadGEM2-ES present climate (1976-2005) of average maximum five-day precipitation RX5. On middle and right column, percentage changes for RCP45 (middle) and RCP85 (right) for period 2070-2099 are shown. Changes are significant on 5 % level.

Figure A-16 Present value and change in RX1-30 for NWE The left column shows HadGEM2-ES present climate (1976-2005) of maximum one-day precipitation in 30 years RX1-30. On middle and right column, percentage changes for RCP45 (middle) and RCP85 (right) for period 2070-2099 are shown. Changes are significant on 5 % level.

Figure A-17 Present value and change in RX5-30 for NWE The left column shows HadGEM2-ES present climate (1976-2005) of maximum five-day precipitation in 30 years RX5-30. On middle and right column, percentage changes for RCP45 (middle) and RCP85 (right) for period 2070-2099 are shown. Changes are significant on 5 % level, except for JJA RCP45 scenario.